





**PALAEO-ENVIRONMENTAL HISTORY OF THE SOUTHWESTERN BLACK  
SEA DURING THE LATE HOLOCENE: AN ELEMENTAL AND STABLE  
ISOTOPIC STUDY**

Anna E. Linegar, B.Sc

A Thesis submitted to the  
School of Graduate Studies in  
partial fulfilment of the requirements  
for the degree of

**Master of Science**

**Department of Environmental Science, Faculty of Science**

Memorial University of Newfoundland

**September 2012**

St. John's

Newfoundland





## ABSTRACT

The palaeo-environmental evolution of the SW Black Sea shelf during the last ~11,500 years is studied using the geochemical results from a long piston core (MAR05-50P) and its gravity core (MAR05-51G). Nine radiocarbon dates are used to erect a chronology for a composite core, constructed by splicing the upper 50 cm of MAR05-51G on top of MAR05-50P. On the basis of lithological, geochemical and regional geological data three units (Units A, B and C) are identified in the composite core. A local unconformity,  $\alpha_1$ , is identified in the lower portion of the core, with the hiatus spanning from ~10,735 – 8,420 cal yr BP. The TOC and TS values as well as  $\delta^{13}\text{C}$  and  $\delta^{34}\text{S}$  data documented that the lower Unit C (~11,500 – 10,735 cal yr BP) was deposited in a geochemically closed oxie, brackish system, where >80% of the organic matter originated from terrestrial/lacustrine sources. The middle Unit B (~8,420 – 4,700 cal yr BP) above the  $\alpha_1$  unconformity represents a transition from Unit C environment to an open marine oxie-dysoxic system associated with the reconnection of the Black Sea with the World's Oceans. These sediments contain  $\geq 40\%$  marine organic matter, and host evidence for active sulphate reduction showing isotopic fractionation, indicative of an open benthic system. The upper Unit A (~4,700 cal yr BP to Present) was deposited in a fully marine, mainly dysoxic environment where ~30% of the organic matter originated from marine sources. The stable isotopic data reveal a full-scale sulphate reduction during this interval. Regional correlations with two previously studied cores show good agreements with MAR05-50. The overall results from this study cannot refute the conclusions made by the *Outflow Hypothesis II* and the *Oscillating Sea Level Hypothesis*, however are in disagreement with some components of the *Flood Hypothesis*.

## ACKNOWLEDGEMENTS

First and foremost, I would like to express my deepest appreciation and gratitude to my co-supervisors, Dr. Ali Aksu and Dr. Richard Hiscott for the opportunity to take part in this research project. I am very grateful for all your continuous patience, guidance and constructive feedback that you have given me during the course of this thesis. Without your endless support, this would never have been possible.

I would like to send a special thanks to Alison Pye for her guidance and expertise in the Stable Isotope Lab, especially while retrieving my (ever so finicky) sulphur data. I would also like to thank Helen Gillespie for her direction during the geochemical sample preparation, to Dr. Geert Van Biesen for his assistance with mass spectrometry and Michael Shaffer for his instruction and direction with the scanning electron microscope.

To my friend, co-worker and officemate from day one, Lorna Williams: Thank you for all the encouragement, assistance, conversations and (of course) baked goods you have shared with me during the course of our theses. To two of my best friends, Michael Hamilton and Katey Roberts, thank you for all the emotional support, hour-long talks and never ending empathy you both provided me as we concurrently completed our MSc programs – we all finally made it! I want to say thanks to fellow grad students Chris Lister, Alex Chafe, Angela Buchanan, *et alia* for all the chats and tea parties that kept my sanity intact and enriched my time as a graduate student. To the rest of my friends and family: thank you to all who lent emotional, moral, financial and even physical (brute-force) support throughout the duration of this thesis. And of course, for putting up with my long and sporadic hours as I pursued this degree: some things never change.

Last but certainly not least, I want to thank my parents, Derm and Florence Linegar, and my wonderful boyfriend Mike Noseworthy for loving me unconditionally, for all the encouragement (even when unwanted) and for being there for me unflinchingly. I could not ask for a better support group – I literally could not have done this without the three of you. And of course, special thanks to my cat, The Bobz, for remaining generally indifferent throughout this whole process – sometimes that was just what I needed.

## Table of Contents

ABSTRACT .....	ii
ACKNOWLEDGEMENTS .....	iii
Table of Contents .....	iv
List of Tables .....	xi
List of Figures .....	xii
List of Equations .....	xiv
List of Plates .....	xv
List of Symbols, Nomenclature or Abbreviations .....	xvi
List of Appendices .....	xvii
Chapter One: Introduction .....	1
1.0 Introduction .....	1
1.1 Location .....	2
1.2 Organic matter .....	2
1.3 Regional Geology .....	5
1.4 Physical Oceanography .....	7
1.4.1 Black Sea Oceanography .....	7
1.4.2 Anastomosed Channel Network .....	11

1.5 Reconnection Hypotheses .....	14
1.5.1 Flood Hypothesis .....	14
1.5.2 Outflow Hypothesis .....	16
1.5.3 Oscillating Sea Level Hypothesis .....	19
1.6 Previous Work .....	21
1.6.1 Channel Network Mapping.....	21
1.6.2 Core Descriptions.....	21
1.6.2.1 MAR05-51G .....	21
1.6.2.2 MAR05-50P .....	23
1.6.3 Radiocarbon Dating .....	27
1.6.4 Related Cores .....	28
1.6.4.1 MAR02-45P and MAR02-45T .....	30
1.6.4.2 MAR05-13P and MAR05-04G.....	31
1.7 Carbon Isotopes and Total Organic Carbon (TOC).....	31
1.8 Sulphur Isotopes and Total Sulphur (TS) .....	32
1.9 Rationale .....	33
1.10 Research Questions.....	34
Chapter Two: Methodology and Analytical Procedures.....	36
2.1 Coring .....	36

2.2 Sampling .....	36
2.3 Sample Preparation .....	38
2.3.1 Processing of Sediments .....	38
2.3.2 Sediment Weighing.....	39
2.3.3 Gypsum Crystals.....	39
2.3.4 Gypsum Weighing .....	43
2.4 Analytical Techniques .....	43
2.4.1 Principles of Isotope-Ratio Mass Spectrometry .....	43
2.4.2 Elemental Analyzer.....	44
2.4.3 Continuous-Flow Isotope-Ratio Mass Spectrometry .....	44
2.4.4 Sulphur Samples .....	46
2.4.5 Carbon Samples .....	48
2.4.6 Gypsum Samples .....	48
2.4.7 Scanning Electron Microscopy (SEM) .....	48
2.5 Calculations.....	49
2.5.1 Terrestrial and Marine Fractions.....	49
2.5.2 Age Calibration .....	50
2.5.3 Age-Depth Conversion .....	53
2.6 Limitations to the Methodology.....	54

2.6.1 Mineral Dissolution Efficiency .....	54
2.6.2 Mass Spectrometry Error .....	55
2.6.3 Bioturbation .....	55
2.6.4 Sampling Intervals .....	55
Chapter Three: Chronology .....	57
3.1 Radiocarbon Dates .....	57
3.1.1 Radiocarbon Results .....	57
3.1.2 Reservoir Corrections .....	57
3.1.3 Calibrated Radiocarbon Dates for MAR05-50P and MAR05-51G .....	60
3.1.4 Calibrated Dates for MAR02-45P/MAR02-45T & MAR05-13P/MAR05-04G .....	62
3.2 Age Model .....	62
3.2.1 Core-Top Loss .....	62
3.2.2 Considerations.....	65
3.2.3 Resulting Age Model .....	66
3.2.4 Age Models for cores MAR02-45 and MAR05-13 .....	67
3.2.5 Conversion of Geochemical Data .....	67
Chapter Four: Results .....	71
4.0 Results.....	71

4.1 Carbon Results .....	71
4.1.1 Total Organic Carbon (TOC) Results .....	71
4.1.2 $\delta^{13}\text{C}$ Isotope Ratios .....	73
4.2 Sulphur Results .....	74
4.2.1 Total Sulphur (TS) Results .....	74
4.2.2 $\delta^{34}\text{S}$ Isotopic Ratios.....	74
4.3 TOC/TS Ratio .....	75
4.4 TS/TOC Ratio .....	76
4.5 Sediment Sources.....	78
4.5.1 Terrestrial Fraction.....	78
4.5.2 Marine Fraction.....	78
4.6 Gypsum Results .....	79
4.6.1 Crystal Abundance .....	79
4.6.2 Scanning Electron Microscope (SEM) Results.....	81
4.6.3 Isotopic ( $\delta^{34}\text{S}$ ) Ratios in Gypsum .....	81
4.6.4 Effect of Gypsum on Sulphur Geochemistry .....	83
Chapter Five: Interpretation .....	84
5.0 Age Domain .....	84
5.1 Lithological Correlation.....	84

5.2 Environmental Interpretation of the Geochemical Data .....	91
5.2.1 Total Organic Carbon .....	91
5.2.2 Stable Isotopic Composition of Total Organic Carbon.....	92
5.2.3 Total Sedimentary Sulphur .....	94
5.2.4 Stable Isotopic Composition of Sedimentary Sulphur.....	96
5.2.5 Ratios of TOC/TS and TS/TOC.....	98
5.3 Interpretation of Geochemistry from MAR05-50.....	101
5.3.1 Unit C.....	101
5.3.2 Unit B.....	103
5.3.3 Unit A.....	105
5.4 MAR05-50 Micropalaeontology Correlation .....	108
5.5 Geochemical Interpretations of cores MAR02-45 and MAR05-13.....	110
5.5.1 Core MAR02-45 Geochemistry .....	110
5.5.2 Core MAR05-13 Geochemistry .....	113
5.5.2.1 MAR05-13 Sulphur Isotopes .....	115
5.5.2.2 MAR05-13 Geochemical Results .....	116
5.6 Geochemical correlations between MAR05-50, MAR02-45 and MAR05-13 .....	117
5.6.1 Carbon Results .....	118
5.6.2 Sulphur Results .....	123

5.6.3 Results from Carbon to Sulphur and Sulphur to Carbon Ratios.....	128
Chapter Six: Discussion.....	131
6.1 Last Glacial Maximum – Interglacial Transition (~20,000 – ~12,630 cal yr BP).	131
6.2 Period of basin isolation (~11,300 – ~9,160 cal yr BP).....	133
6.3 Initial saline inflow and two way flow exchange (~9,160 – ~4,400 cal yr BP) ....	135
6.4 Late Holocene to Present (~4,400 – present day) .....	138
Chapter Seven: Conclusion.....	139
7.1 Summary .....	139
7.2 Recommendations for Future Work.....	145
Bibliography .....	147
Appendix A: Carbon and Sulphur Sediment Geochemistry .....	I
Appendix B: Gypsum Crystal Counts and Geochemistry .....	XXIX
Appendix C: Gypsum Crystals .....	XXXIII

## List of Tables

Table 1: Uncalibrated radiocarbon dates for cores MAR05-51G and MAR05-50P.....	29
Table 2: Reference materials used for instrument, element and isotope calibration . ....	40
Table 3: Parameters used to classify the abundance of gypsum grains .....	42
Table 4: Raw radiocarbon dates from core MAR05-50P .....	57
Table 5: Calibrated radiocarbon dates from cores MAR05-51G and MAR05-50P .....	61
Table 6: Calibrated dates for cores MAR02-45P and MAR02-45T .....	63
Table 7: Calibrated dates from core MAR05-13P and MAR05-04G. ....	64
Table 8: Age model used for composite core MAR05-50 .....	68
Table 9: Age model used for composite core MAR02-45 .....	69
Table 10: Age model used for composite core MAR05-13 .....	70
Table 11: Geochemistry results of post-collection gypsum crystals .....	83

## List of Figures

Figure 1: Location map of the Black Sea.....	3
Figure 2: Regional geology map.....	6
Figure 3: Simplified cross section of the Black Sea and the Bosphorus Strait.....	8
Figure 4: Surface water circulation in the Black Sea.....	10
Figure 5: Sun-illuminated image of the saline-underflow channel network.....	12
Figure 6: Comparative illustration of the Flood Hypothesis versus the Outflow Hypothesis II.....	17
Figure 7: Seismic tie between the MAR05-50P core site and the nearby first order saline density-current channel.....	22
Figure 8: Graphic core logs for cores MAR05-50P and MAR05-51G.....	24
Figure 9: Grain size analysis of core MAR05-50P.....	26
Figure 10: Location of cores MAR05-50P/MAR05-51G, MAR02-45P/MAR02-45T and MAR05-13P/MAR05-04G on the southwestern Black Sea shelf.....	37
Figure 11: Simplified diagram of an elemental analyzer.....	45
Figure 12: Simplified schematic of an isotope-ratio mass spectrometer.....	47
Figure 13: $\delta^{13}\text{C}$ ranges for various sources of organic matter.....	51
Figure 14: Plot of various suggested reservoir ages versus time.....	59
Figure 15: MAR05-50P/MAR05-51G geochemical results (TOC, $\delta^{13}\text{C}$ , TS & $\delta^{34}\text{S}$ ).....	72
Figure 16: MAR05-50P/MAR05-51G geochemical results (TOC/TS, TS/TOC, Terrestrial Fraction and Marine Fraction).....	77
Figure 17: Gypsum abundance counts in core MAR05-50P and MAR05-51G.....	80

Figure 18: Sulphur geochemistry of gypsum from MAR05-50P .....	82
Figure 19: Comparison of calibrated age models versus depth for cores MAR05-50, MAR05-13 and MAR02-45 .....	85
Figure 20: Lithological correlation of cores MAR05-50, MAR02-45 and MAR05-13 ....	87
Figure 21: Geochemical results of composite core MAR05-50 in time domain .....	102
Figure 22: Correlation between geochemistry and ostracod species abundance in composite core MAR05-50.....	109
Figure 23: Geochemistry of composite core MAR02-45 in time domain .....	111
Figure 24: Geochemistry of composite core MAR05-13 in time domain .....	114
Figure 25: Correlation of carbon elemental and isotopic values for cores MAR05-50, MAR02-45 and MAR05-13 .....	119
Figure 26: Correlation of sediment source fractions for cores MAR05-50, MAR02-45 and MAR05-13 .....	120
Figure 27: Correlation of elemental and isotopic sulphur data for cores MAR05-50, MAR02-45 and MAR05-13 .....	125
Figure 28: Correlation of TOC/TS and TS/TOC for cores MAR05-50, MAR02-45 and MAR05-13 .....	129
Figure 29: Scanning electron microscope compositional spectrum of inclusions found in a gypsum crystal .....	XXXVII

## List of Equations

Equation 1: General bacterial sulphate reduction chemical equation.....	5
Equation 2: Carbon-13 isotopic composition equation.....	32
Equation 3: Sulphur-34 isotopic composition equation.....	32
Equation 4: Equation for calculating terrigenous organic matter fraction in sediments....	50
Equation 5: Equation for calculating marine organic matter fraction in sediments.....	50

## **List of Plates**

- Plate 1: Low magnification secondary electron scanning electron microscope image of a gypsum crystal .....XXXIII
- Plate 2: Low magnification secondary electron scanning electron microscope image of a gypsum crystal showing a twinned crystal .....XXXIV
- Plate 3: Low magnification backscatter electron image of a gypsum crystal ..... XXXV
- Plate 4: High magnification image of an iron (Fe) inclusion in a gypsum crystal ...XXXVI
- Plate 5: High magnification backscatter electron image of an inclusion containing iron (Fe), magnesium (Mg) and aluminium (Al) in a gypsum crystal. .... XXXVIII

## List of Symbols, Nomenclature or Abbreviations

$\alpha$	A lowstand subaerial erosion surface combined with a shelf-crossing transgressive unconformity on the southwestern Black Sea shelf.
$\alpha_1$	A local unconformity present in the southwestern Black Sea shelf region above the $\alpha$ erosion surface.
$\alpha_2$	A local unconformity present in the southern Black Sea shelf region above both the $\alpha$ erosion surface and the $\alpha_1$ unconformity.
ka BP	Abbreviation for thousands of years before present.
$^{14}\text{C}$ yr BP	Abbreviation for uncalibrated radiocarbon years before present.
cal yr BP	Abbreviation for calibrated calendar years before present.

## **List of Appendices**

Appendix A: Carbon and Sulphur Sediment Geochemistry .....	I
Appendix B: Gypsum Crystal Counts and Geochemistry .....	XXIX
Appendix C: Gypsum Crystals .....	XXXIII

## **Chapter One: Introduction**

This thesis constitutes an important component of a larger research project in the Marmara Sea Gateway (i.e., Straits of Dardanelles and Bosphorus, and the intervening Marmara Sea) which deals with the watermass communication history of the Black Sea, Marmara Sea and the Aegean Sea associated with the climatic and oceanographic changes during the Quaternary glacial-interglacial cycles. The goal of this study is to develop a palaeo-environmental reconstruction of the southwest Black Sea shelf using the elemental and stable isotopic data collected from a long piston core and its co-located gravity core from the southwest Black Sea shelf. Below, various elements necessary for the understanding of the Black Sea germane to the thesis subject are introduced. The specific scientific objectives are given in Section 1.10.

### **1.0 Introduction**

The Black Sea is currently the largest anoxic basin on Earth. Here, anoxia occurs when vertical mixing and ventilation of the bottom waters are prevented by strong watermass stratification (e.g., Neuman, 1942; Caspers, 1957; Sorokin, 1983 as referenced in Murray et al., 1991). The dissolved oxygen is progressively consumed by oxidation and respiration of fauna, leading completely anoxic bottom waters. In such settings, the organic matter that rains through the water column is entirely preserved as high total organic carbon (TOC) muds, which become black shales when lithified. The anoxic environment allows the Black Sea to act as a prototype for Earth's earliest ocean, which was considered to be anoxic until atmospheric oxygen levels rose in the late Archean,

forming a two-layer oxic/anoxic system during the Proterozoic (Holland, 1973; Berner and Canfield, 1989). Because of its unique chemical oceanography and distinct physical geography, the Black Sea has long been used as a natural laboratory for a wide array of scientific inquiries (e.g., Glenn and Arthur, 1985; Canfield, 1989; Codispoti et al, 1991; Jørgensen et al., 2001). Results from previous studies can provide analogues for economically valuable processes (hydrocarbon and economic mineral formation), chemical processes (anaerobic respiration and redox reactions) and the effects of climate on ocean dynamics. These processes have occurred over the course of the Earth's history (with some still occurring today); consequently, the Black Sea provides unique conditions that cause it to be the target of intensive research today (Arthur and Dean, 1998; Murray et al., 2007).

### **1.1 Location**

The Black Sea is an east–west-tending elliptical basin located between latitudes 40°55' and 46°32' N and longitudes 27°27' and 41°42' E (Figure 1). It is connected to the Marmara Sea via the Bosphorus Strait; the Marmara Sea is then connected to the Aegean Sea (Mediterranean) via the Dardanelles Strait. Bulgaria, Georgia, Romania, Russia, Turkey and Ukraine all have Black Sea coastlines.

### **1.2 Organic matter**

Organic matter preserved in marine sediments can be from two main sources: degraded products of terrestrial vegetation delivered by rivers, or phytoplankton that live photosynthetically in the upper ~100 m of the water column (e.g., Deuser, 1971;

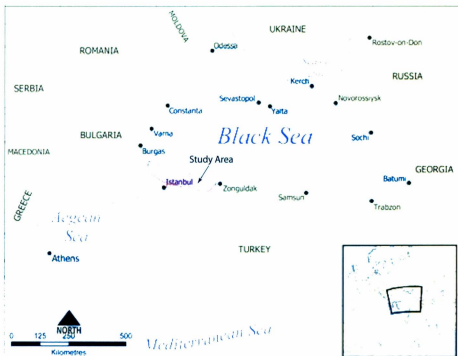


Figure 1: Location map of the Black Sea in relation to neighbouring countries, as well as other bodies of water. Inset shows map location in a global context while the study area of this research is denoted in red. Modified from Hogan and Saundry (2012).

Fontugne and Calvert, 1992). Initially, when this organic matter enters the water column, most of it (at least 80%) is consumed and respired as  $\text{CO}_2$  by zooplankton or higher trophic-level consumers living at various water depths (Deuser, 1971). However, a small fraction of this organic matter escapes these processes and settles to the bottom of the basin to become part of the sedimentary record (e.g., Deuser, 1971; Canfield, 1994; Arthur and Dean, 1998). The organic matter preserves an isotopic signature indicative of the types of vegetation (such as  $\text{C}_3$  plants, lacustrine algae, marine algae) in the area at the time of deposition, which can be used to determine sediment sources and past climates.

The amount of organic carbon preserved in marine sediments is dependent on several factors including the sedimentation rate, the concentration of dissolved oxygen in the bottom water, and decomposition by bacteria (Canfield, 1994). Organic matter may become oxidized via oxic respiration, as an electron donor during bacterial reduction of seawater sulphate, via denitrification, metal oxide reduction or methanogenesis, with the first two in this list being the most predominant (Canfield, 1991). Oxic respiration uses molecular oxygen as an electron acceptor to convert nutrients into energy in living organisms. (e.g., Abedon et al., 2008). Sulphate reduction refers to a process of respiration performed by heterotrophic microbes in anoxic conditions. Using sulphate ( $\text{SO}_4^{2-}$ ) as the electron acceptor, organic matter is oxidized by these bacteria while reducing sulphate to hydrogen sulphide ( $\text{H}_2\text{S}$ ) in order to obtain energy (Equation 1) (Berner, 1978; Leventhal, 1983). In sediments,  $\text{H}_2\text{S}$  reacts with dissolved iron to form pyrite and related sulphide minerals (Berner, 1984). In general, the overall process of bacterial sulphate reduction can be summarized as follows:



where  $CH_2O$ , representing a idealized organic matter compound, reacts with the sulphate in the water to produce hydrogen sulphide and bicarbonate (Westrich and Berner, 1984).

For the purposes of this project, the composition of organic matter will be used as a proxy for the palaeoclimatic and palaeoceanographic history of the southwestern Black Sea during the Holocene: ~11,700 cal yr BP to present (Walker et al., 2009).

### 1.3 Regional Geology

The Black Sea formed as an extensional basin in the Early Cretaceous Epoch (144–137 my BP) as a result of the subduction of the Tethys oceanic plate that began in the Middle Jurassic (180–159 my BP) (Yılmaz, 2007). Currently, the southern boundary of the Black Sea is marked by the east–west-trending Pontide Mountain belt (Figure 2). These mountains extend along northern Anatolia, creating steep coastal slopes and a relatively narrow southern shelf, only ranging from 1 to 10 km in width (Yılmaz, 2007). The bedrock of the southwestern region around the Bosphorus Strait consists of the Western Pontides Group, which is distributed across four tectonic domains: the Istranca Massif, the Istanbul-Zonguldak Zone, the Armutlu-Almacık Zone and the Sakarya continent. The former two domains are the closest to the MAR05-50P and MAR05-51G coresites on the southwestern shelf (Flood et al., 2009) which are considered in this thesis. The Istranca Massif is a metamorphic complex whose autochthonous basement succession encompasses a suite of high-grade metamorphic rocks including gneisses,

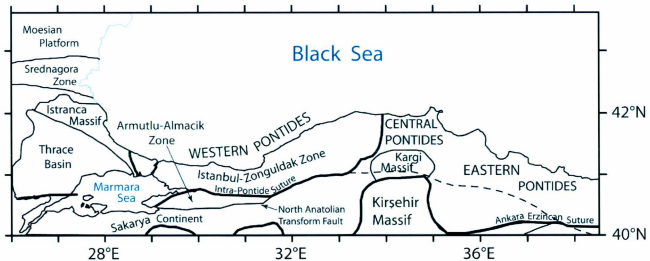


Figure 2: Regional geology map showing the main tectonic zones and features of the southern Black Sea. The Western Pontides Group is closest to the study area for this thesis, and includes the rocks in four tectonic domains: the Istranca Massif, the Istanbul-Zonguldak Zone, the Armutlu-Almacik Zone and the Sakarya continent. Modified from Yılmaz et al. (1997).

schists, migmatic granite and amphibolites, cut by granitic dykes (Yılmaz et al., 1997). It is overlain by a northerly transported allochthon consisting of phyllites, slates and recrystallized limestones. The Istanbul-Zonguldak domain is also a high-grade metamorphic complex and includes metagabbro, metadiabase, dolerite dykes, migmatitic gneiss, schist and intrusive granite in its basement. These rocks are overlain by a Lower Paleozoic sedimentary sequence, which includes red arkosic conglomerate, sandstone, mudstone, quartzites, siltstones, graywackes and chamositic shales (Yılmaz et al., 1997).

## **1.4 Physical Oceanography**

### *1.4.1 Black Sea Oceanography*

The watermass exchange between the Black Sea and the Mediterranean is characterized by a distinct two-layer flow across the straits of Bosphorus and Dardanelles (Figure 3). The low salinity (17–20‰), seasonally cooler (5–15°C) surface waters of the Black Sea flow out the Strait of Bosphorus atop the warmer (15–20°C), more saline (38–39‰) Mediterranean watermass moving northeast from the Aegean Sea. The surface watermass travels southwest from the Black Sea to the Aegean Sea with an average velocity of 10–30 cm/s. The bottom waters originating in the eastern Aegean Sea penetrate into the Marmara Sea through the Strait of Dardanelles and flow northeast forming the bottom watermass in the Marmara Sea. This watermass penetrates into the Strait of Bosphorus and flows north with velocities of 5–15 cm/s (Latif et al., 1991).

Strong stratification of the water column contributes to bottom-water anoxia and hydrogen sulphide (H<sub>2</sub>S) enrichment in the central Black Sea below water depths of

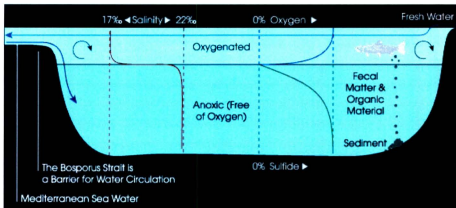


Figure 3: Simplified cross section of the Black Sea and the Bosphorus Strait (left side) showing the boundary between the two water-masses. The low salinity, oxygenated Black Sea watermass forms a layer that sits atop higher salinity, anoxic bottom waters. Dissolved oxygen decreases to zero towards the chemocline, whereas hydrogen sulphide content increases with depth from the same boundary. In reality, the oxic/anoxic interface is not horizontal, but varies from ~110–130 m depth in the central western Black Sea to ~150–170 m depth at the basin margins near shelf edge (Jorgensen et al., 1991). Modified from the Goddard Earth Sciences Data and Information Service Center, 2012.

~100 m. The surface layer (0 to ~50 m) is well oxygenated, but dissolved oxygen decreases slowly with depth. There is a suboxic zone located at the oxic/anoxic boundary from approximately 50–100 m depth, marked by low dissolved oxygen and the first appearance of H<sub>2</sub>S. The thickness of the suboxic zone varies based on location, climate and time (Murray et al., 1989; Codispoti et al, 1991; Jørgensen et al., 1991). The concentrations of O<sub>2</sub> and H<sub>2</sub>S in this layer do not overlap, rather O<sub>2</sub> drops to zero and H<sub>2</sub>S then rises from zero in this transitional zone (İzdar and Murray, 1991; Murray, 1991).

Although significant saline water enters the Black Sea from the Mediterranean via the Strait of Bosphorus, there is a net export of approximately 300 km<sup>3</sup>/yr because freshwater input from several large rivers (the Danube, Don, Dnieper, Dniester and Southern Bug) and precipitation exceed the saline inflow and rate of evaporation. Surface circulation in the Black Sea is dominated by two large cyclonic gyres, as well as several smaller anti-cyclonic coastal eddies. A narrow “Rim Current” circulates along the periphery of the deep basal area in a counter-clockwise direction, separating a set of coastal eddies from the large centrally located gyres (Figure 4) (Latif et al., 1991; Oğuz et al., 1993; Murray et al., 2007). The Rim Current is <75 km in width, and travels at an average velocity of 20 cm/s (Oğuz et al., 1993).

There is a permanent halocline and pycnocline in place due to the vertical stratification in the Black Sea. This boundary has varied over the evolution of the sea: it also varies geographically in the present-day Black Sea ranging from ~75 m in the centre to up to ~210 m along the margin of the basin (Murray et al., 1991). The location of the salinity-density boundary is coincident with the chemocline in the modern Black Sea

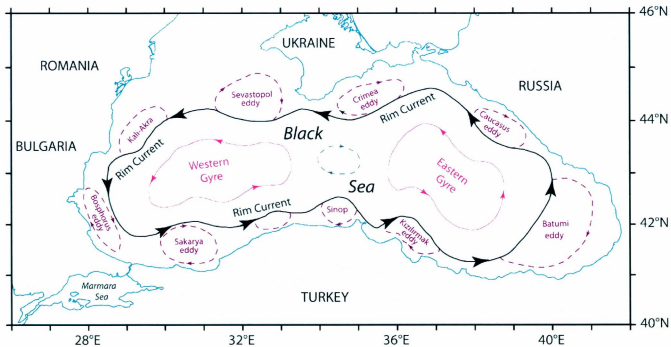


Figure 4: Surface water circulation in the Black Sea showing the cyclonic Rim Current, Western Gyre and Eastern Gyre, as well as several of the smaller anticyclonic eddies (from Oğuz et al., 1993).

(Figure 3), which is now between 110–130 m depth in the centre, and 150–170 m depth away from the basin margins (Jørgensen et al., 1991). Below this boundary the bottom waters are anoxic and above the boundary the water is more oxygenated and supports life (Codispoti et al., 1991). Due to hydrostatic pressure gradients caused by the Rim Current, the oxic-anoxic contact has an overall dome-like shape throughout the Black Sea, resulting in a deeper interface at the shelf edge than in the central regions (Oğuz et al., 1994).

#### *1.4.2 Anastomosed Channel Network*

A saline density current may occur when dense normal marine water enters an area where the ambient water mass is less dense because of a lower salinity. Due to the salinity difference in the two-way flow system at the northern Bosphorus exit (salinity contrast of approximately 12‰ to 16‰), there is a persistent saline underflow that has created a shelf-crossing network of anastomosed channels (Di Iorio et al., 1998; Özsoy et al., 2001). The network consists of first-order channels, in-channel barforms, sediment waves, crevasse channels, levee/overbank deposits and is morphologically similar to that of a terrigenous anastomosed river system (Figure 5) (Flood et al., 2009).

A main saline-underflow channel extends from the mouth of the Bosphorus Strait, meandering northwards over 50 km until it reaches the shelf break. Flood et al (2009), in an overview of the channel system, divide the channel into four general sections: an inner-shelf channel, a mid-shelf region of poorly confined flow, an outer-shelf channel network and an upper-slope channel. The inner shelf channel begins at the mouth of the Bosphorus and continues about 18 km into the Black Sea. Here, the bankfull depth of the

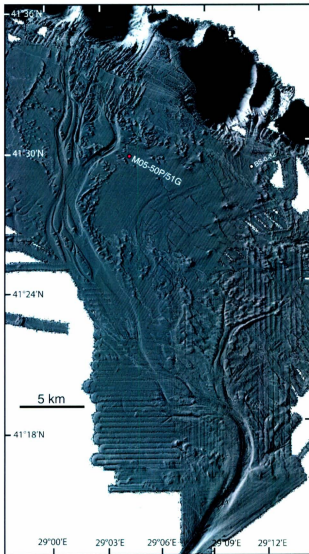


Figure 5: Sun-illuminated image of the saline-underflow channel network created where dense saline Mediterranean water enters the Black Sea through the Bosphorus Strait (bottom of image). The outer-shelf network lies north of 41°24'N (Modified from Flood et al., 2009).

main channel ranges from ~10–35 m and there are several smaller distributaries that branch off. The mid-shelf channel is broad and extends from 18–26 km along the flow path. It is characterized by an irregular floor, little or no levées and includes an exposed basement bedrock ridge that disrupts the general channel flow in this area.

The outer-shelf channel extends from 26–43 km along the centreline of the main channel, and consists of an anastomosed channel network. The levées in this area are mounded and dimpled by partially buried conical mounds; streamlined bars (up to 5 km by 2.5 km) separate anastomosed channels. Channel size ranges from 5–8 m in depth and from ~200 m to 1.3 km in width. The sediments of the banks and intra-channel bars are silty muds radiocarbon dated at younger than ~8,000 uncalibrated radiocarbon years before present (hereafter reported with the units  $^{14}\text{C}$  yr BP) (Flood et al., 2009). The channel floors consist of coarser sand and gravel with some shelly horizons, and are generally at the level of the shelf-crossing early Holocene transgressive unconformity  $\alpha$ . As the channel network continues toward the shelf edge, the number of channel divisions increases and the tops of the bars begin to be dissected by secondary channels. It has been hypothesized that the Rim Current, which is running parallel to the shelf edge, could be suspending the finer sediments in this area, carrying them across the shelf, thus providing the materials to build the levées of the channel (Flood et al., 2009; R.N. Hiscott, pers. comm. 2012). The MAR05-50P and MAR05-51G core sites studied in this thesis are in the eastern levée of the main outer-shelf channel (Flood et al., 2009).

The upper-slope channel extends from 43–51 km along the channel centreline and is marked by complex morphology and increasing channel slope gradients. The channel

ends at about 51 km along the flow path in water depths of ~300 m. It is considered that the density contrast between the Mediterranean inflow and the overlying Black Sea waters has decreased by that point so that there is insufficient contrast to drive the saline underflow, allowing those waters to lift off the seabed as a mid-water plume (Flood et al., 2009). Modern observations of pristine sediment waves and young crevasse channels and young radiocarbon dates from bar top cores (Flood et al., 2009) indicate that channel processes are active today.

## **1.5 Reconnection Hypotheses**

Due to the Black Sea's interesting geology and oceanography, geologists have been researching for the past seven decades the evolution of the sea at various stages of its reconnection with the world's ocean following the last glacial cycle. During the last glacial maximum (~20,000 yr BP) the Black Sea was disconnected from the global oceans. This was due to relative sea level being lower than the shallow sill depth of the Strait of Bosphorus (~40 m); the only connection to the Mediterranean. The process by which the Black Sea became reconnected, however, is under intense debate. Currently, there are three reconnection hypotheses: the *Flood Hypothesis*, the *Outflow Hypothesis* and the *Oscillating Sea Level Hypothesis*.

### *1.5.1 Flood Hypothesis*

The *Flood Hypothesis* was initially proposed by Ryan et al. (1997a/b) and Ryan and Pittman (1998) as a part of a joint US-Russia-Turkey research collaboration, and hypothesizes a catastrophic reconnection of the Black Sea with the world's oceans. The

authors challenged the widely accepted hypothesis that there was a gradual post-glacial inflow of saline Mediterranean water entering a full Black Sea “lake”, commencing around 9,000 <sup>14</sup>C yr BP (e.g., Ross et al., 1970, Degens and Ross, 1972, Deuser, 1972). The authors instead propose that from 14,700 to 10,000 <sup>14</sup>C yr BP, the Neoeuxinian lake (now the Black Sea) was partially emptied due to evaporation and reduced river input, with the lake level standing at -140 m, ~100 m below the Bosphorus sill depth. Then, rising global sea level ruptured a hypothetical sediment dam in the Bosphorus at 7,150 <sup>14</sup>C yr BP, resulting in a catastrophic flooding of the continental shelf. The authors argued that the flood caused the simultaneous and sudden appearance of marine organisms in the Black Sea, caused a decrease in sedimentation rate and produced ubiquitous organic-rich sediments. Ryan and co-workers estimated that the exposed shelf was over 100,000 km<sup>2</sup> in area and due to the geometry of the Bosphorus inlet, it was possible that an excess of 50 km<sup>3</sup> of Mediterranean water invaded the Black Sea lake once the sill was breached. They proposed that the lake level rose at a rate of approximately 15 centimetres per day, rising over 100 meters in a matter of two years. This flooding submerged over 100,000 km<sup>2</sup> of the previously exposed shelf, abruptly forcing early human inhabitants inland (Ryan et al., 1997a; Ryan et al., 1997b). Ryan and Pitman (1998) further suggested that this flood might be the basis of the ancient flood myths (e.g., found in the Epic of Gilgamesh, the Epic of Atrahasis, and the Epic of Ziusudra [Keller, 1981; Lambert and Millard, 1969; Best, 1999]), including the biblical account of “Noah’s Flood”. The evidence for the 1997/1998 proposal of the *Flood Hypothesis* was mainly radiocarbon ages of the oldest marine shells (7,150 <sup>14</sup>C yr BP)

found in marine sediment cores from the northern Black Sea shelf, as well as about 350 km of high-resolution seismic profiles (Ryan et al., 1997a; Ryan et al., 1997b).

Major (2002) and Ryan et al. (2003) modified the date of the flooding to 8,400 <sup>14</sup>C yr BP based on a sudden shift in the strontium isotope ratio in biogenic carbonate at that time. They then attributed the younger 7,150 <sup>14</sup>C yr BP shell date to a salinization time lag. Ryan et al. (2003) also proposed a second older high water level (due to river inflow) at 11,000 to 10,000 <sup>14</sup>C yr BP that resulted in export of water into the Marmara and Mediterranean seas. As a result, according to the *Flood Hypothesis*, the Black Sea experienced two lowstand periods (-120 m at 13,400 <sup>14</sup>C yr BP through to 11,000 <sup>14</sup>C yr BP and -95 m from 10,000 to 8,400 <sup>14</sup>C yr BP) that preceded the two flooding events. It should be noted that the younger flood at 8,400 <sup>14</sup>C yr BP is referred to as the “Great Flood”, which is still considered by some researchers to be associated with biblical accounts.

### *1.5.2 Outflow Hypothesis*

Multi-proxy data from Memorial University of Newfoundland researchers (among other institutions) conflicts with the *Flood Hypothesis*. Instead, Aksu et al. (2002a) initially proposed the *Outflow Hypothesis I*, which suggested a gradual reconnection of the Black Sea and the eastern Mediterranean over thousands of years, accompanied by significant time lags, rather than one catastrophic event (Figure 6). This hypothesis was based on work completed in the Aegean Sea, Marmara Sea and Black Sea area (Aksu et al., 1999b; Aksu et al., 2002b; Hiscott et al., 2002), as explained below.

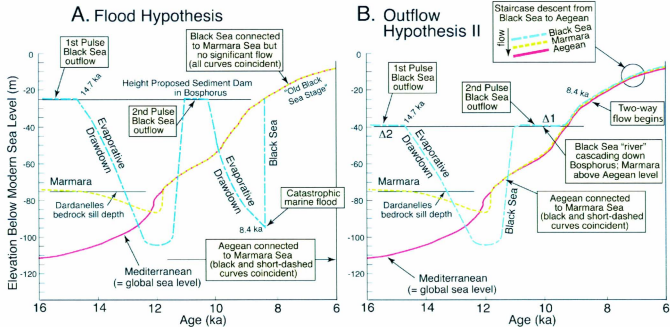


Figure 6: Comparative illustration of the Flood Hypothesis (A) versus the Outflow Hypothesis II (B). The Flood Hypothesis shows the potential flooding time of  $\sim 8.4$   $^{14}\text{C}$  ka BP from Major et al. (2002) and Ryan et al. (2003). The Outflow Hypothesis II is based on Hiscott et al. (2007a, b). Lines show the elevation below modern sea level for the Black Sea (turquoise), the Marmara Sea (fuchsia) and the Aegean Sea (green) as suggested by each hypothesis. Modified from Hiscott et al. (2007a, b).

The *Outflow Hypothesis I* stated that the Black Sea rose to the level of the Bosphorus sill (-40 m) at approximately 11,000 to 10,000  $^{14}\text{C}$  yr BP. At this point, the Marmara Sea level was approximately 20 m below the sill depth, cut off from the Black Sea but connected to the Aegean Sea since approximately 12,000  $^{14}\text{C}$  yr BP through the deeper Dardanelles Strait (Çatağay et al., 2000). Brackish waters from the Black Sea began to flow south through the Bosphorus, forming a delta ( $\Delta 1$ ) in the Marmara Sea. This outflow was propelled by the drainage of the major eastern European rivers and left an imprint in the microfossil assemblage as well as the geochemistry of Marmara Sea sediments. The one-way outflow continued until approximately 9,000  $^{14}\text{C}$  yr BP, when the level of the Marmara Sea reached the Bosphorus sill depth. From here, it was hypothesized that over the course of 500 to 1,000  $^{14}\text{C}$  yr, the denser, saline Mediterranean waters intruded into the Bosphorus Strait and eventually into the Black Sea, establishing the current two-way flow exchange, likely by 8,000  $^{14}\text{C}$  yr BP. The *Outflow Hypothesis I* proposed that the pycnocline gradually rose with the inflow of saline waters, and by 7,500  $^{14}\text{C}$  yr BP (in accordance with the arrival of the first Mediterranean immigrants), the salinity on the shelf rose to a level suitable for colonization by marine species (Aksu et al., 2002a).

After the proposal of the two outflow events at 16,000 to 14,700  $^{14}\text{C}$  yr BP and 11,000 to 10,000  $^{14}\text{C}$  yr BP by Ryan et al. (2003), a modified *Outflow Hypothesis II* was proposed by Hiscott et al. (2007a, b) that included both of these events. Hiscott et al. (2002) noted an older delta ( $\Delta 2$ ) in the north-eastern Marmara Sea below  $\Delta 1$ . The

16,000–14,700  $^{14}\text{C}$  yr BP outflow was offered as an explanation for the formation of  $\Delta 2$ , although Hiscott et al. (2007a) had no age control for  $\Delta 2$ .

Eriş et al. (2007) have claimed that  $\Delta 1$  and  $\Delta 2$  have ages of 3,800 – 6,200  $^{14}\text{C}$  yr BP and 10,500 – 11,500  $^{14}\text{C}$  yr BP, respectively, seriously compromising a component of the *Outflow Hypothesis II*. However, multibeam and seismic surveys conducted by Memorial University of Newfoundland researchers in 2011 suggest that Eriş et al. (2007) miscorrelated their giant piston core MD-2750 to the seismic stratigraphy, so that these younger ages might be invalid (R.N. Hiscott, personal communication, 2012).

### *1.5.3 Oscillating Sea Level Hypothesis*

A third hypothesis for the reconnection of the Black Sea with the world's ocean in the Holocene is the *Oscillating Sea Level Hypothesis*, based initially on the conclusions of Kerey et al. (2004) and Yanko-Hombach et al. (2004). They suggest that the increase in sea level in the Black Sea was neither catastrophic nor gradual. Instead, they suggest that it rose to present-day levels in an oscillating manner. This hypothesis is based on extensive multi-proxy data collected by the former Union of Soviet Socialist Republics and former eastern bloc scientists throughout the Black Sea since 1971. The timeline for this hypothesis begins at 27,000  $^{14}\text{C}$  yr BP during the Würm (Middle Weichselian) glaciation within the Last Glacial Period (Yanko-Hombach, 2007). Up until this time, the authors state that brackish Tarkhankutian Basin (coincident with the modern Black Sea) was connected to the Marmara Sea via the Bosphorus Strait, based on palynological evidence found within the strait. Then, the connection was interrupted due to drop in sea

levels and drought conditions brought on by the Last Glacial Maximum (~27,000 – 18,000 <sup>14</sup>C yr BP). This resulted in a drop of ~100 m in water level, transforming the Tarkhankutian basin into the completely isolated Early Neoeuxinian lake. At ~17,000 <sup>14</sup>C yr BP, the climate began to warm which caused water from most likely the Caspian Sea to enter the Late Neoeuxinian lake via the Manych Spillway, raising the water level to approximately –20 m. This also produced a small overflow effect, releasing brackish water into the Marmara Sea and eventually into the Aegean Sea. The Younger Dryas (~11,000–10,000 <sup>14</sup>C yr BP) brought on cooler climates, reducing the water level to about –50 m. The level rose again to –20 m due to inflowing dense, saline Mediterranean waters, and by 10,000 <sup>14</sup>C yr BP, according to this hypothesis, the surface never fell below –40 m again. However, the authors propose that these waters entered the Black Sea via an alternative route, such as Izmit Bay to Sapanca Lake to the Sakarya River since there is a lack of evidence of marine organisms in the Bosphorus Strait prior to 5,300 <sup>14</sup>C yr BP (Kerey et al., 2004; Yanko-Hombach et al., 2004). Based on this route and the sea level of the Mediterranean at 10,000 <sup>14</sup>C yr BP, saline waters began to enter the Black Sea in an oscillatory manner. The oscillatory reconnection is suggested to have raised the water level at a rate of, on average, 3 cm/100 yr, which could not be deemed catastrophic. Likewise, due to the oscillatory exchange, the outflow from the Black Sea would be periodically broken after 10,000 <sup>14</sup>C yr BP, which is in contrast to the *Outflow Hypothesis II* (Yanko-Hombach, 2007).

## 1.6 Previous Work

### 1.6.1 Channel Network Mapping

Cores MAR05-50P and MAR05-51G studied in this thesis were taken due to their close proximity to the anastomosed channel network northwest of the mouth of the Bosphorus Strait (Özsoy et al, 2001, Flood et al., 2009). The evolution and morphology of this channel system are discussed by Flood et al. (2009). A sun-illuminated image (Figure 5) and seismic profile (Figure 7) show the proximity of the cores to the channel network. As well, both the early Holocene transgressive unconformity  $\alpha$  and the  $\alpha_1$  unconformity can be seen relative to the core site MAR05-50P in cross-section (Figure 7). Flood et al. (2009) attribute the  $\alpha_1$  unconformity to subaqueous erosion beneath wind-driven currents and this boundary can be seen throughout the southwestern shelf region.

### 1.6.2 Core Descriptions

Cores MAR05-51G and MAR05-50P were described by Dr. Ali Aksu on November 9<sup>th</sup>, 2005, at Memorial University. Standard lithological and palaeontological notations were made as well as sediment colour using the Geological Society of America Rock-Colour chart. Grain size for core MAR05-50P was determined by Dr. Richard Hiscott using a Horiba® model LA-950 laser particle-size analyzer, which can detect particles within the range 0.01  $\mu\text{m}$  to 3000  $\mu\text{m}$ .

#### 1.6.2.1 MAR05-51G

As described by Dr. Aksu in 2005, gravity core MAR05-51G is composed of mainly silty mud. The core is divided into two lithostratigraphic units, Unit 1 and Unit 2

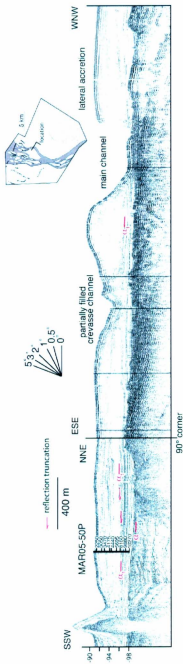


Figure 7: Seismic tie between the MAR05-50P core site and the nearby first order saline density-current channel. Water depth at the core site is  $-91$  m (shown on sidebar) and the depth of the main channel is approximately  $8.5$  m from levee crest to floor. Regional unconformities  $\alpha$  and  $\alpha_1$  are visible in the profile, however only the  $\alpha_1$  unconformity is penetrated by MAR05-50P. Modified from Flood et al. (2009).

on the basis of sediment texture. Unit 1 extends from the top of the core to about 58 cm. It is characterized by colour banded and colour mottled silty-mud. The colour alternates between dark gray (N3) and olive gray (5Y4/1). The texture shows moderate bioturbation, specifically large concentric burrows. Isolated shells are present throughout the unit. Unit 2 extends from 58 cm to the bottom of the core. This unit is predominately olive gray (5Y4/1) slightly colour mottled silty-mud. There are two shelly horizons at depths of 90 cm and 107 cm. Similar to Unit 1, Unit 2 shows moderate bioturbation with isolated shells throughout (Figure 8). At 145 cm depth, an *in-situ* *Mytilus galloprovincialis* mollusc shell was radiocarbon dated to 3105 ± 90 calibrated calendar years before present (hereafter reported with the units cal yr BP) (Table 1).

#### 1.6.2.2 MAR05-50P

The upper part of piston core MAR05-50P is similar to core MAR05-51G and is composed mostly of silty mud. Three lithostratigraphic units are identified in this core: Units 1, 2 and 3, as described below.

Unit 1 extends from 0 cm to approximately 45 cm depth, and exhibits colour banded and colour mottled layers. There are some burrows as well as a small number of shells within this unit, including *Parvicardium exiguum*. Unit 2 extends from about 45 cm to 645 cm depth. It is olive gray (5Y4/1) in colour, slightly colour mottled and shows moderate bioturbation, isolated shells, as well as four shelly horizons (Figure 8). Notable shells include *Mytilus galloprovincialis*, *Spisula subtruncata*, *Abra alba* and *Cyclope donovania*. Both Units 1 and 2 have a mean grain size of ~6.5 $\phi$  (Flood et al., 2009), with

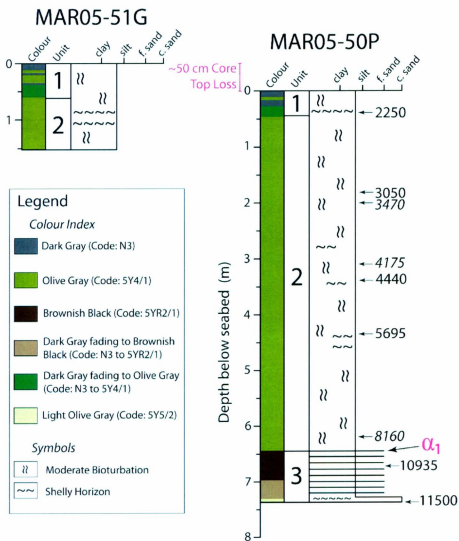


Figure 8: Graphic core logs for piston core MAR05-50P and gravity core MAR05-51G showing grain size, lithological units, sediment colour and textures. Ages shown are in calibrated calendar years before present, and previously unpublished dates are italicized. Modified from Flood et al. (2009).

all standard deviations falling within the silt classification limits. The sand fraction for both units is generally less than 10% (Figure 9).

At 645 cm depth in core MAR05-50P, there is an inferred unconformity that is marked by an abrupt change in colour, mean grain size, sand fraction and texture (Figures 8 and 9). This unconformity is correlated with the  $\alpha_1$  marker of Hiscott et al. (2007b) based on its similar  $^{14}\text{C}$  age and lithology seen above and below the boundary, as well as attributes of the corresponding seismic units which are separated by a truncation surface at the MAR05-50P core site (Figure 7; Flood et al., 2009). Unit 3 extends from the  $\alpha_1$  unconformity to the bottom of the core at 738 cm depth. From 645 cm to 698 cm depth, the core shows slightly coloured mottled brownish black (5YR2/1) burrowed muds with frequent fine sand and silt laminae. From 698 cm to 734 cm depth, the colour passes from dark grey (N3) to brownish black (5YR2/1), but the sediment maintains the same grain size and texture. Finally, at the base of the core from 734–738 cm, there is a spike in the mean grain size. This is due to the presence of light olive gray (5Y5/2) gravelly sandy mud with shells. The shells are rounded and reworked – most are large juvenile *Dreissena polymorpha*, with the largest shell dimension being ~0.7 cm. The sand fraction also increases to approximately 40% at the base of the core within this 4 cm interval. Due to the intermittent fine sand laminae seen in Unit 3, the mean grain size rises to ~5.5 $\phi$  (Figure 9).

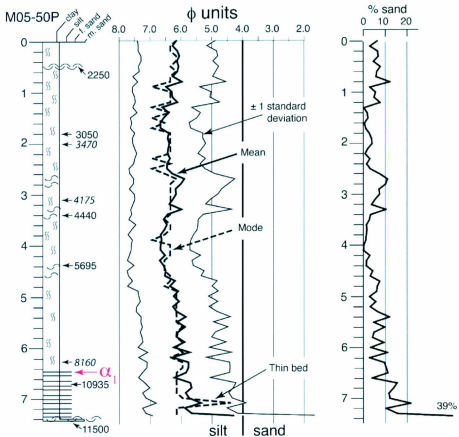


Figure 9: Grain size analysis for 75 samples from core MAR05-50P. Data were collected with a Horiba® model LA-950 laser particle-size analyzer. Radiocarbon dates shown adjacent to the lithological log are given in calibrated calendar years before present and previously unpublished dates are italicized. Modified from Flood et al. (2009).

### *1.6.3 Radiocarbon Dating*

Radiocarbon dating uses the steady decay of  $^{14}\text{C}$  to date materials that are of late Pleistocene to Holocene age. The production of the radioactive isotope  $^{14}\text{C}$  occurs naturally as a secondary effect of the cosmic-ray bombardment of the upper atmosphere. The radiogenic isotope quickly oxidizes (on the order of hours to days) to form  $^{14}\text{CO}_2$ . Stratospheric winds then distribute these molecules throughout the atmosphere, resulting in a relatively well-mixed distribution of  $^{14}\text{CO}_2$  at the Earth's surface. The world's oceans absorb approximately 85% of these molecules, while only 1% is absorbed by terrestrial material, primarily through photosynthetic processes. As a result, the  $^{14}\text{C}$  ratio of living organisms is the same as the  $^{14}\text{C}$  ratio in the atmosphere at the time of absorption. This content is maintained in equilibrium with the atmosphere through metabolic processes until the living organism dies. Given that  $^{14}\text{C}$  decays at a steady rate (half-life =  $5730 \pm 40$  years), the age of biomineralization by the dead organism can be calculated (Taylor and Aitken, 1997).

Radiocarbon dates are reported in years before present (yr BP), where "present" is 1950 by international convention. During the 1955–1963 Common Era, the detonation of nuclear and thermonuclear bombs created an artificial and dramatic increase in  $^{14}\text{C}$  in the atmosphere. As a result, dates after 1950 generally are not available using the radiocarbon dating technique. Dates taken directly from the samples are considered raw or uncalibrated, as they do not account for the variation of the levels of atmospheric  $^{14}\text{C}$  over the course of geologic time. However, the raw dates can be calibrated using the results of dendrochronology and computer software such as OxCal or Calib, to produce calibrated

years before present (cal yr BP). This calibration process uses dendrochronology to align raw radiocarbon ages with known, constant solar ages obtained by counting tree rings (Taylor and Aitken, 1997), or by using other absolute dates to calibrate the raw results. This calibration method is further explained in Chapter 2.

Previously dated material from cores MAR05-50P and MAR05-51G has been published in the Flood et al. (2009) (Table 1). These samples were sent to the IsoTrace Radiocarbon Laboratory, Accelerator Mass Spectrometry Facility at the University of Toronto in Ontario, Canada. They were processed in an accelerator mass spectrometer using a conventional analytical  $^{14}\text{C}$  half-life of 5,568 years, and the errors represent 68.3% confidence limits. The raw dates as well as the calibrated dates for these samples, and the new, previously unpublished dates, are further discussed in Chapter 3.

#### *1.6.4 Related Cores*

On the southwestern shelf of the Black Sea, previous Memorial University of Newfoundland projects have provided some insight into the history of organic-matter deposition in Holocene muds. Using short cores slightly northwest of the MAR05-50P site on the Black Sea shelf (the closest at 41°42'N, 28°43'E), Adetona (2005) found that in the shallow sediments, the signatures of the organic material are consistent with the mixing of isotopically heavier marine matter (~ -23‰) with lighter terrestrial matter (~ -27‰), with ~50% of the organic matter being of marine origin (e.g., algal). In the deeper sediments, the organic matter was predominantly (~80%) from terrestrial and/or lacustrine sources. Cranshaw (2007) also found that the organic component of the deeper

Table 1: Uncalibrated radiocarbon dates ( $^{14}\text{C}$  yr BP) for cores MAR05-51G and MAR05-50P, as published in Flood et al., 2009.

Core	Depth	Dated Material	$^{14}\text{C}$ date	$\sigma$	Lab ID
MAR05-51G	145	<i>Mytilus galloprovincialis</i>	3280	$\pm 60$	TO-13101
MAR05-50P	44	<i>Mytilus galloprovincialis</i>	2590	$\pm 90$	TO-13095
MAR05-50P	180	<i>Mytilus galloprovincialis</i>	3240	$\pm 50$	TO-13096
MAR05-50P	279	<i>Mytilus galloprovincialis</i>	3250	$\pm 70$	TO-13097
MAR05-50P	340	<i>Mytilus galloprovincialis</i>	4320	$\pm 60$	TO-13098
MAR05-50P	435	<i>Mytilus galloprovincialis</i>	5330	$\pm 70$	TO-13099
MAR05-50P	670	<i>Dreissena polymorpha</i>	9880	$\pm 110$	TO-13100
MAR05-50P	737	<i>Dreissena</i> spp.- <b>pristine</b>	10270	$\pm 90$	TO-12915
MAR05-50P	737	Bivalve fragments- <b>worn</b>	32190	$\pm 280$	TO-12734

sediments was mostly terrestrial and/or lacustrine in origin (82–100%) on the southwestern Black Sea Shelf, using a core located at 41°09.987'N, 31°07.686'E.

The proposed research will augment this database with new work closer to the Bosphorus exit into the Black Sea, and will synthesize these new results with past data to extract general conclusions regarding deposition of organic matter in this unique environment.

#### *1.6.4.1 MAR02-45P and MAR02-45T*

Piston core MAR02-45P and its co-located trigger-weight core MAR02-45T were collected from the transgressive succession on the southwestern Black Sea shelf during the 2002 RV *Koca Piri Reis* research cruise. Both cores were raised from 69 m water depth at 41°41.170'N, 28°19.080'E, which is approximately 66 km west-northwest of the MAR05-50P/MAR05-51G core site. MAR02-45T is 180 cm in length and MAR02-45P 836 cm in length. It was determined using radiocarbon dates that there is approximately 110 cm missing section from the top of the piston core (Hiscott et al., 2007b). Consequently, a composite core of 946 cm total length was created, which is conformable at the  $\alpha_1$  level, is unconformable at the  $\alpha_2$  level, and spans most of the Holocene (up to 10,350 cal yr BP). This composite core is referred to as MAR02-45. Sedimentological, geochemical, palynological and palaeontological analyses were completed on the core and published in Hiscott et al. (2007b), Marrett et al. (2009) and Mertens et al. (2012). These data will be used for correlation purposes in Chapter 5.

#### *1.6.4.2 MAR05-13P and MAR05-04G*

During the 2005 RV *Koca Piri Reis* research cruise, gravity core MAR05-04G and piston core MAR05-13P were collected at 41°09.947'N, 31°07.715'E and 41°09.987'N, 31°07.686'E, respectively at a water depth of 75 meters. These core sites are located approximately 175 km east-southeast of the MAR05-50P core site, east of the mouth of the Strait of Bosphorus. Core MAR05-04G is 171 cm in length and core MAR05-13P is 813 cm in length. The lithological descriptions of each can be found in Cranshaw (2007). There is approximately 30 cm of core-top loss in MAR05-13P. As a result, a composite core was created with MAR05-04G. The composite core will be referred to as MAR05-13 and will be used in Chapter 5 for correlation purposes with MAR05-50. Ages at the base of the composite core extend to the late Holocene (11,236 cal yr BP). Geochemical data, some palynological results, as well as seismic profiles for cores MAR05-04G and MAR05-13P have been previously presented in Cranshaw (2007) and published in Mertens et al. (2012).

### **1.7 Carbon Isotopes and Total Organic Carbon (TOC)**

Carbon, atomic number 6, has two stable isotopes:  $^{12}\text{C}$  = 98.89 percent abundance and  $^{13}\text{C}$  = 1.11 percent abundance. Carbon has one radioactive isotope,  $^{14}\text{C}$ , which is often used for dating material due to its presence in organic material, as well as its half-life of  $5730 \pm 40$  years. Natural processing of carbon such as atmospheric cycling, mineralization and photosynthesis all have their own distinct isotopic carbon ( $\delta^{13}\text{C}$ ) signature. Generally, biogenic processes tend to result in an enrichment of the light isotope,  $^{12}\text{C}$ , whereas isotope exchange reactions between carbon dioxide and carbonate

minerals result in the enrichment of the heavier isotope,  $^{13}\text{C}$ . The carbon isotopic composition is expressed in delta notation; that is, the ratio of  $^{13}\text{C}$  to  $^{12}\text{C}$ . By convention, this ratio is presented as in Equation 1 (Faure, 1977):

$$\delta^{13}\text{C} = \left[ \frac{(^{13}\text{C}/^{12}\text{C})_{\text{sample}} - (^{13}\text{C}/^{12}\text{C})_{\text{standard}}}{(^{13}\text{C}/^{12}\text{C})_{\text{standard}}} \right] \times 1000\text{‰} \quad (2)$$

where standard refers to the international reference standard Vienna PeeDee Belemnite (VPDB).

Total organic carbon (TOC) refers to the amount of carbon bound in an organic compound of biological origin. TOC is useful in delineating the sediment source, whether marine or terrestrial, determined using the  $\delta^{13}\text{C}_{\text{TOC}}$  and the equations of Fontugne and Calvert, 1992; elaborated in Section 2.5). It is also useful for determining the local sedimentation rate (as rapid burial can enhance organic matter preservation), as well it is an indicator of anoxia, drinking water quality and petroleum source-rock quality (Waples, 1985).

### 1.8 Sulphur Isotopes and Total Sulphur (TS)

Sulphur, atomic number 16, has four stable isotopes, with the following abundances:  $^{32}\text{S} = 95.02\%$ ,  $^{33}\text{S} = 0.75\%$ ,  $^{34}\text{S} = 4.21\%$  and  $^{36}\text{S} = 0.02\%$ . With respect to isotopic abundances, ratios are determined using the light  $^{32}\text{S}$  isotope and the heavier  $^{34}\text{S}$ , expressed in terms of  $\delta^{34}\text{S}$  (Faure, 1977):

$$\delta^{34}\text{S} = \left[ \frac{(^{34}\text{S}/^{32}\text{S})_{\text{sample}} - (^{34}\text{S}/^{32}\text{S})_{\text{standard}}}{(^{34}\text{S}/^{32}\text{S})_{\text{standard}}} \right] \times 1000\text{‰} \quad (3)$$

where standard refers to the international reference standard Canyon Diablo troilite (FeS) meteorite.

Variations in the isotopic ratio of sulphur can be due to several environmental factors. One such process is known as biogenic fractionation, which refers to the reduction of sulphate ions by anaerobic bacteria that live in buried marine or lake sediments. Through anaerobic respiration, bacteria remove the oxygen from sulphate ions ( $\text{SO}_4^{2-}$ ) in organic matter and excrete hydrogen sulphide ( $\text{H}_2\text{S}$ ). This product is enriched in the lighter  $^{32}\text{S}$  isotope, which can be used as an indicator of this process. The hydrogen sulphide produced in these reactions often goes on to react with iron found in the sediments to produce the mineral pyrite ( $\text{FeS}_2$ ). Total sulphur (TS) can also serve as a proxy for the amount of pyrite in marine sediments, which can be used as a reflection of the quantity of sulphate reduction occurring in the sediments (Faure, 1977).

## **1.9 Rationale**

Since the amount of organic matter found in sediments is regulated by sea level, salinity, depositional environment, dissolved oxygen content, and the vigour of primary production relative to input from terrestrial sources, the study of preserved organic matter in a marine core can yield valuable information regarding the local environmental conditions. Such information can then be used in conjunction with other published data to interpret conditions during the Holocene reconnection of the Black Sea with the world's oceans.

### **1.10 Research Questions**

The specific scientific objectives of this thesis are:

- to correlate the lithologies in cores MAR05-50P/MAR05-51G and to create a final composite core MAR05-50 using the organic geochemical multiproxy data and radiocarbon ages in selected shell samples;
- to erect a chronostratigraphic framework for cores MAR05-50P/MAR05-51G, using several radiocarbon dates, calibrated to correct for the apparent reservoir offsets;
- to determine the source of the organic matter (i.e., whether marine or terrestrial) in the southwest Black Sea shelf sediments extracted in MAR05-50P/MAR05-51G, using the organic geochemical data in samples extracted at 10 cm intervals;
- to construct a palaeo-environmental and palaeoceanographic history of the core sites, and to compare these results with previous work;
- to compare the geochemical findings in cores MAR05-50P/MAR05-51G with other multi-proxy data to identify any trends within the data set that can constrain specific environmental changes. Currently, students and colleagues of Aksu and Hiscott are working on the micropalaeontology (ostracods) and palynology of the same cores. These data will be available for comparison purposes, which will help to develop a more holistic story of the watermass evolution and the history of reconnection for future research;

- to correlate the geochemical data of the composite core MAR05-50 with two southwest Black Sea shelf composite cores, MAR05-13 and MAR02-45 to identify regional trends; and
- to evaluate the data to see if there are contributions to be made to the validity of three existing hypotheses regarding the watermass reconnection history of the Black Sea with the eastern Mediterranean Sea.

## **Chapter Two: Methodology and Analytical Procedures**

### **2.1 Coring**

The field area for this project is located in the southwestern Black Sea. During a 2005 cruise (MAR05), several sediment cores were collected from the southwestern shelf, using a Mooring Systems Inc. piston and gravity corer and the research vessel *RV Koca Piri Reis* of the Institute of Marine Sciences and Technology, Dokuz Eylül University. The cores were collected to recover various sedimentary features associated with a saline density current channel where Mediterranean water cascades, at depth, into the lower-salinity Black Sea (Figure 10). The piston core MAR05-50P (41°29.634' N and 29°04.445' E) and a near by gravity core MAR05-51G (41°29.471' N and 29°04.393' E) are selected for a detailed organic geochemical and stable isotopic study. According to the GPS coordinates, there is approximately 310 meters between these two core sites. The gravity core MAR-51G has a total length of 157 cm, while the piston core is 738 cm in length. The water depth at the core sites is 91 m (Flood et al., 2009); this places the core site above the permanent halocline/pycnocline, as well as the chemocline.

### **2.2 Sampling**

Eighty-nine wet sediment samples were taken from the centre of the working halves of the split cores at 10 cm intervals in both MAR05-50P and MAR05-51G. Each individual sample was put in a clear plastic package and labelled accordingly. All samples were kept in a cold storage unit in the Department of Earth Sciences, at a

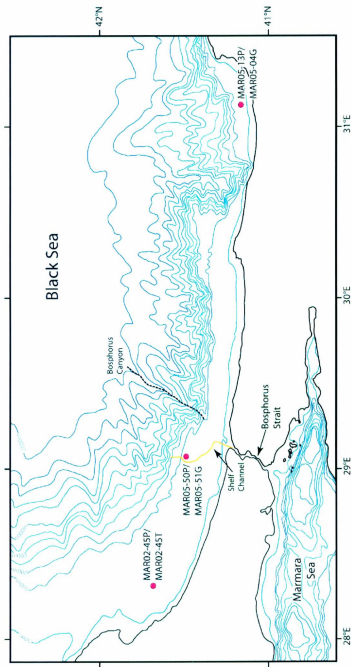


Figure 10: Location of cores MAR05-50P and MAR05-51G on the southwestern Black Sea shelf, showing bathymetry. Also shown are the saline-density current channel (solid orange line), the axis of the Bosphorus Canyon (dotted black line), seismic grid (grey) and cores MAR02-45P/MAR02-45T and MAR05-13P/MAR05-04G that will be used for correlation purposes. Modified from Flood et al. (2009).

temperature of  $-6^{\circ}\text{C}$ . The time between sample collection and processing for this thesis was approximately 48 months.

## **2.3 Sample Preparation**

### *2.3.1 Processing of Sediments*

Once the individual depth intervals were noted, the samples were then processed to remove carbonate material from the sediment in order to eliminate the inorganic carbon component. Approximately  $1\text{ cm}^3$  of wet sediment was placed in a 100 ml plastic measuring cup. Reagent-grade 38% hydrochloric acid was diluted using equal parts of acid and distilled water. This resulted in an approximately 19% hydrochloric acid solution which was added to the plastic measuring cups in a standard fume hood. Samples were left to react for 24 hours, with periodic stirring to that ensure the HCl digested all carbonate material.

The dissolution process was determined to be complete when there was no longer any bubbling or fizzing in the sample cup. Once complete, the acid solution was decanted from the cups, the samples were transferred to 50 ml plastic vials and rinsed with distilled water. The vials were then centrifuged to rapidly settle the sediments to the bottom. The water was then decanted from the vials and replaced with distilled water, and the samples were then returned to the centrifuge. This process was repeated three times in order to ensure the acid was fully removed from the sediments.

Next, the samples were transferred to aluminium cups and placed in an oven set at  $40^{\circ}\text{C}$  to dry overnight. The dry carbonate-free sediments were then removed from the

oven and ground by hand with a mortar and pestle. Finally, the samples were transferred to small glass vials and labelled for geochemical analysis.

### *2.3.2 Sediment Weighing*

The dry sediments were then brought to the Stable Isotope Laboratory in the Department of Earth Sciences where each sample was weighed into 7x7 mm tin capsules. Approximately 15 mg of sample was weighed out for sulphur elemental and isotopic determination using a Metler Toledo AT21 balance. Approximately 14 mg of sample was weighed into a second set of capsules for carbon analysis. Approximately 0.2 mg of vanadium pentoxide was added to the samples, which acts as a catalyst for oxidation. The tin cups were then folded over and compressed into tiny balls and placed in a labelled 96-welled plastic tray. Once the samples were weighed, sets of internal and sample calibration standards were also prepared in the same manner to be added to each run. The standards used are listed in Table 2.

### *2.3.3 Gypsum Crystals*

Euhedral gypsum crystals were discovered in the >63-micron fractions of cores MAR05-50P and MAR05-51G that were collected by fellow MSc candidate Lorna Williams. The fractions were collected as part of her thesis on ostracod biostratigraphy. The sediment samples required for her project were collected at the same time as the geochemistry samples used in this thesis, in December 2005. The gypsum crystals were not present in the freshly split cores when they were initially described (R.N. Hiscott, personal communication), so it is concluded that they formed during the several months

Table 2: Known/accepted values for the reference materials used for instrument, element and isotope calibration. MUN-CO-2 and IAEA-CH-6 are used for carbon isotope calibration and USGS-24 is a standard for carbon isotope and elemental analyses. Sulphanilamide and MUN Sulfanilamide are primers used for elemental calibration of carbon and sulphur. IAEA-S-2 (NZ-2) and IAEA-S-3 are used for sulphur isotope calibration, and B2150 (high organic sediment) is a standard for sulphur isotope and elemental analyses. IAEA-S-1 (NZ-1) is used as a check standard for sulphur isotopes, while W95-32 PY is used as an internal primer for assessing the stability of the instrument. Carbon isotopic values are measured with respect to the international reference standard Vienna PeeDee Belemnite (V-PDB), while the sulphur isotopic values are measured with respect to the Vienna Canyon Diablo Troilite (V-CDT) international reference standard.

Standard ID	Carbon wt %	$\delta^{13}\text{C}$ (V-PDB)	Sulphur wt %	$\delta^{34}\text{S}$ (V-CDT)
IAEA-CH-6	42.11	$-10.45 \pm 0.13$		
USGS-24	100	$-16.05 \pm 0.11$		
MUN-CO-2	12.00	$-41.11 \pm 0.09$		
MUN Sulfanilamide	41.85		18.62	
Sulphanilamide	41.85		18.62	
IAEA-S-1 (NZ-1)			12.94	-0.30 (exact)
IAEA-S-2 (NZ-2)			12.94	$+22.67 \pm 0.15$
IAEA-S-3			12.94	$-32.55 \pm 0.12$
B2150			$0.92 \pm 0.01$	$+5.19 \pm 0.16$
W95-32 PY				$+7.24 \pm 0.66$

after core splitting and before the samples were prepared for geochemical and palaeontological analysis. Because gypsum is a sulphate mineral, the effects of crystal formation on sediment analysis had to be considered, specifically to determine if gypsum crystallization involved isotopic fractionation and if HCl treatment of bulk samples dissolved some of the gypsum. According to laboratory experiments conducted by Li and Demopolous (2005), gypsum is stable in low concentrations of HCl at room temperature. The following process was completed by Williams to obtain the >63 micron fractions.

Starting in December 2009, samples were first disaggregated in a 1% solution of sodium hexametaphosphate (calgon) and left overnight. Then, each sample was transferred to a glass beaker, where approximately 10–15 ml of a 30% solution of hydrogen peroxide was added. The beakers were then boiled for approximately 10 minutes using a hot plate in order to assist with disaggregation. Samples were then cooled, wet sieved through a 63  $\mu\text{m}$  screen and dried in an oven at approximately 30°C. The >63  $\mu\text{m}$  fractions were then weighed and placed in individually labelled sample vials. These samples are referred to as Batch 1. Due to damage to the original ostracod separates while being transported by air, this process was then repeated in August 2010 by Williams using fresh sediment samples from the archive half of core that had been stored in the cold storage unit. This resulted in a second round of >63  $\mu\text{m}$  samples known as Batch 2. This batch was processed in the same manner as Batch 1, however the hydrogen peroxide bath and boiling step was omitted as it was deemed unnecessary.

For this thesis, the number of gypsum crystals in each sample of Batch 1 and Batch 2 was counted using a stereographic binocular microscope. For samples with large

amounts of gypsum crystals, a micro-splitter was used to divide the sample evenly. Weights, grain counts and gypsum abundance results for both Batch 1 and Batch 2 are presented in Chapter 3. The semi-quantitative scale for gypsum abundance (Table 3) was devised by the author, based roughly on the conventional ACFOR abundance scale used in ecological studies (i.e., abundant, common, frequent, occasional, rare) (e.g., Allen et al., 2006). Gypsum abundance results are presented in Chapter 4.

Table 3: Parameters used to classify the abundance of gypsum grains in each sample interval. Abundance scale based on conventional ecological ACFOR scales (e.g., Allen et al., 2006).

Abundance	Grains per mg	Classification
Abundant	500 +	5
Common	200 to 499	4
Frequent	50 to 199	3
Occasional	10 to 49	2
Rare	1 to 9	1
None	0	0

Using sample intervals with high gypsum abundances, 6 samples of crystals were collected from Batches 1 or 2. Each sample consisted of ~50 gypsum grains of various sizes, with enough mass to produce >4 mg of powdered gypsum. Of those, samples 430, 460 and 470 were taken from intervals with a mean bulk total sedimentary  $\delta^{34}\text{S}$  value of  $-35.72 \pm 0.92\%$ . Meanwhile, samples 490, 520 and 540 were taken from intervals with total sedimentary  $\delta^{34}\text{S}$  values that ranged from  $-16.4\%$  to  $+2.6\%$ . Each sample was crushed using an agate mortar and pestle, then transferred to individually labelled vials and put in a desiccation chamber in the Stable Isotope Laboratory to prevent excess water vapour absorption from the atmosphere.

### *2.3.4 Gypsum Weighing*

Using the Metler Toledo AT21 balance in the Stable Isotope Laboratory, approximately 2.4 mg of powdered gypsum was weighed out into 7x7 mm tin capsules and approximately 0.2 mg of the catalyst vanadium pentoxide was added. The 12 sample capsules, along with 3 duplicates, were compressed into tiny balls and stored in a 96-well plastic tray. The calibration standards, prepared in the same manner, are listed in Table 2. For this run, only the standards containing elemental and isotopic sulphur were used.

## **2.4 Analytical Techniques**

All samples and standards in this thesis were analyzed using high-precision continuous-flow isotope-ratio mass spectrometers in the Stable Isotope Laboratory. High-precision with respect to mass spectrometry indicates that results have a standard deviation of 4 to 6 significant figures, as defined by Brenna et al. (1997). Each sediment sample was analyzed for the carbon and sulphur stable isotopes ( $\delta^{13}\text{C}$  and  $\delta^{34}\text{S}$ ) of the bulk organic matter, as well as total organic carbon (TOC) and total sulphur (TS) contents of the sediments.

### *2.4.1 Principles of Isotope-Ratio Mass Spectrometry*

A mass spectrometer is commonly used in chemical analyses to separate and count charged atoms and molecules based on their mass/charge ratio ( $m/z$ ). Detection of mass and charge is done electronically when particles are passed through an electromagnetic field (Faure, 1977). In order to obtain the desired results, continuous-flow

isotope-ratio mass spectrometry requires the use of both an elemental analyzer, as well a gas-source isotope-ratio mass spectrometer (IRMS).

#### *2.4.2 Elemental Analyzer*

Elemental analyzers are used to automatically prepare samples by converting the solid sample into a pure gas for analysis in the isotope-ratio mass spectrometer (Figure 11). First, the prepared tin capsules containing either sample of sediment or standard are loaded in the automatic sampler carousel in the specified run order. One at a time, samples are dropped into the heated reactor where they are flash combusted with oxygen. Using a continuous flow of helium as a carrier gas, the products then travel through oxidation and reduction chambers for the removal of any excess oxygen. Next, the gases pass through a  $\text{Mg}(\text{ClO}_4)_2$  trap to remove water. Then, the gas passes through a 1.2-m Poropak QS 50/80 gas chromatograph at  $70^\circ\text{C}$  to separate the gas-phase products before sending the gaseous sample to the isotope-ratio mass spectrometer via the helium carrier gas (Brenna et al., 1997). In these experiments, the elemental analyzer used was the Carlo Erba NA1500 Series II, located in the Stable Isotope Laboratory at the Department of Earth Sciences. The unit was interfaced with the mass spectrometers using a ConFloIII interface and was used to determine carbon and sulphur elemental and isotopic abundances.

#### *2.4.3 Continuous-Flow Isotope-Ratio Mass Spectrometry*

Once the pure gases are prepared in the elemental analyzer, they travel into the mass spectrometer. Continuous-flow analysis uses a constant flow of a carrier gas,

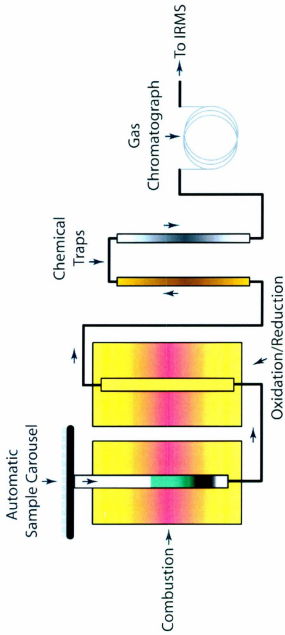


Figure 11: Simplified diagram of an elemental analyzer. Modified from "Forensic Isotope Ratio Mass Spectrometry" (2012).

helium in this case, in order to bring the combusted sample to the mass spectrometer. Modern mass spectrometers are comprised of three essential components: an ion source, a magnetic analyzer and an ion collector (Figure 12). All components are evacuated to pressures of the order of  $10^{-6}$  to  $10^{-9}$  mm Hg (Faure, 1977).

The  $\text{CO}_2$  or  $\text{SO}_2$  gas molecules are first introduced into the ion source where they interact with a focused electron beam. This beam strips the electrons from gas molecules creating positive ions, which are then propelled down a flight tube toward a negatively charged plate. Part of the ion beam passes through a slit in the plate and then enters the magnetic field of an electromagnet whose field is perpendicular to the direction of travel of the ion beam. This causes the ions to deflect in a circular path with radius proportional to the individual mass of each ion— heavier ions are less deflected than the lighter ions. The separated ion beams continue onto the collector array that consists of three or more Faraday cup collectors. The collision of the ion with its specific cup is counted and converted into a digital output (Faure, 1977). The result is the isotope count in parts per mil (‰) as well as the bulk element composition of the specific sample. The calculated isotope ratios,  $^{13}\text{C}/^{12}\text{C}$  and  $^{34}\text{S}/^{32}\text{S}$ , are compared to the international reference standards (as previously seen in Equations 2 and 3 in Chapter 1) which determines the isotopic ratio in the sample, given in delta notation.

#### *2.4.4 Sulphur Samples*

The sulphur samples and standards were run in July 2010 using the Finnigan MAT252 gas-source isotope-ratio mass spectrometer in the Stable Isotope Laboratory.

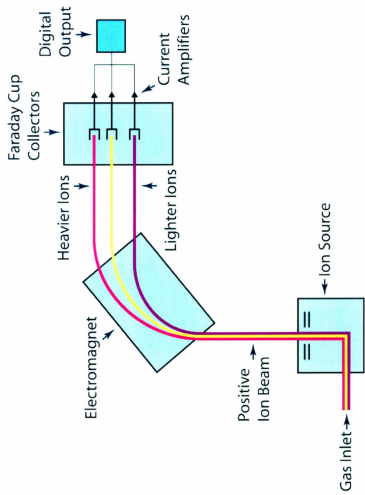


Figure 12: Simplified schematic of an isotope-ratio mass spectrometer. Modified from “Forensic Isotope Ratio Mass Spectrometry” (2012).

Each run included 20 samples, along with 34 calibration standards for instrument and sample calibration.

#### *2.4.5 Carbon Samples*

The carbon samples and standards were run in September 2010 using the ThermoElectron DeltaVPlus gas-source isotope-ratio mass spectrometer in the Stable Isotope Laboratory. Runs for the carbon samples included 30 samples, as well as 27 calibration standards.

Results for elemental and isotopic analyzes are presented in Chapter 4, while raw data are presented in Appendices A.

#### *2.4.6 Gypsum Samples*

Gypsum samples and standards were run in December 2011 using the MAT252 gas-source isotope-ratio mass spectrometer in the Stable Isotope Laboratory. Sulphur elemental and isotopic composition was determined using 15 samples including 3 duplicates, as well as 29 calibration standards.

Results for elemental and isotopic analyzes are presented in Chapter 4, while raw data are presented in Appendix B.

#### *2.4.7 Scanning Electron Microscopy (SEM)*

When the post-core-splitting gypsum crystals were discovered in the >63  $\mu\text{m}$  fractions, they were originally of unknown composition. To confirm that the grains were in fact gypsum, 15 grains were picked from the MAR05-50P 490 cm depth interval in

June 2011. The grains were then placed on a mount and brought to the Angus Bruno Innovation Centre at Memorial University for analysis with the FEI Quanta 400 environmental Scanning Electron Microscope (SEM). Samples were coated in gold, which is an electrically conductive material that prevents the build up of electrostatic charge on the surface of the sample during SEM analysis. Secondary electron and backscattered electron images were taken, as well as a compositional analysis with energy discriminated X-rays (EDX). The Roentec Quantax EDX system uses the Xflash SDD detector to bombard the grain with electrons. The X-rays that are emitted by the grain are analysed for their energies, which are then used to determine the specific elemental composition of the sample.

## **2.5 Calculations**

### *2.5.1 Terrestrial and Marine Fractions*

Estimations of the amount of terrestrial and marine carbon that contributed to the total organic carbon in each sample were made using the carbon isotopic abundance and known local end members for each sediment input in the Black Sea. The equation, modified from simple mixing equations in Calder and Parker (1968) and Fontugne and Calvert (1992) (Equation 4) uses the end-member values  $\delta^{13}\text{C}_{\text{terr}} = -27\text{‰}$  and  $\delta^{13}\text{C}_{\text{mar}} = -22\text{‰}$  to calculate the individual percent fractions:

$$F_{\text{terrestrial}} = \frac{(\delta^{13}\text{C}_{\text{sample}} - \delta^{13}\text{C}_{\text{marine}})}{(\delta^{13}\text{C}_{\text{terrestrial}} - \delta^{13}\text{C}_{\text{marine}})} \quad (4)$$

$$\begin{aligned} F_{\text{terrestrial}} + F_{\text{marine}} &= 1 \\ F_{\text{marine}} &= 1 - F_{\text{terrestrial}} \end{aligned} \quad (5)$$

The terrestrial end-member ( $\delta^{13}\text{C}_{\text{terr}}$ ) is taken from the  $\delta^{13}\text{C}$  of  $\text{C}_3$  plants found in temperate climate zones, akin to the Black Sea region (Deines, 1980; Meyers, 1994) (Figure 13). However, isotopic results from this thesis necessitate that the terrestrial end-member be changed from  $-27\text{‰}$  to  $-28\text{‰}$ , in order to accommodate the range seen in the data set. It is important to note that isotopic values of lacustrine algae also fall within this range, and are included in the terrestrial fraction (Meyers, 1994). The marine end-member ( $\delta^{13}\text{C}_{\text{mar}}$ ) was chosen based on known local marine values, where Fontugne (1983) noted that marine plankton in the East Mediterranean and Black Sea have a  $\delta^{13}\text{C}$  value of  $-22\text{‰}$ . Then, the marine fraction of organic matter can be simply calculated from knowledge of the terrestrial fraction. This is based on the assumption (Equation 5) that all organic matter in a system is the sum of the terrestrial input and the marine input.

### 2.5.2 Age Calibration

As mentioned in Chapter 1, raw  $^{14}\text{C}$  dates do not account for the natural fluctuations in the amount of atmospheric  $^{14}\text{C}$  over geological time, nor do they account for the disparity between different contemporaneous carbon reservoirs (i.e., atmospheric, terrestrial, marine). For this reason, it is necessary to convert these sample ages to calibrated years before present (cal yr BP) in order to interpret the dates with respect to actual solar years. There are many software programs used for this calibration process,

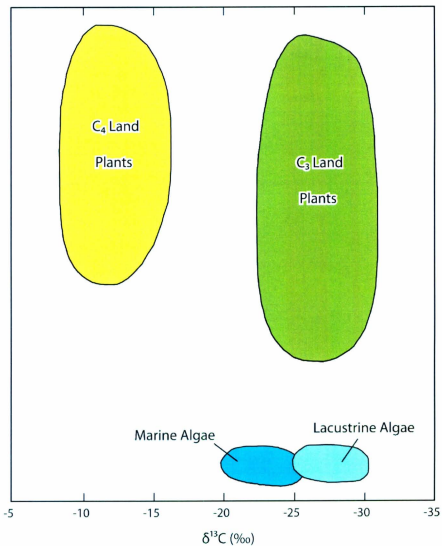


Figure 13: Simplified diagram of the  $\delta^{13}\text{C}$  ranges for various sources of organic matter. Modified from Meyers (1994).

but for this thesis the program used was OxCal 4.1 maintained by Professor Christopher Bronk Ramsey, that is hosted by the University of Oxford's Radiocarbon Accelerator Unit (Ramsey, 2012).

The calibration process corrects for the temporal variation of atmospheric  $^{14}\text{C}$  production, as well as the offsets produced by reservoir effects. Modern carbon reservoirs (in this instance, the dissolved  $\text{CO}_2$  in marine water) have inherited ages older than zero because of time delays in arrival of the carbon in the water column, and because of contamination of the carbon reservoir by old, perhaps even "dead" carbon from terrestrial weathering of bedrock older than ~50,000 years. The latter is referred to as the "Hard Water Effect" (Soulet et al., 2011a). On average, the difference in  $^{14}\text{C}$  age between contemporary terrestrial and marine organisms is about 400 radiocarbon years (Stuiver and Braziunas, 1993). In order to account for this apparent age difference, a reservoir correction that is associated with the specific marine reservoir in question must be applied (Higham, 2012).

The OxCal program processes chronological data in two distinct ways. The first is the calculation of probable age ranges for the specific dates through radiocarbon calibration. The second is the assessment of several related events that are linked either through generic grouping or through stratigraphic relationships (Ramsey, 2012). The former technique was used in this instance.

There has been extensive research in recent years trying to determine the proper reservoir correction for the Black Sea through the late Quaternary. For this thesis, proposals by Siani et al. (2000), Kwiecien et al. (2008) and Soulet et al. (2011a, 2011b)

were considered. The resulting reservoir corrections used for cores presented in this thesis are 415  $^{14}\text{C}$  yr for ages younger than 7,150  $^{14}\text{C}$  yr BP and 280  $^{14}\text{C}$  yr for ages older than 8,400  $^{14}\text{C}$  yr BP. The reservoir correction is on a linear sliding scale between 7.15  $^{14}\text{C}$  ka and 8.4  $^{14}\text{C}$  ka. The basis for these chosen reservoir corrections are further explained in Chapter 3: Chronology. These reservoir corrections were inserted into the OxCal 4.1 software, along with the raw radiocarbon dates for the cores used in this thesis. All dates were calibrated using the Marine09 calibration curve, which is currently the most recent collection of modelled ocean averages, based on Reimer et al., 2009 (Ramsey, 2012). The Marine09 curve has a built-in reservoir correction of 405  $^{14}\text{C}$  yr. In order to apply the southwestern Black Sea specific corrections of 415  $^{14}\text{C}$  yr and 280  $^{14}\text{C}$  yr,  $\Delta R$  values of +10  $^{14}\text{C}$  yr and -125  $^{14}\text{C}$  yr were applied, respectively. Calibrated ages for cores MAR05-50P and MAR05-51G, as well as composite cores MAR02-45 and MAR05-13 are present in Chapter 3.

### *2.5.3 Age-Depth Conversion*

Once the calibrated ages were determined, an age model was constructed (Chapter 3) and the geochemical data was converted from a depth domain to a time domain. This conversion was made using two programs: Ager and Timer. The Ager program is used to determine the sedimentation rate between each date given in the age model. It then uses linear interpolation and/or extrapolation to allocate an age to each geochemical measurement throughout the core. This information is then entered into the Timer program, which places the geochemical data at equal time increments that are defined by

the user (100 year increments in the case of this thesis). The results of this conversion to an age domain are presented and discussed in Chapter 5.

## **2.6 Limitations to the Methodology**

### *2.6.1 Mineral Dissolution Efficiency*

In sediment samples, carbon is usually preserved in two separate forms: organic and inorganic. Organic carbon refers to carbon bound in organic compounds, whereas inorganic carbon is usually found in minerals such as carbonates (e.g., calcite, aragonite and dolomite). In order to analytically measure total organic carbon (TOC), the inorganic carbon within the sample must be removed. All samples were bathed in a hydrochloric acid solution to remove carbonate minerals. However, there are limitations to this procedure, as stated by Galy et al. (2007). When dissolving the inorganic material, the results are constrained by both the efficiency of the mineral dissolution, as well as a desire to preserve all organic carbon. In practice, the organic carbon that remains is actually the total insoluble carbon. The acid treatment likely attacks and dissolves some of the more labile organic components such as carbohydrates found in plant materials. It might also have dissolved a small amount of gypsum (Li and Demopoulous, 2005). As well, the carbonate minerals may not fully dissolve, which may result in trace inorganic carbon included in the TOC determination. However, it should be noted that this method of equating total insoluble carbon with total organic carbon is common practice.

### *2.6.2 Mass Spectrometry Error*

During the sulphur mass spectrometry runs, the Finnigan MAT252 gas-source isotope-ratio mass spectrometer had just re-entered commission after a lengthy maintenance down time. As a result, there was an energy-source failure during the two of the eight sulphur runs, which prevented the inclusion of all of the end-of-run calibration standards (Appendix A). Without these standards, a second set of peak size check standards could not be included, which might have led to a slightly higher standard deviation than normal for the sulphur isotopic values of these two sulphur runs. However, the total sulphur results from these runs would not be affected by these energy-source failures (A. Pye, personal communication).

### *2.6.3 Bioturbation*

Bioturbation refers to the disturbances due to organisms present in sediments, and is a common occurrence in marine environments. When organisms move within the sediment column for feeding purposes, they cause a mixing or smearing of the original sedimentary layering. Because each layer that was deposited represents an instant of geologic time, this mixing results in a reduction of the time resolution.

### *2.6.4 Sampling Intervals*

There are certain limitations created by the sampling intervals, both the intervals between sediment samples and irregular intervals between radiocarbon-dated shells. For this project, sediment samples were taken at 10 cm intervals. However, because the sedimentation rate on the Black Sea shelf has varied throughout the Holocene, the time

interval between each sampling level varies. Estimations of the sedimentation rate can be made using the available calibrated radiocarbon ages; however accuracy of the interpolated ages that can be assigned to individual samples includes error caused by several factors. The error depends on (a) the degree to which sedimentation rates fluctuated between levels with radiocarbon dates (i.e., levels where a shell was extracted), (b) the stratigraphic proximity of the particular sediment sample to a dated level (the more distant, the greater the potential error), (c) standard deviations associated with the radiocarbon dates and their calibrated equivalents, and (d) the degree to which the dated shells are synchronous with their sampling depths (shells can be reworked upward, can be shifted upward or downward by burrowers, or can live below the sediment-water interface, as is the case for infaunal molluscs). Some of these uncertainties cannot be quantified, so ages assigned to individual samples must be considered approximate, particularly if there is not a stratigraphically nearby radiocarbon date.

## Chapter Three: Chronology

### 3.1 Radiocarbon Dates

#### 3.1.1 Radiocarbon Results

Three new radiocarbon dates were acquired during the course of the thesis research and consequently have not been previously published. *Mytilus galloprovincialis* shells at depth intervals 200 cm and 310 cm were collected in June 2011 by supervisor Dr. Ali Aksu and sent to the Radiocarbon Dating Laboratory at the Université Laval in Québec City, Québec, Canada. Dr. Ali Aksu also collected a foraminifera sample in October 2011 at 625 cm depth, consisting of ~500 individual forams. This sample was sent to Beta Analytic Inc., Miami, Florida, USA for dating. The resulting uncalibrated  $^{14}\text{C}$  dates are presented in Table 4.

Table 4: Raw radiocarbon dates in years before present (yr BP) from core MAR05-50P at depths 200 cm, 310 cm and 625 cm. All samples were collected by Dr. Ali Aksu and have not been previously published.

Core	Depth	Dated Material	$^{14}\text{C}$ date	$\sigma$	Lab Number
M05-50P	200	<i>Mytilus galloprovincialis</i>	3590	$\pm 15$	UCIAMS-96128
M05-50P	310	<i>Mytilus galloprovincialis</i>	4130	$\pm 20$	UCIAMS-96127
M05-50P	625	Foraminifera	7570	$\pm 40$	BETA307981

#### 3.1.2 Reservoir Corrections

As mentioned previously in Chapter 2, radiocarbon dates from marine sample generally have to be corrected for reservoir offsets. Currently, there is a large amount of

research occurring in the Black Sea area that is trying to determine what the appropriate reservoir correction should be (Figure 14). Siani et al. (2000) proposed that an appropriate modern reservoir correction for the Black Sea area extending to the Dardanelles Strait should be  $415 \pm 90$   $^{14}\text{C}$  yr. Kwiecien et al. (2008) concurred with this value, however suggested that it should apply to samples collected from the upper 0–400 meters depth and for the uncalibrated ages of younger than 7,100  $^{14}\text{C}$  yr BP, which corresponds to the disappearance of lacustrine species of Ryan et al., 1997. The results of Kwiecien et al. (2008), in agreement with Major et al. (2002) and Bahr et al. (2005), further suggested that dates older than 8,400  $^{14}\text{C}$  yr BP (the initial marine inflow as described in Major et al., 2002) and younger than  $\sim 12,000$   $^{14}\text{C}$  yr BP (i.e., the beginning of the Younger Dryas stadial) should have a reservoir correction of 0  $^{14}\text{C}$  yr for samples collected from water depth of less than 400 m. Soulet et al. (2011a, b) disagreed with this suggestion and instead indicated that, due to hard water effects, the offset for that time interval is closer to 280–350  $^{14}\text{C}$  yr for samples collected from less than 400 m water depth. Specifically, Soulet et al. (2011b) suggested that a 280  $^{14}\text{C}$  yr BP correction should be used for samples that range in age from 13,800  $^{14}\text{C}$  yr BP until the end of the Younger Dryas event at  $\sim 11,500$   $^{14}\text{C}$  yr BP. At this point they propose a slight increase to 300  $^{14}\text{C}$  yr until the initial saline inflow ( $\sim 8,400$   $^{14}\text{C}$  yr BP). They then propose a linear increase to the modern value, from this point until the disappearance of lacustrine species at 7,100  $^{14}\text{C}$  yr BP. Based on these contrasting studies (0  $^{14}\text{C}$  yr versus 280–350  $^{14}\text{C}$  yr), a reservoir correction of 280  $^{14}\text{C}$  yr was selected for dates older than 7,500  $^{14}\text{C}$  yr BP, as the variation in standard deviation of dates calibrated this way would be more likely to

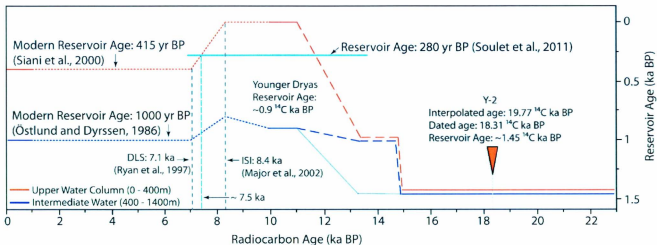


Figure 14: Figure modified from Kwiecien et al. (2008) detailing the variation of the suggested reservoir age ( $^{14}\text{C}$  ka) over time ( $^{14}\text{C}$  ka BP). Ages relevant to the cores found in this thesis lie within the upper water column (red line). The turquoise line was superimposed by the author to identify the recommendations put forth by Soulet et al. (2011a, b) for ages older than 7,500  $^{14}\text{C}$  yrBP. ISI = initial saline inflow; DLS = disappearance of lacustrine species; Y-2 = late-glacial marine tephra that correlates with the Cape Riva ignimbrite layer found in basins in the East Mediterranean area. This was a result of the eruption of the Santorini volcano, which has been dated at 18.31  $^{14}\text{C}$  ka BP (Pichler and Friedrich, 1979; Eriksen et al., 1999).

encompass the true age. Soulet et al. (2011b) assigned no error bars were to the reservoir ages in their study. Since the water depths of the three cores used in this thesis fall within the upper water column, only the 415 <sup>14</sup>C yr and 280 <sup>14</sup>C yr corrections were applied to the calibration process. Notably, Mertens et al. (2012) followed this same protocol, however used a reservoir value of 300 <sup>14</sup>C yr for ages older than 8,400 <sup>14</sup>C yr. For ages between 7,100 <sup>14</sup>C yr and 8,400 <sup>14</sup>C yr, a reservoir value was calculated by linear interpolation between 280 <sup>14</sup>C yr and 415 <sup>14</sup>C yr. Given that the difference between the reservoir value used in this thesis (i.e., 280 <sup>14</sup>C yr) compared to Mertens et al (2012; i.e., 300 <sup>14</sup>C yr) is only 20 <sup>14</sup>C yr, the age output of these two calibrations are very similar. Also, considering the standard deviation of the measured radiocarbon dates, calibrated results from both procedures overlap within the margin.

### *3.1.3 Calibrated Radiocarbon Dates for MAR05-50P and MAR05-51G*

Using the aforementioned reservoir corrections of 280 <sup>14</sup>C yr for samples older than 7,100 <sup>14</sup>C yr and 415 <sup>14</sup>C yr for samples younger than 7,100 <sup>14</sup>C yr in the OxCal 4.1 online program (<https://c14.arch.ox.ac.uk/oxcal/OxCal.html>), all available radiocarbon dates from MAR05-51G and MAR05-50P were calibrated using the Marine09 calibration curve. The uncalibrated and calibrated ages are present in Table 5, as well as their respective standard deviations and median calibrated ages. The median age is presented to confirm that the distribution of probable calibrated ages is not significantly skewed.

Table 5: Calibrated radiocarbon dating results for cores MAR05-51G and MAR05-50P, showing both uncalibrated years before present (yr BP) and calibrated years before present (cal yr BP). Raw  $^{14}\text{C}$  dates were originally presented by Flood et al. (2009), excluding those newly collected dates (italicized in this table) that are presented in Table 4.

Core	Depth (cm)	$^{14}\text{C}$ date (yr BP)	$\sigma$	Mean cal yr BP	$\sigma$	Median cal yr BP	Lab Number
Reservoir correction: 415 yr BP							
M05-51G	145	3280	$\pm 60$	3105	$\pm 90$	3105	TO-13101
M05-50P	44	2590	$\pm 90$	2250	$\pm 120$	2250	TO-13095
M05-50P	180	3240	$\pm 50$	3050	$\pm 80$	3050	TO-13096
<i>M05-50P</i>	<i>200</i>	<i>3560</i>	<i><math>\pm 15</math></i>	<i>3470</i>	<i><math>\pm 40</math></i>	<i>3470</i>	<i>UCLAMS-96128</i>
M05-50P	279	3250	$\pm 70$	3065	$\pm 100$	3065	TO-13097
<i>M05-50P</i>	<i>310</i>	<i>4130</i>	<i><math>\pm 20</math></i>	<i>4175</i>	<i><math>\pm 45</math></i>	<i>4175</i>	<i>UCLAMS-96127</i>
M05-50P	340	4320	$\pm 60$	4440	$\pm 90$	4440	TO-13098
M05-50P	435	5330	$\pm 70$	5695	$\pm 80$	5685	TO-13099
Reservoir correction: 280 yr BP							
<i>M05-50P</i>	<i>625</i>	<i>7570</i>	<i><math>\pm 40</math></i>	<i>8160</i>	<i><math>\pm 60</math></i>	<i>8160</i>	<i>BETA-307981</i>
M05-50P	670	9880	$\pm 110$	10935	$\pm 150$	10950	TO-13100
M05-50P	737	10270	$\pm 90$	11500	$\pm 175$	11490	TO-12915
M05-50P	737	32190	$\pm 280$	35390	$\pm 450$	35255	TO-12734

### *3.1.4 Calibrated Dates for MAR02-45P/MAR02-45T & MAR05-13P/MAR05-04G*

The calibration process mentioned above was repeated for radiocarbon dates reported for cores MAR02-45P and MAR02-45T (Hiscott et al., 2007) and MAR05-13P and MAR05-04G (Cranshaw, 2007). All dates were converted using the Marine09 calibration curve in the OxCal 4.1 program, and using consistent reservoir corrections. The calibrated dates are presented in Tables 6 and 7.

## **3.2 Age Model**

### *3.2.1 Core-Top Loss*

Using the carbon and sulphur geochemical results (Figure 15, Chapter 4), it was determined that there was approximately 50 cm of core-top loss during the collection of core MAR05-50P (also seen lithologically in Figure 8, Chapter 1). Core-top loss is common in marine piston coring: if the freefall wire is set too long, the topmost sediments are bypassed by the corer because the piston remains at the tip of the core barrel until the freefall wire is pulled tight. In order to compensate for this core-top loss in the age model and presentation of the results, the geochemical data collected from the uppermost 50 cm of gravity core MAR05-51G were spliced onto the top of core MAR05-50P, creating a composite core that is referred to as MAR05-50. This causes the depths of samples taken from MAR05-50P to increase by 50 cm so that they are assigned a correct sub-seabed depth, resulting in a new total core length of 787 cm.

Table 6: Calibrated dates for cores MAR02-45P and MAR02-45T. Raw dates were first published by Hiscott et al. (2007), excluding the date at depth 174 cm (italicized) – it has not been previously published.

Core	Depth (cm)	<sup>14</sup> C date (yr BP)	$\sigma$	Mean cal yr BP	$\sigma$	Median cal yr BP	Lab Number
Reservoir correction: 415 yr BP							
M02-45T	92	730	±50	365	±50	365	TO-11433
M02-45T	145	770	±50	395	±55	395	TO-11434
M02-45P	33	730	±40	365	±45	365	TO-11435
M02-45P	158	2400	±60	2025	±80	2020	TO-11006
<i>M02-45P</i>	<i>174</i>	<i>5115</i>	<i>±20</i>	<i>5480</i>	<i>±45</i>	<i>5480</i>	<i>UCIAMS-85907</i>
M02-45P	220	5190	±50	5535	±55	5540	TO-11436
M02-45P	302	5900	±60	6310	±65	6310	TO-11437
Reservoir correction: 280 yr BP							
M02-45P	406	7560	±60	8145	±75	8145	TO-11438
M02-45P	495	8380	±70	9140	±95	9140	TO-11142
M02-45P	569	8570	±70	9355	±80	9365	TO-11439
M02-45P	639	8620	±70	9405	±75	9415	TO-11440
M02-45P	754	8840	±70	9655	±105	9640	TO-11441
M02-45P	810	9370	±70	10350	±80	10350	TO-11007
M02-45P	822	9340	±70	10325	±80	10320	TO-11442
M02-45P	835	9070	±70	9985	±115	9995	TO-11443

Table 7: Calibrated dates from core MAR05-13P and MAR05-04G. Raw  $^{14}\text{C}$  ages were originally presented by Cranshaw, 2007.

Core	Depth (cm)	$^{14}\text{C}$ date (yr BP)	$\sigma$	Mean cal yr BP	$\sigma$	Median cal yr BP	Lab Number
Reservoir correction: 415 yr BP							
M05-04G	17	540	$\pm 50$	155	$\pm 70$	160	TO-13196
M05-04P	137	2600	$\pm 60$	2255	$\pm 80$	2260	TO-13197
M05-13P	16	1380	$\pm 50$	915	$\pm 60$	915	TO-13198
M05-13P	87	2230	$\pm 60$	1820	$\pm 75$	1820	TO-12906
M05-13P	253	3940	$\pm 60$	3920	$\pm 90$	3915	TO-12907
M05-13P	384	4170	$\pm 60$	4235	$\pm 90$	4235	TO-12908
M05-13P	441	4770	$\pm 70$	5035	$\pm 110$	5025	TO-12909
M05-13P	504	5960	$\pm 80$	6375	$\pm 85$	6370	TO-12910
M05-13P	620	6370	$\pm 90$	6835	$\pm 115$	6835	TO-12911
M05-13P	647	7020	$\pm 100$	7505	$\pm 90$	7505	TO-12912
Reservoir correction: 280 yr BP							
M05-13P	696	8740	$\pm 70$	9540	$\pm 80$	9525	TO-12834
M05-13P	784	9870	$\pm 90$	10935	$\pm 135$	10950	TO-12913

### 3.2.2 Considerations

There were two samples taken from 737 cm depth in core MAR05-50P that returned very different ages (Table 1 & Table 5). The first sample contained a pristine-looking *Dreissena* sp. shell, with patina clearly visible under the microscope. The second sample was a collection of bivalve fragments that were visibly worn and pitted by dissolution. The worn sample revealed an age of 35,390 cal yr BP, while the pristine sample gave an age of 11,500 cal yr BP (Table 5). Consequently, it was decided that the worn shells must have been reworked. Thus, the oldest sample age is not included in the age model.

Another consideration was the 3,065 cal yr BP age from a *Mytilus galloprovincialis* shell recovered from 279 cm depth in core MAR05-50P (Table 1 & Table 5). Interestingly, this sample was only 15 calibrated years older than another *Mytilus galloprovincialis* sample from 180 cm depth in the same core (Table 5). Two additional *Mytilus galloprovincialis* samples were sent for dating to determine whether or not the age from 279 cm depth was reliable. These samples were from 200 and 310 cm depth in the core, which bracketed the suspect age. The ages obtained from the new samples were 3,470 and 4,175 cal yr BP respectively, which were also inconsistent with the age obtained from the 279 cm depth (Table 5). On the basis of these new dates, sample 279 cm was excluded from the age model.

When constructing the age model, there were three samples relatively close in age and depth: 3,050 cal yr BP from 180 cm depth and 3,470 cal yr BP from 200 cm depth in piston core MAR05-50P, and 3,105 cal yr BP from gravity core MAR05-51G (Table 5).

In a linear age model there cannot be a reversal in sedimentation rate (that is, an older age at a depth above that of a younger age) without evidence of a hiatus. As a result, one of the three ages could not be included in the age model. Given that there is often some compression associated with the collection of gravity cores (Skinner and McCave, 2003) and that only the top 50 cm of the gravity core were considered for the construction of the composite core, the date from MAR05-51G (3,105 cal yr BP) was omitted from the age model.

### *3.2.3 Resulting Age Model*

Once the dates were chosen for the age model, the age of the hiatus at the  $\alpha_1$  unconformity could be estimated using linear extrapolation downward from above the unconformity, and upward from beneath the unconformity. During visual description, it was noted that a facies change occurs at 645 cm depth (695 cm depth in the composite core). Using the ratio of age difference to depth difference of the two dates above the boundary, the expected age of the upper limit of the hiatus could be calculated. An identical calculation was then used for the expected age of sediment just below the boundary (plotted at 696 cm depth in the composite core), which resulted in the ages 8,420 and 10,735 cal yr BP for sediments just above and just below the unconformity, respectively. Repeated calculations using all combinations of maximum and minimum ages (mean + one standard deviation, mean - one standard deviation) for the control points above and below  $\alpha_1$  allowed error estimates of  $\pm 65$  yr and  $\pm 215$  yr to be assigned to these ages, respectively. Each calculation assumes a constant sedimentation rate,

which might not have been true through the intervals considered. As a result, the  $\alpha_1$  hiatus is at best only approximately estimated to have lasted for  $2,315 \pm 280$  solar years.

Additionally, there was some linear interpolation used to calculate the age at the top of the piston core. It was assumed that the top of the composite core (0 cm depth) represents present day, having an age of 0 cal yr BP. Due to the previously mentioned restrictions in radiocarbon dating methods, “present day” here is actually 1950 CE, 55 solar years before the core retrieval date. Using the previous technique, an apparent age for 50 cm composite depth was calculated using the two control points below this level in the piston core. It should be noted that as a result of this calculation, the geochemistry versus age data for the top of the core (Figure 19, Chapter 5) is modified and interpolated as well. The final age model for composite core MAR05-50P is presented in Table 8.

### *3.2.4 Age Models for cores MAR02-45 and MAR05-13*

The age models for composite cores MAR02-45 and MAR05-13 were constructed in the same manner using linear interpolation and extrapolation for both the tops of the piston cores as well as upper and lower boundaries of the local unconformities, either  $\alpha_2$  or  $\alpha_1$ . Finalized age models for each core are presented in Tables 9 and 10.

### *3.2.5 Conversion of Geochemical Data*

Using the finalized age model, the geochemical data were entered into the Ager and Timer programs. The data were converted into a time domain for each of the three composite cores, accounting for the known changes in sedimentation rate. This

information is presented in Chapter 5, and it used for correlational purposes between the three composite cores: MAR05-50, MAR02-45 and MAR05-13.

Table 8: Calibrated ages used for constructing the age model used for site MAR05-50 in this thesis. Depth is listed as composite depth to account for 50 cm core-top loss in MAR05-50P. Ages at 50, 695 and 696 cm were calculated using linear interpolation and extrapolation to assign ages to both the top of the piston core, as well as sediment just above and just below the  $\alpha_1$  unconformity.

Depth in Composite (cm)	Age (cal yr BP)
0	0
50	1200
94	2250
230	3050
250	3470
360	4175
390	4440
485	5695
675	8160
695	8420
696	10735
720	10935
787	11500

Table 9: Age model for composite core MAR02-45 (110 cm core top loss). Ages at 110, 270, 271 and 950 cm were calculated by linear extrapolation to determine the ages at both the top and bottom of the piston core, as well as the ages of the upper and lower boundaries of the  $\alpha_2$  unconformity.

Depth in Composite (cm)	Age (cal yr BP)
0	0
110	280
143	365
145	395
268	2025
270	2050
271	5465
284	5480
330	5535
412	6310
516	8145
605	9140
679	9355
749	9405
864	9655
920	10350
950	10720

Table 10: Age model used for composite core MAR05-13 (30 cm core top loss). Ages at 0, 30, 689, 690 and 833 cm are linearly extrapolated values for the ages at the top and bottom of the piston core, as well as the ages of sediment just above and just below the  $\alpha_1$  unconformity.

Depth in Composite (cm)	Age (cal yr BP)
0	0
17	155
30	495
46	915
117	1820
137	2255
283	3920
414	4235
471	5035
534	6375
650	6835
677	7505
689	7805
690	8970
726	9540
814	10935
833	11235

## Chapter Four: Results

### 4.0 Results

The results from the analytical geochemistry, as well as laboratory work to assess the implication of the gypsum that formed after core splitting are presented in detail in this chapter. Raw data from the sediment and gypsum isotope-ratio mass spectrometer runs, as well as scanning electron microscope images are included in Appendices A, B and C respectively.

### 4.1 Carbon Results

#### *4.1.1 Total Organic Carbon (TOC) Results*

The total organic carbon (TOC) values in cores MAR05-50P and MAR05-51G range from a minimum of 0.82% to a maximum of 1.85% (Figure 15). From the base of the piston core until 490 cm depth, TOC varies within the range of 0.82% to 1.32%, with a mean value of 1.06%. At 480 cm, there is a sudden increase to 1.43%, marking a zone of relatively high TOC (range 1.38% to 1.85%, mean = 1.63%) that persists until 350 cm. At 340 cm, the TOC shifts downwards again, oscillating between 1.03% and 1.65%, with a mean value of 1.42%. This zone extends to the top of the piston core, and it also describes the entirety of the gravity core MAR05-51G. The TOC data show an oscillating pattern throughout both cores, but notably the lower region shows a greater variance in its fluctuation than the two zones above.

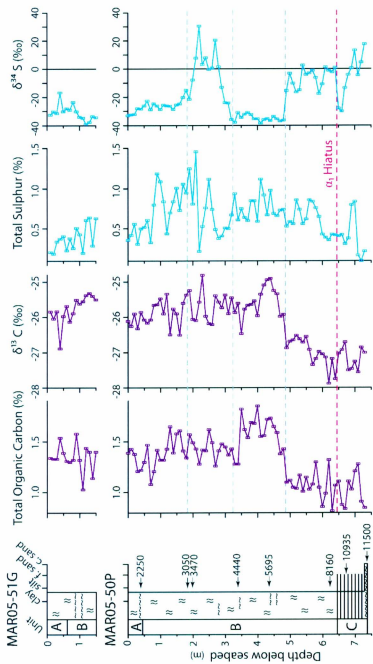


Figure 15: Geochemical results from carbon and sulphur mass spectrometer runs, showing Total Organic Carbon,  $\delta^{13}\text{C}$ , Total Sulphur and  $\delta^{34}\text{S}$ . Ages shown are given in calibrated years before present (cal. yr BP).

Kidd et al. (1978) define a *sapropel* as “a discrete layer, greater than 1 cm in thickness, set in open marine pelagic sediments and containing greater than 2.0% organic carbon by weight”. They go on to describe *sapropelic layers* as similar, but they “differ in that [they] contain between 0.5% and 2.0% organic carbon”. While sapropels are common throughout the Marmara Sea gateway region (e.g. Aksu et al., 1999b; Çağatay et al., 2002; Aksu et al., 2002c; Mudie et al, 2002b; Adetona, 2005; among many others), cores MAR05-50P/MAR05-51G do not contain any sapropels. However, by definition, the entire succession can be considered sapropelic mud.

#### 4.1.2 $\delta^{13}\text{C}$ Isotope Ratios

The  $\delta^{13}\text{C}$  isotope results range from a minimum of  $-27.88\text{‰}$  to a maximum of  $-24.81\text{‰}$ , and show two separate general zones (Figure 15). From the base of the piston core until 490 cm depth, the  $\delta^{13}\text{C}$  values oscillate within the range of  $-27.88\text{‰}$  to  $-26.51\text{‰}$  (mean =  $-27.05\text{‰}$ ). At the 480 cm level, there is a sudden, positive increase in the  $\delta^{13}\text{C}$  isotopes from  $-26.87\text{‰}$  to  $-25.92\text{‰}$ , indicating a relative enrichment in the heavier carbon isotope  $^{13}\text{C}$ . From this point, the values continue to become  $^{13}\text{C}$ -enriched the next 40 cm, where they then begin to fluctuate within the range of  $-26.50\text{‰}$  to  $-24.81\text{‰}$  (mean =  $-25.75\text{‰}$ ) to the top of the piston core. All  $\delta^{13}\text{C}$  values in gravity core MAR05-51G fall within this relative  $^{13}\text{C}$ -enriched range seen in the top of the piston core, excluding one point at 40 cm that is noticeably depleted ( $-26.88\text{‰}$ ). The  $^{13}\text{C}$ -depleted zone at the base of the core ( $\sim -27.05\text{‰}$ ) is close to the terrestrial end member suggested by Deines (1980) ( $-27\text{‰}$ ) and this thesis ( $-28\text{‰}$ ), while the values from the  $^{13}\text{C}$ -enriched

top zone ( $\sim -25.75\text{‰}$ ) indicate a greater proportion of the Black Sea marine end member ( $-22\text{‰}$  according to Fontugne, 1983).

## 4.2 Sulphur Results

### 4.2.1 Total Sulphur (TS) Results

The total elemental sulphur (TS) in the sediments of cores MAR05-50P and MAR05-51G ranges between 0.08% and 1.46% (Figure 15). While the values fluctuate greatly throughout the cores, there are some very general trends. At the base of core MAR05-50P, the total sulphur is low from 730 cm until 600 cm depth, ranging from 0.10% to 0.84%. Although there is a localized, two-sample peak from 700–690 cm, the average for this interval is generally low, at 0.40%. From 590 cm to 320 cm, the TS values increase slightly and stay steady in their fluctuations between 0.53% and 1.12% (mean = 0.74%). However, at around 310 cm depth, the TS results begin to oscillate within a much wider range (0.22% to 1.46%, with a mean of 0.78%) until about 80 cm in the top section of the piston core. The values begin to settle down at this point, with the remaining top of the piston core and entire gravity core staying within the range of 0.08% to 0.64% (mean = 0.39%). As well, there is a gradual upward decreasing trend in the elemental sulphur results throughout this top section.

### 4.2.2 $\delta^{34}\text{S}$ Isotopic Ratios

The  $\delta^{34}\text{S}$  isotopic ratios within cores MAR05-50P and MAR05-51G show clear zones throughout the Holocene interval, with a wide isotopic range between  $-39.02\text{‰}$  and  $+30.52\text{‰}$  (Figure 15). The bottom section of the piston core shows a general upward

enrichment of the light  $^{32}\text{S}$  isotope, beginning at 730 cm (+17.68‰) and increasing to -27.83‰ at 640 cm. This interval coincides roughly with the  $\alpha_1$  hiatus (645 cm). At this point, the isotope values shift dramatically to a  $^{34}\text{S}$ -enriched zone from 630 cm to 490 cm, that ranges between -17.58‰ and +2.63‰ (mean = -6.75‰). The isotopes then, once again, shift suddenly to become enriched in the lighter isotope  $^{32}\text{S}$ . This interval, 480 cm to 320 cm, has very little variance in isotopic values, ranging from -38.21‰ to -30.71‰ with a mean of -34.80‰. At 310 cm,  $\delta^{34}\text{S}$  begins to rise again in a local  $^{34}\text{S}$ -enrichment zone extending upward to 180 cm. Values are dispersed from -24.14‰ to +30.52‰, with a mean of -2.33‰. From 170 cm in the piston core to the top of the gravity core, the isotopes become enriched in the lighter  $^{32}\text{S}$  isotope once again, fluctuating within a much smaller range (-39.02‰ to -16.60‰, mean = -28.73‰).

### 4.3 TOC/TS Ratio

The ratio between elemental (organic) carbon and elemental sulphur is useful as it is used as a palaeo-environmental proxy for salinity changes in a basin (Berner and Raiswell, 1983; Berner, 1984). As stated in Berner and Raiswell (1984), sediments with a lower TOC/TS ratio (less than ~2) are indicative of marine environments, while sediments with higher TOC/TS ratios (greater than ~5) likely indicate a low-salinity to freshwater environment. The relationship between organic carbon and sulphur in sediments is linear. As a result, graphical analysis can be completed to reveal more about the local environment at the time of organic matter deposition (Leventhal, 1983).

The ratio of organic carbon to sulphur is simply the TOC value divided by the TS value at each individual depth. The TOC/TS ratio fluctuates throughout both cores,

ranging from 0.98 to 9.10 (Figure 16). At the base of core MAR05-50P, the TOC/TS ratio fluctuates below the  $\alpha_1$  hiatus from a minimum of 1.29 to a maximum of 9.10. Above the hiatus, the ratio remains reasonably stable, oscillating between 0.98 and 3.86, excluding one outlier at 220 cm that reaches 5.82. The mean ratio for this zone is 2.21. The gravity core MAR05-51G shows a general upward increasing trend, ranging from 2.19 at the base to 7.00 toward the top of the core.

#### **4.4 TS/TOC Ratio**

The ratio of sulphur to organic carbon is calculated by dividing the total sulphur by the total organic carbon, and it too yields valuable information about the depositional environment, as well as the presence of microbial sulphate reduction in the water column (Leventhal, 1983). Overall, the TS/TOC ratio in MAR05-50P and MAR05-51G ranges from a minimum value of 0.052 to a maximum value of 1.02 (Figure 16). Despite the smaller range in comparison to TOC/TS, the values of TS/TOC appear to fluctuate more aggressively with no specific pattern. However, the TS/TOC ratio generally increases from a low point at the base of the piston core (0.11 at 720 cm depth) to a maximum of 1.02 at 210 cm depth. From that point upwards, the ratio generally decreases throughout the rest of the piston core to the top of the gravity core where it reaches a low of 0.052 at 40 cm.

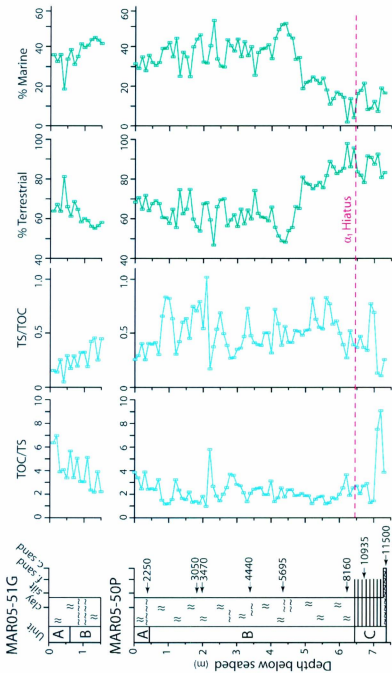


Figure 16: Calculated geochemistry results showing Total Organic Carbon over Total Sulphur, Total Sulphur over Total Organic Carbon, Terrestrial Source fraction and Marine Source fraction. Ages are given in calibrated years before present (cal yr BP).

## 4.5 Sediment Sources

Sediment source fractions were calculated using the  $\delta^{13}\text{C}$  isotope data and equations 4 and 5 that were presented previously in Chapter 2.

### 4.5.1 Terrestrial Fraction

The calculated terrestrial fraction of organic matter found in sediments is indicative of the amount of organic matter that likely came from the regional terrain, based on isotopic patterns of the local vegetation. This fraction also includes any lacustrine organic matter, given that the isotopic range of lacustrine algae falls within that of  $\text{C}_3$  land plants. Throughout cores MAR05-50P and MAR05-51G, the terrestrial fraction ranges from 47% to 98% (Figure 16). The most abundant terrestrial zone occurs at the base of the piston core. From 730 cm to 490 cm, the organic matter source ranges between 75–98% terrestrial, averaging about 84%. From 480 cm to 440 cm, there is a steep decline in terrestrial sources, declining to 48%. For the rest of the piston core, the terrestrial fraction fluctuates within the range of 47% to 75% (mean = 63%). The gravity core shows a slight upward enrichment in terrestrial material, but possesses the same mean value of 63%.

### 4.5.2 Marine Fraction

The marine fraction describes the percent of the organic matter that yields similar  $\delta^{13}\text{C}$  isotopic signatures to local marine organic sources (such as regional phytoplankton blooms). Given that logically there are only two sources for organic matter (from either the land or the sea), the marine fraction results are a mirror image of the terrestrial

fraction (Figure 16). As a result, the transitions from marine depleted zones to marine enrichment occur at the same levels. At the base of the piston core, the marine fraction ranges from 2–25% (mean = 16%). Values increase from 13% to 52% at 440 cm. The trend then stabilizes between 25% and 53% to the top of the piston core (mean = 38%). The gravity core shows a slight trend toward depletion at the top, but still contains, on average, 38% marine fraction.

## **4.6 Gypsum Results**

### *4.6.1 Crystal Abundance*

Since gypsum crystals were not observed when cores were split and described, the gypsum must have formed during storage in the repository. Gypsum crystals were counted in the >63 micron fractions from two dry sediment batches collected at different times, 48 months and 56 months after core splitting. Overall, Batch 1 has a lower abundance of crystals than Batch 2 (Figure 17). Excluding one outlier in MAR05-51G (130 cm), the gravity core and top 340 cm of the piston core have no gypsum crystals. The interval between 340 cm and 560 cm shows occasional (10–49 grains per mg) to abundant (500+ grains per mg) gypsum crystals. Below this point, there are no gypsum crystals to the bottom of the core, excluding one local occurrence at the 630 cm depth.

Batch 2 shows no gypsum crystals in the gravity core, as well as the top 120 cm of the piston core. From 130 cm to 340 cm, there are intervals of rare (1–9 grains per mg) to abundant (500+ grains per mg) gypsum crystals spaced between intervals containing no gypsum. At 410 cm, after 60 cm of zero gypsum, the abundance jumps to common (200–



499 grains per mg), then to abundant. The abundance stays high to the base of the core, excluding 3 samples at the base. The counts are presented in Appendix B.

#### *4.6.2 Scanning Electron Microscope (SEM) Results*

Five scanning electron microscope images were taken of gypsum crystals from Batch 2, 490 cm, to confirm that the post-splitting crystals are, in fact, gypsum. Images are presented in Appendix C. Crystals were euhedral (Plates 1, 2 and 3) with twinning in some instances (Plate 2), as observed under low magnification. A compositional analysis was performed using energy discriminated X-Rays (EDX) on the crystals and their various inclusions. The spectrum associated with an iron inclusion (Plate 4) shows peaks of oxygen, sulphur and calcium in addition to iron, as well as smaller peaks of magnesium, aluminium and silicon (Figure 29). This confirms that the crystal is a calcium sulphate, or gypsum:  $\text{CaSO}_4 \cdot 2\text{H}_2\text{O}$ . Other inclusions were found throughout the crystal, but were predominately iron, magnesium and aluminium in composition (Plate 5).

#### *4.6.3 Isotopic ( $\delta^{34}\text{S}$ ) Ratios in Gypsum*

In order to assess whether gypsum crystals growing in core MAR05-50P compromised the sediment sulphur isotope results, crystals were collected for geochemical analysis from six sample intervals where they are abundant. Results show that the gypsum sulphur generally mirrors the isotope ratios of the sediment sulphur (Figure 18; Table 11). The isotopes from the gypsum samples are, on average, 6‰ to 8‰ heavier than those of the corresponding sediments, indicating a relative enrichment in the heavy  $^{34}\text{S}$  isotope. Duplicate samples were run to compare different crystals from the

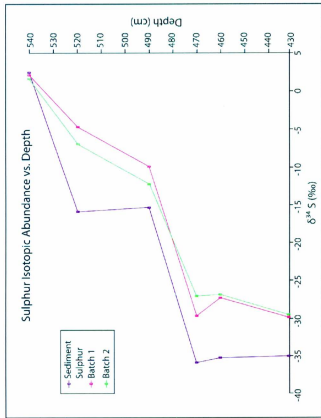


Figure 18: Sulphur isotopic abundance in the MAR05-50P sediments versus the isotope results of Batch 1 and Batch 2 gypsum crystals for the same depth intervals.

same batch/interval and the results show that the difference is only between 0.08‰ and 0.3‰, which is well within the standard deviations of the isotopic values (Table 11).

Table 11: Geochemistry results from sulphur isotope runs for sediment, Batch 1 gypsum, Batch 2 gypsum, as well as duplicate gypsum runs. All depths given are in centimetres and all results are in per mille (‰).

Depth (M50P)	Sediment $\delta^{34}\text{S}$	Batch 1 $\delta^{34}\text{S}$	Batch 2 $\delta^{34}\text{S}$	Duplicate $\delta^{34}\text{S}$
430	-35.14	-29.72	-28.98	-28.67 (Batch 2)
460	-35.25	-27.27	-26.87	
470	-36.78	-29.32	-27.06	-29.40 (Batch 1)
490	-15.25	-9.93	-12.47	
520	-16.44	-4.48	-7.00	
540	+2.63	+1.85	+1.07	+1.19 (Batch 2)

#### 4.6.4 Effect of Gypsum on Sulphur Geochemistry

Readers are reminded that bulk samples used to determine sediment  $\delta^{34}\text{S}$  were not sieved, so retained any gypsum that might have formed in the sediment between splitting of the cores and the time of laboratory work. Gypsum is very insoluble in HCl (Li and Demopoulos, 2005) so it would have remained in solid form with only very minor loss during the removal of carbonates, and would have been ground to powder with the rest of the sediment before isotopic analysis. Even wholesale gypsum dissolution during HCl treatment would have minimally affected the bulk  $\delta^{34}\text{S}$  ratios (Figure 18), so it is concluded that minor dissolution would in no way compromise the variations ascribed to geological processes (Figure 15).

## Chapter Five: Interpretation

### 5.0 Age Domain

The conversion of data from a depth domain into a time domain assists in the interpretation of geochemical data on local, regional and worldwide scales. Once converted to calibrated years before present, it is much less complicated to compare events in a specific core with data from other sites. This allows a more secure interpretation of the palaeo-environmental conditions at the time of deposition using all available data. Cores MAR05-50, MAR05-13 and MAR02-45 were converted using the age models mentioned in Chapter 3, and results from all three sites are integrated into the interpretation (Figure 19).

Because the data are described in time domain, the stratigraphic term “unconformity” is replaced by the time term “hiatus”. The Glossary of Geology (1980) describes hiatus as “*a lapse in time, such as the time interval not represented by rocks at an unconformity: the time value of an episode of non-deposition or of non-deposition and erosion together*”. From this point onward, the terms  $\alpha$ ,  $\alpha_1$  and  $\alpha_2$  unconformities will be referred to as the  $\alpha$ ,  $\alpha_1$  and  $\alpha_2$  hiatuses.

### 5.1 Lithological Correlation

Multi-proxy data derived from composite cores MAR02-45 and MAR05-13 have been previously published (Cranshaw, 2007; Hiscott et al., 2007b) and are available for correlation with the composite core MAR05-50 presented in this thesis. Lithological and

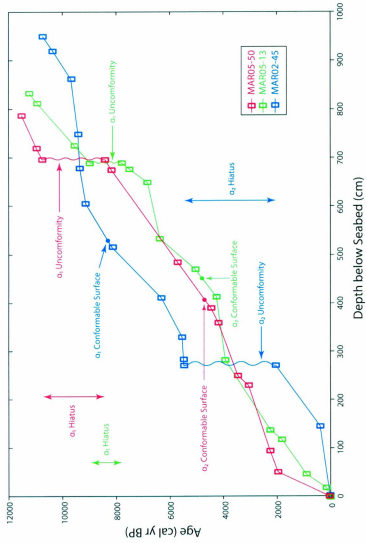


Figure 19: Comparison of calibrated age models versus depth for cores MAR05-50 (red), MAR05-13 (green) and MAR02-45 (blue). The locations of the  $\alpha_1$  and  $\alpha_2$  surfaces in each core are denoted using the same colour scheme.

geochemical comparisons between the three cores in conjunction with conclusions from the previous studies will assist in a more holistic understanding of the regional palaeo-environment over the course of the Holocene.

Lithological correlation in the age domain shows key similarities in cores MAR05-50, MAR05-15 and MAR02-45, and provides a snapshot of the regional lithology of the southwestern Black Sea shelf. All cores can be divided into the same three separate regional units – Unit A, Unit B and Unit C – which have been previously identified and described in Cranshaw (2007), Hiscott et al. (2007b) and Flood et al. (2009) and correlated with regional seismic stratigraphy identified in Aksu et al. (2002b) (Figure 20).

Regional Unit C exists at the base of the three cores and is the oldest of the three units (Figure 20). This regional unit corresponds to lithological Unit 3 of core MAR05-50P, discussed in Chapter 1 (Figure 8). It extends from the  $\alpha$  unconformity to the  $\alpha_1$  level. Although  $\alpha$  was not recovered in cores MAR05-50, MAR05-15 and MAR02-45, core MAR05-03 terminates in and consequentially recovered sediment from the level of this unconformity, as discussed in Reynolds (2012). Core MAR05-03 was taken ~481 m from the MAR02-45 core site and was precisely correlated with MAR02-45 as part of an honours dissertation project (Reynolds, 2012). The lowest radiocarbon age above the  $\alpha$  hiatus at the MAR05-03 site, and by extension at the MAR02-45 site, is from 1014 cm below present day seabed and is 11,880 cal yr BP (Figure 20). Based on Huntce DTS boomer profiles, the  $\alpha$  unconformity at site MAR05-50 is estimated to be ~9 m

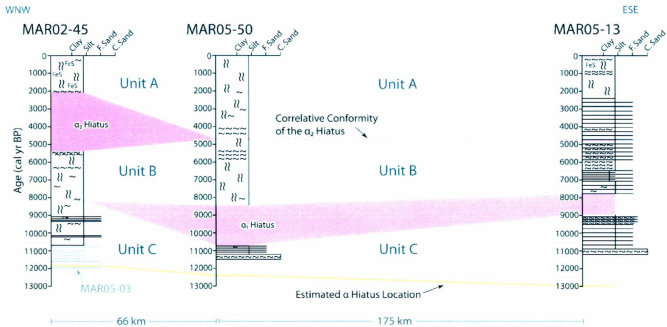


Figure 20: Lithological correlation between cores MAR05-50, MAR02-45 and MAR05-13. Core MAR05-03 from Reynolds (2012) has been superimposed at the base of core MAR02-45 (light gray) to show the location of the  $\alpha$  unconformity in that area.

below the seabed (A.E. Aksu, pers. comm., 2012). Using a linear extrapolation of the oldest two dates from the MAR05-50 age model (Figure 19), the age of sediment immediately above the  $\alpha$  unconformity at this site is approximately 12,400 cal yr BP.

The same technique could not be used on core MAR05-13 as recent work suggests that the lower section of the core had been compressed during coring (Bradley et al., in press). These authors indicated that *"the best facies matches between core MAR05-13 and the crossing seismic profile suggest that the core is compressed, so that its basal sediment (833 cm core depth; sand and gravel) comes from a sub-seafloor depth of ~11 m (based on 1500 m s<sup>-1</sup> acoustic velocity). This length difference is probably a combination of true compression because of inadequate piston suction and possible spotty bypassing (without full recovery) of particular intervals toward the top of the core"*. Using the 11 m depth for the  $\alpha$  unconformity and constant average sedimentation rates from the MAR05-13 age model (e.g., Figure 19), the age of the sediments directly above the  $\alpha$  unconformity is extrapolated to be ~13,000 cal yr BP. Although slightly older, this extrapolated age is in good agreement with the age estimated at core sites MAR05-50 and MAR02-45 (Figure 20). However, this age must be viewed as a conservative estimate: a slightly higher sedimentation rate would result a younger age for the sediments immediately above the hiatus.

In all three cores, Unit C is largely bioturbated muds with frequent fine sand and silt laminae, as well as shelly horizons. Core MAR02-45 is noted to have some Chondrites trace fossils within the lower part of this unit. At the base of cores MAR05-50, MAR05-13 and MAR05-03, there is a grain size peak that includes coarse sand and

some gravel. This coarser lithology is similar to sediments found along the thalweg of the saline channel where it has cut down to the  $\alpha$  level (Flood et al., 2009). According to Hiscott et al. (2007b), the fine sand and silt interbeds are event deposits, probably storm deposits. While the top of Unit C appears to be lost because of erosion at the  $\alpha_1$  unconformity in cores MAR05-50 and MAR05-13, a conformable surface is present at 525 depth in piston core MAR02-45P (Hiscott et al., 2007b), which dates the upper boundary of Unit C to  $\sim 8,200$  cal yr BP in MAR02-45.

Regional Unit B is bounded by the  $\alpha_1$  and  $\alpha_2$  surfaces, and is characterized by bioturbated muds with frequent shelly horizons of various molluscan fauna (Hiscott et al., 2007b) (Figure 20). This unit correlates with the “crinkly” seismic subunit 1C of Aksu et al. (2002b), which consists of acoustically discontinuous and distorted reflections lying atop of the  $\alpha_1$  unconformity, making the unit easy to identify. In core MAR02-45, the top of Unit B is cut by the  $\alpha_2$  unconformity so that the youngest sediment below the unconformity has an age of 5,465 cal yr BP; however, this unconformity is not present at core sites MAR05-50 and MAR05-13. Using the crossing seismic profile, Cranshaw (2007) identified  $\alpha_2$  as a conformable surface at 455 cm depth in core MAR05-13P, giving the boundary an age of  $\sim 4,800$  cal yr BP. The same boundary in MAR05-50 is 4.1 m below the seabed (Figure 7, Chapter 1) (A.E. Aksu, pers. comm., 2012) in sediment with an age of  $\sim 4,700$  cal yr BP. Given the abundance of benthic macro-fauna in Unit B, it can be inferred that the contemporary benthic environment was well oxygenated (Hiscott et al., 2007b). Since the  $\alpha_2$  level is not a lithological boundary in core MAR05-

50P, regional Unit B only encompasses the lower portion of lithological Unit 2 in that core (Figure 8, Chapter 1).

Regional Unit A, the youngest of the three units, extends from the  $\alpha_2$  unconformity/conformable surface to the sediment-water interface so has an age of ~5,200–5,400 cal yr BP to present (Figure 20). Sediments equivalent to the basal point of Unit A are missing in core MAR02-45 due to the presence of the  $\alpha_2$  unconformity and its associated protracted hiatus. In core MAR05-50, regional Unit A encompasses the top portion of lithological Unit 2 and the entirety of lithological Unit 1, both of which are colour-mottled bioturbated muds hosting some isolated shells (Figure 8, Chapter 1). In cores MAR05-13 and MAR02-45, Unit A is identical muds; however, both cores show Fe-monosulphide staining toward the core top. Hiscott et al. (2007b) hypothesized that the decrease of shell abundance might indicate a reduction of benthic oxygen levels.

The  $\alpha$  unconformity formed during the Last Glacial Maximum, when the Black Sea level stood ~100 m below present-day level (Hiscott et al., 2007b). At that time, the entire shelf was exposed to subaerial processes including erosion. During the subsequent post-glacial sea-level rise, the landward movement of the shoreline associated with transgression allowed near-shore and shallow shelf processes to further rework and erode the sediments across the shelf, modifying the original unconformity. Therefore, the  $\alpha$  unconformity is a composite unconformity developed by subaerial erosion and subsequent ravinement (as defined by Swift, 1968).

## 5.2 Environmental Interpretation of the Geochemical Data

Given the wide array of potential depositional conditions and/or environments that could be associated with a particular variable (such as TOC,  $\delta^{34}\text{S}$ , etc), a basic framework is needed for the environmental interpretation of each geochemical variable. This basic framework must provide the full range of conditions/environments for each variable, but also must provide an average value that is most probable for a given environment, such as marine, lacustrine, terrestrial, etc. Below, a succinct summary of the literature is used to create this basic framework, and is summarized in Table 12, located at the end of this section.

### 5.2.1 Total Organic Carbon

The environmental interpretation of the total organic carbon percentage data is straightforward: the sedimentary total organic carbon abundance is a function of the balance between input and consumption. Input can be *in situ* primary productivity within the basin as well as terrestrial supply to the basin via fluvial and aeolian processes. Consumption can be associated with scavenging by biological organisms within the water column when the organic and inorganic particulate matter sinks toward the bottom, as well as scavenging on and in the surface sediments. Removal of organic carbon from the environment can also be associated with oxidation in the water column or sediments. The total organic carbon content of most marine sediments ranges from <0.1% to ~0.3% by weight (e.g., Holser et al., 1988). These sedimentary organic carbon values represent the balance between the primary and secondary production in the ocean, the consumption by predation and oxidation, and the rate of sedimentation which in turn determines the rate

of burial of the organic carbon. When the amount of total organic carbon notably increases from these background values it reflects changes in this balance by either an increase in the biological productivity, an increase in the preservation of organic carbon on the seafloor, or a combination of the two processes. When the total organic carbon values reach 0.5% to 2.0%, these sediments are classified as sapropelic muds (Kidd et al., 1978). When sedimentary organic carbon values are >2.0%, these sediments are called sapropels, or black shales once lithified. Sapropels develop beneath anoxic bottom water conditions as well as in fully oxygenated bottom water beneath upwelling zones with very high primary productivity (e.g., Hagen, 2001). Regardless, any marine sediment that contains >~0.3% total organic carbon is potentially anomalous and might reflect a change in the palaeo-environment.

#### *5.2.2 Stable Isotopic Composition of Total Organic Carbon*

The environmental interpretation of the stable isotopic composition of carbon is complicated. The carbon isotopic signatures of marine ( $\delta^{13}\text{C} \sim -22\text{‰}$ ) and terrestrial ( $\delta^{13}\text{C} \sim -28\text{‰}$ ) organic carbon can be related to numerous biological and physical and chemical environmental processes. Environmental and metabolic effects control fractionation of the isotopes of organic carbon during photosynthesis. Maximum fractionation is achieved when pH and water temperature are low, the dissolved  $\text{CO}_2$  concentrations are high and the growth rate of the phytoplankton is moderate (Degens, 1969). Plankton that live in lower temperature ocean waters produce isotopically depleted organic carbon  $\delta^{13}\text{C}$  values (Fontugne and Duplessy, 1978; Sackett, 1986). Most marine phytoplankton exhibit  $\delta^{13}\text{C}$  values ranging from  $-8\text{‰}$  to  $-24\text{‰}$  (Meyers, 1994).

One step up the food chain, the  $\delta^{13}\text{C}$  composition of marine microfauna (mostly zooplankton) ranges from  $-7\text{‰}$  and  $-19\text{‰}$ . Thus, it is generally accepted that relatively heavy  $\delta^{13}\text{C}$  values ranging between  $-20$  and  $-25\text{‰}$  (with an average of  $-22\text{‰}$ , see Chapter 2) are marine in origin.

In land plants, the metabolic effect becomes important in three photosynthetic pathways (Fry and Sherr, 1984): (a) the Calvin or  $\text{C}_3$  pathway where  $\text{CO}_2$  is taken and incorporated from the atmosphere by carboxylation of ribulose diphosphate (RUDP); (b) the Hatch Slack or  $\text{C}_4$  pathway where  $\text{CO}_2$  is first fixed by carboxylation of phosphoenolpyruvate (PEP) – this is followed by transportation of the carboxylation product to the outer layer of the photosynthetic cell where it is decarboxylated and refixed by ribulose diphosphate; and (c) Crassulacean Acid Metabolism (CAM) pathway which can utilise either RUDP or PEP carboxylase for  $\text{CO}_2$  fixation. The selected carboxylase is dependent on the environment. A quick review of the land plants reveals that  $\text{C}_3$  plants have lighter  $\delta^{13}\text{C}$  composition ( $-23\text{‰}$  to  $-31\text{‰}$ ), whereas  $\text{C}_4$  plants have slightly heavier  $\delta^{13}\text{C}$  composition ( $-9\text{‰}$  to  $-17\text{‰}$ ; Meyers, 1994). Similarly, the lacustrine primary and secondary productivity ranges from  $-25\text{‰}$  to  $-30\text{‰}$ . In this thesis, the end member for terrestrial organic carbon is taken to be  $-28\text{‰}$  (see Chapter 2) as the regional environment and palaeo-environment supported both  $\text{C}_3$  plants and lacustrine algae.

Based on these parameters, the  $\delta^{13}\text{C}$  of the total organic carbon is expected to fluctuate between a terrestrial end member of  $-28\text{‰}$  and a marine end member of  $-22\text{‰}$ . A systematic shift from relatively enriched to depleted  $\delta^{13}\text{C}$  values would signal a

progressive increase in the proportion of terrestrial/lacustrine organic carbon, whereas the opposite would signal a progressive increase in the proportion of marine organic carbon. The sharpness of a transition in the downcore  $\delta^{13}\text{C}$  values is representative of the geological time involved in the creation of the shift from one predominant source to the other.

### *5.2.3 Total Sedimentary Sulphur*

Sedimentary sulphur is generally very low in marine sediments, ranging from <0.1% to ~0.2% (e.g., Holser et al., 1988). High total sedimentary sulphur is often associated with sapropels/sapropelic muds as well as black shales, where there is a strong positive correlation between the total organic carbon and total sedimentary sulphur. If the predominant total sulphur mineral is a sulphide (such as pyrite), a total sulphur content ranging between 1.0% and 1.2% is generally considered to reflect euxinic or sulphidic bottom water condition (e.g., Masuzawa et al., 1992). In the case of this thesis however, given the presence of extensive micro- and macro-fauna and moderate bioturbation, it is unlikely that the sediments are fully-euxinic. Therefore, these areas are interpreted with caution, and the benthic environment is suggested to have small concentrations of dissolved oxygen and therefore is likely dysaerobic (Raiswell and Berner, 1986).

An increase in total sulphur values in sediments of marginal seas implies the input of dissolved sulphate (e.g., seawater sulphate associated with a full marine connection) and active sulphate reduction if most of the sedimentary sulphur is present as sulphide minerals, such as pyrite. Conversely, a decrease in total sulphur in marine sediments would suggest either a decrease in the supply of sulphate or a decrease in the importance

of bacterial sulphate reduction. For example, if there is a decrease in the sulphate and/or bacterial reduction, then this would decrease the amount of  $\text{H}_2\text{S}$  available to react with cations (e.g.,  $\text{Fe}^{2+}/\text{Fe}^{3+}$ ) to produce sulphide minerals (e.g., pyrite).

Downward diffusion and sulphur fixation by bacteria living in sediments that accumulated centuries earlier are important processes that complicate the interpretation of the sulphur elemental and isotopic data in marine sediments (Jørgensen and Kasten, 2006). In such cases, quoting Jørgensen and Kasten (2006), “... *the age of the particular authigenic mineral does not correspond to the age of the sediment layer, in which it is formed, but is much younger. Counter-intuitive as it may seem, in the case of downward moving sulphidization fronts the age of the mineral precipitate becomes younger with increasing sediment depth. From these considerations, it becomes obvious that the post-depositional alterations of mineral phases generated in this way complicate and even prevent interpretation of the geochemical environment during the time of original sediment deposition...*” Despite this ominous statement, the elemental and isotopic sulphur data in this thesis are carefully interpreted, but with caution. Any uncertainty in the interpretation is clearly highlighted.

In the following discussion, high total sedimentary sulphur values are interpreted to represent a strong association with sapropel and sapropelic sediments, thus with high total organic carbon values. High total sedimentary sulphur values can also represent the presence of pyrite in the sediment.

#### *5.2.4 Stable Isotopic Composition of Sedimentary Sulphur*

The  $\delta^{34}\text{S}$  values of sulphide minerals in sedimentary rocks show wide variations, ranging from  $\sim -45\text{‰}$  to  $\sim +42\text{‰}$  (Brownlow, 1979). Much of these variations are due to bacterial reduction of the sulphate ion ( $\text{SO}_4^{2-}$ ) to hydrogen sulphide ( $\text{H}_2\text{S}$ ). In nature, the extent of bacterial fractionation may be quite variable, depending on the rate and continuity of the relevant biogeochemical reactions, the availability of organic matter and oceanographic environmental conditions. Negative  $\delta^{34}\text{S}$  values in sediments signify bacterial fractionation. The presence of reduced sulphur in marine sediments is a key indicator of microbial sulphate reduction. In cases where the stable isotopic ratio is determined in total sedimentary sulphur, rather than the sulphur-bearing host mineral phase, then the  $\delta^{34}\text{S}$  values reflect the relative contributions of sulphur from pore water or adsorbed sulphate, sulphide and organic matter (Brownlow, 1979).

Providing all other conditions are met (e.g., readily available organic matter), fractionation due to bacterial sulphate reduction is dependent on whether the benthic conditions represent an open or closed system (e.g., Goldhaber and Kaplan, 1980; Thode, 1991). Open systems provide a renewable source of seawater sulphate, which allows the bacteria to preferentially fractionate, absorbing the lighter  $^{32}\text{S}$  isotope and preserving it in the sediment record. However, in cases of closed systems (i.e., poor renewal of marine waters), only a limited amount of seawater sulphate is available. Here, the bacteria reduce all of the accessible sulphate, therefore the final isotopic ratio is equal to that of the original seawater sulphate (Thode, 1991). Sufficient burial and pore-water diffusion can also create closed system conditions. In this case, sulphate-reducing bacteria use up

both the light  $^{32}\text{S}$  and heavy  $^{34}\text{S}$  isotopes, and even use sulphate provided by adjacent sedimentary layers via diffusion. This results in the closed system effect, producing isotopic signatures akin to the local seawater sulphate. Often, this process is associated with areas having higher rates of sedimentation (Goldhaber and Kaplan, 1980).

The  $\delta^{34}\text{S}$  composition of seawater sulphate ranges from +17‰ to +22 ‰ (Paytan et al., 1998). Thus, when the  $\delta^{34}\text{S}$  value of the sedimentary sulphur in a core ranges between these values, the data will be interpreted to represent seawater sulphate. The seawater sulphate value is important in the interpretation of the downcore  $\delta^{34}\text{S}$  data because when the  $\delta^{34}\text{S}$  values become depleted, the simplest interpretation is that  $^{32}\text{S}$  was preferentially extracted from the seawater sulphate pool by sulphate-reducing bacteria. Thus, an upward transition from strongly positive to strongly negative  $\delta^{34}\text{S}$  values in a core should represent an incoming supply of seawater which would have provided the ideal conditions for bacterial sulphate reduction leading to a shift in the sulphur isotopic values to progressively more negative values. Vinogradov et al. (1962; as referenced in Holser et al., 1988) found that the isotopic fractionation by bacterial sulphate reduction ranges between approximately -34‰ to approximately -19‰ in the Black Sea.

An abrupt transition in the  $\delta^{34}\text{S}$  values in a core, closely corresponding to similarly abrupt changes in other multi-proxy data over a few centimetres thickness (or few tens of years in age) cannot be fully reconciled with the migration of a zone of diffusion, and therefore must reflect a near-real-time change in the palaeo-environment. For example, a dramatic shift in the  $\delta^{34}\text{S}$  values in core MAR05-50 that is recorded from 7,500 to 6,300 cal yr BP correlates exactly with a dramatic faunal turnover from Caspian

to Mediterranean ostracod species: this example is fully discussed in Sections 5.3 and 5.4. Because the ostracod assemblage of the sediments is independent of molecular diffusion, this shift in the  $\delta^{34}\text{S}$  values can only be interpreted as representing real-time changes in the palaeo-environment. Less abrupt isotopic changes may represent a diagenetic overprint that post-dates the sediments at that stratigraphic level.

#### *5.2.5 Ratios of TOC/TS and TS/TOC*

The values of TOC/TS and TS/TOC are calculated by a straightforward division of one elemental weight percent by the other, but provide important information about the ratio of carbon to sulphur present in the sediments. These ratios can yield details about the palaeo-environmental deposition conditions.

The ratio of total organic carbon content to total sulphur content (TOC/TS) is used to determine depositional salinity conditions. Berner (1984) and Raiswell and Berner (1986) defined a ratio of  $2.8 \pm 0.8$  to be the normal-marine value for Quaternary sediments deposited under an oxic water column. Values ranging from 3 to 6 are considered to indicate sediments of brackish settings, while TOC/TS values  $>10$  imply freshwater conditions (Berner and Raiswell, 1983). Leventhal (1983) and Berner (1989) proposed that sediment with TOC/TS ratios less than the oxic marine value of 2.8 have been deposited under anoxic conditions. The premise for this interpretation is based on the fact that in anoxic conditions, there is a higher degree of sulphate reduction, which consumes the organic material (and therefore, reduces the TOC amount) and produces higher TS (e.g., pyrite) amounts. So mathematically, the larger the value of TS in relation to TOC, the smaller the ratio will be.

Given that the TS/TOC ratio is the inverse of TOC/TS, interpretations are essentially the inverse of those outlined above. As noted in Rullkötter (2006), sediments with high TS/TOC ratios indicate anoxic depositional environments because the consumption of the readily available organic matter by bacteria produces excess H<sub>2</sub>S, which leads to increased pyrite precipitation and thus a higher TS weight percent. Given the TOC/TS benchmark of 2.8 for the oxic/anoxic transition, the resulting inverse benchmark is simply 0.357. Any values higher than this potentially indicate an anoxic water column at the time of deposition. In practise, intervals hosting anoxic sediments are better interpreted using TS/TOC ratios while variations within oxic sediments can be assessed in more detail using TOC/TS ratios. TOC/TS ratios are especially useful because they can be used to differentiate between freshwater, brackish and oxic marine sediments.

In the context of this thesis, however, the reader is reminded that each of the three composite cores show moderate bioturbation, as well as abundant micro- and macro-fauna throughout. These organisms and ichnofabrics require the presence of some degree of dissolved oxygen within the benthic environment in order to sustain life, with the exception of the *Chondrites* trace fossil, as it is known indicator of seafloor dysoxia with anoxic sediments and pore waters (e.g., Bromley and Ekdale, 1984). As a result, carbon to sulphur ratios that plot within the anoxic sediment ranges (TOC/TS < 2.0 and TS/TC > 0.5) are likely not indicators of fully anoxic conditions. These situations will be clearly noted and interpreted as low dissolved oxygen environments or dysoxia.

Table 1: Summary of the ranges of parameters (Section 5.2) used for identification of depositional environments in this thesis.

Geochemical Indicators of Various Organic Matter and Depositional Environments					
TOC	$\delta^{13}\text{C}$	TS	$\delta^{34}\text{S}$	TOC/TS	TS/TOC
Normal Marine Sediments: <0.1% to <0.3% (Holser et al., 1988)	$\text{C}_3$ Plants: -23‰ to -31‰ (Meyers, 1994)	Normal Marine Sediments: <0.1% to 0.2% (Holser et al., 1998)	Seawater Sulphate: +17‰ to +22‰ (Paytan et al., 1998)	Freshwater: >10 (Bernier and Raiswell, 1983)	Normal Oxidic Marine Quaternary Sediments: <0.357 (modified from Rullkötter, 2006)
Sapropelic Muds: 0.5% to 2.0% (Kidd et al., 1978)	$\text{C}_4$ Plants: -9‰ to -17‰ (Meyers, 1994)	Euxinic/Sulphidic Bottom Waters: 1.0 to 1.2% (Masuzawa et al., 1992)	Sulphate Reduction (Black Sea): -19‰ to -34‰ (Vinogradov et al., 1962)	Brackish: 3-6 (Bernier and Raiswell, 1983)	Anoxic Sediments: >0.357 (modified from Rullkötter, 2006)
Sapropels: >2% (Kidd et al., 1978)	Lacustrine Algae: -25‰ to -30‰ (Meyers, 1994)		Range of $\delta^{34}\text{S}$ in Sedimentary Rocks: -45‰ to +42‰ (Brownlow, 1979)	Normal Oxidic Marine Quaternary Sediments: 2.8 ± 0.8 (Bernier, 1986)	
$\delta^{13}\text{C}$ Marine End Member: -22‰ (Fontugne, 1983)	Marine Algae: -20‰ to -25‰ (Meyers, 1994)			Anoxic Sediments: <2.8 (Leventhal, 1983; Bernier, 1989)	
$\delta^{13}\text{C}$ Terrestrial End Member: -28‰ (Modified from Deines, 1980)					

### 5.3 Interpretation of Geochemistry from MAR05-50

Carbon and sulphur elemental and isotopic geochemistry, as well as carbon to sulphur ratios, the sediment source fractions and the composite core lithology were converted to the time domain (Figure 21) using the MAR05-50 age model (Table 8). Within the framework of regional Units A, B and C, the geochemical data can be interpreted as follows.

#### 5.3.1 Unit C

Regional Unit C extends from the base of the core (~11,500 cal yr BP) to the  $\alpha_1$  unconformity (hiatus extrapolated to start at ~10,735 cal yr BP). The organic carbon is isotopically light (~-27‰), which indicates that the source is predominately (>80%) terrestrial or lacustrine. At ~11,200 cal yr BP, there is a slight increase in the quantity of TS and an associated positive shift to high  $\delta^{34}\text{S}$  values >+10‰. This could indicate a temporary increase in microbial sulphate reduction and pyrite production. Since there is an associated shift in the  $\delta^{34}\text{S}$  to isotopically heavier values, this would indicate that benthic conditions resembled a closed system. Presumably the microbes were not able to preferentially fractionate the sulphur isotopes due to the limited quantities of seawater sulphate available (Thode, 1991). Excluding a peak of 8.1 at the base of the core, TOC/TS ratios in Unit C are approximately 2.3, which according to Leventhal (1983) and Berner (1989) potentially indicate deposition under anoxic conditions. Given that the ratio is not consistently <3, it cannot be conclusively stated that the bottom waters on this part of the Black Sea shelf were deficient in oxygen during the entirety of Unit C.

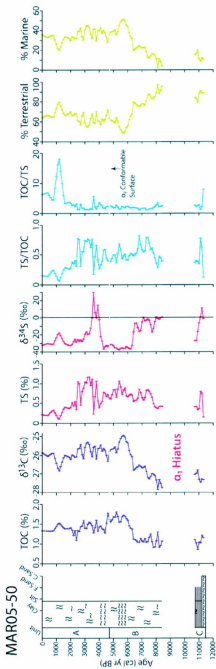


Figure 21: Carbon and sulphur geochemical results of composite core MAR05-50 presented in the time domain. Geochemical data were converted using the Ager and Tinner programs, as well as the age model (Table 8; Figure 19) as discussed in Chapter 3.

Instead, the TOC/TS values in the range ~3–6 might indicate normal brackish waters (Table 12; Berner and Raiswell, 1983). However, since the TS values decrease toward the  $\alpha_1$  hiatus, this indicates a decrease in sulphide minerals in the sediment and, in turn, a decrease in the activity of sulphate reducing microbes. Excluding a short-duration peak (involving two samples and averaging ~0.77%), the TS values for Unit C average ~0.31%, which is only slightly higher than the TS content of normal marine sediments (<0.1% to 0.2%; Holser et al., 1988). Coupled with the borderline oxic/anoxic predictions from the TOC/TS and TS/TOC ratios, the available data are compatible with the proposal of predominately brackish benthic conditions with reduced oxygen levels (but not anoxic) for this time interval (e.g., as proposed by Mudie et al., 2007; Marret et al., 2009; Mertens et al., 2012).

Overall, the geochemical findings indicate that the depositional environment of Unit C was likely brackish in salinity, with low to moderate rates of microbial sulphate reduction indicated by the low amount of total sulphur. There is evidence for poor bottom water oxygenation during this interval (i.e., dysoxia), based on the TOC/TS ratio. Organic carbon that was deposited during this time is  $^{34}\text{S}$ -depleted, which indicates that its source was either from terrestrial input (e.g., fluvial, aeolian) or from primary production in the upper water column by lacustrine species of algae (Meyers, 1994).

### 5.3.2 Unit B

Regional Unit B begins at the resumption of sedimentation after the  $\alpha_1$  hiatus at ~8,420 cal yr BP and extends to the  $\alpha_2$  conformable surface at ~4,700 cal yr BP (Figure 21). This unit shows a general trend of increasing marine organic matter deposition

(beginning at <10% marine fraction before 8,000 cal yr BP, increasing to >40% by 6,000 cal yr BP). Throughout this unit,  $\delta^{34}\text{S}$  becomes more negative and TS values increase. This pattern is indicative of microbial sulphate reduction (e.g., Berner, 1984). From ~8,149 cal yr BP to ~6,400 cal yr BP, the  $\delta^{34}\text{S}$  values range from ~0‰ to -17‰ but at 6,300 cal yr BP there is a sudden shift to more negative (less than -30‰) values. This is in association with a slight increase in the amount of TS found in the sediments. The sudden isotopic shift could indicate the presence of a constant supply of seawater sulphate (that is, an open system such as a permanent, sustained connection with the Mediterranean that today is associated with a two-way hydrological flow system). This would allow the colonies of microbes to flourish, preferentially incorporating the light  $^{32}\text{S}$  isotope during respiration and resulting in increased accumulation of sedimentary sulphur. TS/TOC ratios for Unit B are greater than 0.357 (excluding one value of 0.283 at 8,100 cal yr BP), indicating that the benthic conditions might have been anoxic at the time of deposition (Rullkötter, 2006), although persistent bioturbation suggests otherwise (see below).

Overall, the geochemistry of Unit B indicates a transition in the depositional environment from brackish to more marine salinities. The organic carbon isotopic signature becomes increasingly marine, which could mean that there is (1) a decrease in terrestrial sourcing and an increase of marine algae primary productivity, (2) a transition from lacustrine-type algae to marine-type algae productivity, or (3) potentially both. The increase in sulphate reduction and sulphide formation suggests that oxygen levels in the benthic environment and near-surface sediments became lower with time. This is

believed to be a direct result of development, by ~6,300 cal yr BP, of a sustained two-way flow system between the Black Sea and the Mediterranean Sea, through the Bosphorus Strait and other connecting water bodies, allowing the microbial community to thrive.

### *5.3.3 Unit A*

Regional Unit A ranges from ~4,700 cal yr BP to the sediment water interface (roughly present day) (Figure 21). The organic carbon content in this unit is relatively stable at ~1.25% TOC and the organic matter fractions are ~70% terrestrial and ~30% marine, on average. The TOC/TS ratio remains ~2.1, indicating marine salinities and oxygen-deficient depositional environments, until ~2,500 cal yr BP. From this point onward, there is a general upward increase in TOC/TS caused by upward declining TS (Figure 21). This is likely not due to actual changes in the basinal water chemistry, but instead is attributed to incomplete early diagenesis. The fixation of sulphur by sulphate-reducing bacteria is interpreted to not be complete above this core depth (~150 cm), so the sulphur destined for precipitation and burial may still be in the pore water and not bound in relatively insoluble sulphide minerals. As a result, this would decrease the amount of TS, and consequently increase the TOC/TS ratio. By the same principle, the general upward decreasing trend in the TS is not believed to be indicative of a decrease in the availability of sulphur.

The sulphur isotopes are mostly negative throughout Unit A, indicating bacterially-driven isotopic fractionation. However, at ~4,200 cal yr BP, there is a sudden shift to positive, isotopically heavy values that lasts until ~3,400 cal yr BP. Above and below this interval, TS weight percentages are of ~1.0% or higher. According to

Masuzawa et al. (1992), TS values in this order indicate euxinic or sulphidic benthic conditions. Associated  $\delta^{34}\text{S}$  values vary between 0‰ – +29.7‰. There are two potential scenarios that could produce these results. Either, (1) this pattern could indicate a period of time when the inflow of Mediterranean waters had weakened, reducing the availability of sulphate for only ~600 yr BP. As a result of this briefly closed system, the microbial fauna could not support their preferential fractionation of the light  $^{32}\text{S}$  isotope. Consequently, the sedimentary  $\delta^{34}\text{S}$  values are closer to those of seawater sulphate (e.g., Thode, 1991). Interestingly, the timing of this weakened exchange correlates within the  $\alpha_2$  hiatus in core MAR02-45 (Figure 19). Or, (2) the closed system effect could be due to burial and diffusion of sulphate from adjacent sedimentary layers (Goldhaber and Kaplan, 1980). During this time frame, the sedimentation rate in core MAR05-50 is slightly elevated in relation to the surrounding time intervals (Figure 19). It is important to note that (a) this environmental change is only present in the sulphur data, as the carbon and ostracod (Section 5.4) data show no discernable shifts and (b) the time of this minor event may not be correctly portrayed in Figure 21. Due to the issues of diffusion during diagenesis and sulphur fixation, neither an exact time nor duration can be determined accurately. In order to decide which one of the two scenarios described above is most probable, an understanding of the thickness of the two-way flow compared to the present-day thickness of the layers is needed. The height of the sea-level, the excess water budget in the Black Sea basin (i.e., riverine input + precipitation – evaporation), and the strength of the Mediterranean inflow are the predominant factors controlling the thicknesses of the individual layers of the two-way flow. It is very difficult to predict the past river influx

and the precipitation versus evaporation in the Black Sea. There are conflicting views about the prevailing climate of the landmass surrounding the Black Sea: Ryan et al. (1997a,b, 2003) and Major et al. (2002) suggested that the Black Sea remained evaporative between 10,000 and 3,000  $^{14}\text{C}$  yr BP (~11,150 and 2,755 cal yr BP), whereas Hiscott et al. (2007a,b), Mudie et al. (2007) and Mertens et al. (2012) suggested that the Black Sea region during the interval from 11,000 to 3,000  $^{14}\text{C}$  yr BP (~12,630 to 2,733 cal yr BP) was very pluvial and not evaporative. Thus, the balance between evaporation and precipitation cannot be unequivocally deciphered within the scope of this thesis. Sea-level is a parameter that can be better evaluated. Fairbanks (1989) suggested that global sea-level nearly reached its present height around 4,000  $^{14}\text{C}$  yr BP (~3,995 cal yr BP) and that it has not changed since. However, a sea-level curve published by Chepalyga (2002) for the Black Sea suggests that there have been ~5–15 m fluctuations in the sea level since ~6,000  $^{14}\text{C}$  yr BP (~6,400 cal yr BP). A notable drop of ~15 m in the sea level is proposed to have occurred at ~4,500  $^{14}\text{C}$  yr BP (~4,700 cal yr BP; Chepalyga, 2002). This proposal was later criticized by Giosan et al. (2006) who argued that the level of the Black Sea has remained stable in this time frame based on work in the Danube delta, only to oscillate between -2 m and +1.5 m of its present day level. Although the results of this thesis would generally support the putative sea-level drop (Chepalyga, 2002) as it coincides with the prominent enrichment in  $\delta^{34}\text{S}$  of ~30-40‰ at ~4,200 cal yr BP (Figure 21), additional data are needed to unequivocally determine which of the above two potential scenarios is correct.

Regional Unit A as a whole has geochemical signatures of a marine depositional environment, akin to the upper part of regional Unit B. Benthic conditions were oxygen poor, potentially anoxic at times, and sulphate-reducing bacteria were present, concentrating the lighter  $^{32}\text{S}$  isotope in early-diagenetic sulphide minerals. From ~4,000–3,400 cal yr BP, the sulphur geochemistry suggests a slight change in benthic conditions, possibly due to a temporary reduction in the availability of seawater sulphate as a result of a change in the volume of incoming Mediterranean bottom waters or due to an increase in the rate of burial. As well, the modern zone of early diagenesis appears to affect sediments younger than ~2,500 cal yr BP, with apparently incomplete precipitation of sulphide minerals so that TS values are lower than anticipated.

#### **5.4 MAR05-50 Micropalaeontology Correlation**

Fellow MSc student Lorna Williams conducted a palaeoecological study using ostracods found within cores MAR05-50P and MAR05-51G as proxies (Williams, 2012). Her results can be compared with the geochemical data (Figure 22). Ostracods are microcrustaceans, ranging from 0.3–30 mm in length, that live at the sediment–water interface, whose fossils can be found from the Cambrian through to present day (Athersuch et al., 1989). They are sensitive to variations in water chemistry, and many Black Sea ostracods have well known salinity tolerances or preferences. Although there are 43 different species of ostracods in cores MAR05-50P and MAR05-51G, they can be divided into two main assemblages: Ponto-Caspian (brackish) and Mediterranean (marine) (Williams, 2012). The species at the base of composite core MAR05-50 are almost entirely brackish, while those at the top of the core are almost entirely marine (Figure 22). There is a

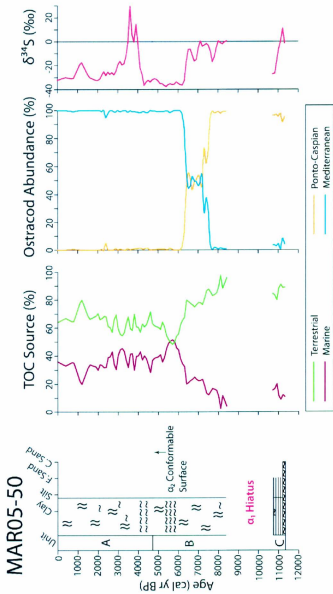


Figure 22: Correlation between organic carbon sources, sulphur isotopes and ostracod species abundance in composite core MAR05-50. Ponto-Caspian species survive in brackish waters while Mediterranean species thrive in higher salinities. Ostracods were collected, identified and counted as part of the Williams (2012) MSc thesis. Modified from Williams (2012).

noticeable transitional zone from ~7,500 cal yr BP to ~6,300 cal yr BP where the brackish species are replaced by marine species. This occurs within the zone of rising marine organic matter input identified in this thesis. The  $\delta^{34}\text{S}$  isotopes oscillate within the range of 0‰ to -20‰ during this transitional zone until 6,300 cal yr BP, when there is a sudden negative shift to values less than -30‰. This shift is associated with the establishment of a sustained two-way flow system and benthic bacterial sulphate reduction, and occurs at the exact same time as the end of the ostracod assemblage transitional zone (Figure 22). Below this transitional zone, the marine fraction is <15%, however by the time the Mediterranean species take over, the marine fraction of the TOC increases to over 40%. This indicates that the benthic conditions at the core site were governed by low salinity (~5‰) until about 7,500 cal yr BP. Then, high salinity Mediterranean water must have entered the area, bringing with it the marine ostracod assemblage. Those species flourished and eventually dominated the seafloor, completely replacing the brackish assemblage by ~6,300 cal yr BP.

## **5.5 Geochemical Interpretations of cores MAR02-45 and MAR05-13**

### *5.5.1 Core MAR02-45 Geochemistry*

Hiscott et al (2007b) published carbon and sulphur elemental and stable isotopic geochemistry (Figure 23) from composite core MAR02-45 in the depth domain, but for correlation purposes, the data have been converted to the time domain using the age model presented in Chapter 3 (Figure 19). Conclusions drawn by Hiscott et al. (2007b), recast into the time domain, are presented below.

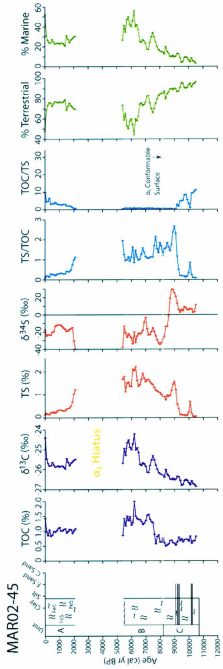


Figure 23: Geochemistry of composite core MAR02-45 (from Hiscott et al., 2007b) presented with respect to time. Data was converted using the age model presented in Chapter 3 (Table 9).

At the base of Unit C, beginning at ~10,700 cal yr BP, TOC sources were predominately terrestrial and/or lacustrine (~90%), total sulphur was under 0.5% and  $\delta^{34}\text{S}$  showed positive isotopic ratios ranging from 0 – +10‰. However, beginning at ~9,400 cal yr BP, there was a marked increase in total sulphur to >1% that coincided with a rapid increase in  $\delta^{34}\text{S}$  which peaked at ~+30‰ by 8,800 cal yr BP. This shift caused the isotopic signature of the sedimentary sulphur to be slightly higher than that of modern seawater sulphate (+17–22‰, Paytan et al., 1998). At this point, there was a dramatic decrease in TS and  $\delta^{34}\text{S}$  until the  $\alpha_1$  conformable surface at ~8,200 cal yr BP. Hiscott et al. (2007b) attribute the  $\delta^{34}\text{S}$  positive shift to a “first pulse” of Mediterranean water into the area rather than a permanent connection. If the connection were complete, the incoming seawater would have provided ideal conditions for bacterial sulphate reduction leading to a negative shift in the sulphur isotopic values to ~-30‰ to -40‰. Instead, Hiscott et al. (2007b) attributed the rise to ~+30‰ to be the result of the complete conversion of the newly introduced sulphate from the Mediterranean waters to sulphides by sulphate-reducing bacteria, but with no replenishment of sulphate so that the final pool of sulphur in the sedimentary sulphides preserved the isotopic signature of seawater sulphate. This was therefore a closed system. The supply of seawater sulphate is reflected in the associated TS peak, as well as an abundance of fine pyrite particles in the palynology samples of the associated intervals (Mudie et al., 2007).

Throughout Unit B (~8,200–5,465 cal yr BP), the  $\delta^{34}\text{S}$  signature becomes lower, averaging around -20‰, and total sulphur ranges between 1–2% until the  $\alpha_2$  unconformity. Hiscott et al. (2007b) attribute this to a rise in sulphate concentration just

before the deposition of Unit B that allowed sulphate-reducing microbes to grow and flourish just below the sediment–water interface. A continuous sulphate supply is indicative of a permanent, two-way connection with the Mediterranean Sea.

Unit A begins after the  $\alpha_2$  hiatus ( $\sim 2,050$  cal yr BP) and extends to the sediment–water interface, which is considered to be roughly present day. Hiscott et al. (2007b) have hypothesized that the  $\alpha_2$  hiatus represents a break in sedimentation on the inner and middle shelf due to surface currents strong enough to prevent deposition. TOC and  $\delta^{13}\text{C}$  stabilize ( $\sim 1.0\%$  and  $\sim 25.7\%$  respectively) while TS gradually decreases toward 0%, representing the same early diagenetic signature as at site MAR05-50 where sulphate reduction and fixation of sulphur in the sediment has not proceeded to completion. The authors note that the TS values directly above the  $\alpha_2$  hiatus are lower than the values in the sediments below the hiatus, however the sulphur isotopes are still  $^{34}\text{S}$ -depleted ( $\sim 20\%$ ) which indicates bacterial fractionation of sulphur associated with poorly oxygenated benthic conditions.

#### *5.5.2 Core MAR05-13 Geochemistry*

The carbon and sulphur geochemistry of MAR05-13 was run in 2007 as part of the Cranshaw (2007) undergraduate dissertation project (Figure 24). As part of that project, the geochemistry was compared in the depth domain to the results from core MAR02-45. The main conclusions of Cranshaw (2007) are converted and summarized here in the time domain using the age model presented in Chapter 3 (Table 10; Figure 19).

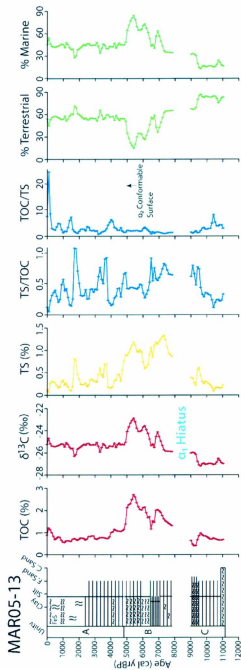


Figure 24: Carbon and sulphur geochemical data for composite core MAR05-13 presented in the time domain. Original data are from Cranshaw (2007) and has been converted from depth to time using the age model presented in Chapter 3 (Table 10).

### *5.5.2.1 MAR05-13 Sulphur Isotopes*

The methodology used for determining the sulphur isotopic values in cores MAR05-13P and MAR05-04G was slightly different than the method described in this thesis (Chapter 2, Section 2.4.4). Instead, one run was performed on the Finnegan MAT252 isotope-ratio mass spectrometer whereby elemental and isotopic abundances were determined for both carbon and sulphur simultaneously. The amount of carbon in these southwestern Black Sea sediments is much greater than the amount of sulphur and, as a result, it is very difficult to obtain reliable data for both elements at the same time. Since the ion counts from the isotope-ratio mass spectrometer are expressed as electric potential, the digital output results in peaks (measured in mV) that can be converted into elemental and isotopic abundances. However, the smaller the peak size, the higher the margin of error. For the MAR05-13 samples, there was a wide variety of sulphur peak sizes dispersed randomly throughout the runs, and several samples had to be re-run since the sulphur peak sizes were far too small to quantify. In order to correct for this, isotope size correction standards (e.g., IAEA-S-2 (NZ-2) and IAEA-S-3, Table 2) were included at the beginning of the run. Since then, industry standards have changed to include two sets of size correction standards: one set at the beginning and one set (including varying standard sizes) at the end of the run, which has increased the accuracy of the data calibration (A. Pye, pers. comm., 2012). Peak size only affects the sulphur isotopic data, and as a result, the margin of error for the MAR05-13 results in Cranshaw (2007) is much greater than that of MAR05-50. Consequently, it was decided that the  $\delta^{34}\text{S}$  data for

MAR05-13 would not be included in comparisons with cores MAR02-45 and MAR05-50.

#### 5.5.2.2 MAR05-13 Geochemical Results

Unit C at the base of the core ranges in age from ~11,236 cal yr BP to ~8,970 cal yr BP at the  $\alpha_1$  unconformity (Figure 24). This unit has low TOC and TS values, as well as low  $\delta^{13}\text{C}$  signatures that are enriched in the light isotope  $^{12}\text{C}$ . The organic carbon sources are predominately terrestrial (~82–100%), indicating high fluvial input and/or lacustrine algal production relative to marine sources (i.e., primary marine algal production in the upper water column). Cranshaw (2007) proposed that these geochemical signatures indicate little watermass exchange with the Mediterranean Sea, suggesting that the Black Sea was a closed basin during this time period. Toward the top of Unit C, beginning at ~9,800 cal yr BP, there is a gradual increase in TS as well as  $\delta^{13}\text{C}$ . Because these changes coincide with a negative shift in  $\delta^{34}\text{S}$  (not included in this study), Cranshaw (2007) proposed that there was increased bacterial reduction of sulphate to sulphide, indicating the potential onset of watermass communication with the Mediterranean Sea.

Unit B extends from the  $\alpha_1$  unconformity to the  $\alpha_2$  level, spanning 7,805 cal yr BP to ~4,800 cal yr BP (Figure 24). TOC and TS values exceed those in Unit C and the  $\delta^{13}\text{C}$  signatures indicate enrichment in the heavy isotope  $^{13}\text{C}$  relative to Unit C. Organic carbon is increasingly marine in origin, ranging from 30–70% marine. Given that the total sulphur in the sediment is consistently high, (~1%) Cranshaw (2007) interpreted a

consistent connection with the Mediterranean Sea and a stratified water column, providing idea benthic conditions for bacterial sulphate reduction.

Unit A begins at ~4,800 cal yr BP and extends to the present day at the sediment–water interface (Figure 24). TOC and  $\delta^{13}\text{C}$  decrease relative to Unit B, but show relatively consistent values (~1% and ~-25‰ respectively). Organic carbon is 30–40% marine. The total sulphur amounts in Unit A oscillate, but are slightly lower than in Unit B. Cranshaw (2007) noted that these geochemical signatures are consistent with continued Mediterranean connection and the initiation of basin-wide low-oxygen bottom-water condition in the Black Sea. Because the TS values always remain below 1.0%, the bottom waters were probably not anoxic, but they must have been dysoxic (cf., Masuzawa et al., 1992).

#### **5.6 Geochemical correlations between MAR05-50, MAR02-45 and MAR05-13**

Correlations between cores MAR05-50, MAR02-45 and MAR05-13 provide a complete geochemical record for the southwestern Black Sea shelf for the entire Holocene Epoch. The hiatus in sedimentation present at the  $\alpha_1$  unconformity in cores MAR05-50 and MAR05-13 is absent in MAR02-45, and *vice versa* for the  $\alpha_2$  unconformity, resulting in data from at least one site for each time step throughout the Holocene.

The MAR05-50 core site is found within a hydrodynamically complex region ~30 km north-northwest of the Strait of Bosphorus. Here the Mediterranean watermass inflow is spreading northward within a saline channel as a distinct bottom watermass, and

significant volumes are spilling over the banks of that channel as the saline water crosses the shelf (R.N. Hiscott, pers. comm., 2012). The Black Sea surface waters are being advected eastward in the Rim Current system. The amount of organic matter preserved in the surface sediments through time is thus a function of the strengths of the surface and bottom currents, the temporal changes in the contribution of organic matter from terrestrial and marine sources, as well as the consumption of organic matter by micro- and meio-benthos and by sulphate reduction. Therefore, the broad and generalized statements about environmental change described below must be view within this context.

The core sites at MAR02-45 ~85 km west-northwest of the Bosphorus Strait and at MAR05-13 ~165 km east-southeast of the Bosphorus entrance represent open shelf settings in the southwestern Black Sea. Here, hydrodynamic conditions are controlled by temporal changes in the position and strength of the Rim Current and the anticyclonic Bosphorus and Sakarya eddies, temporal changes in the depth of the chemocline, the spatial and temporal changes in the contribution of organic matter from terrestrial and marine sources, as well as the oxidation and consumption of organic matter.

#### *5.6.1 Carbon Results*

The elemental carbon and carbon isotopic data (Figure 25) and by association, the balance between marine and terrestrial/lacustrine organic-matter sources (Figure 26) for cores MAR05-50, MAR02-45 and MAR05-13 exhibit good correlations with one another. Both the TOC and the  $\delta^{13}\text{C}$  values follow the same general trend, beginning with low TOC and low  $\delta^{13}\text{C}$  of the organic matter at the base of all three cores and then showing notable increases in the amount of TOC and concomitant enrichments in  $\delta^{13}\text{C}$  values.

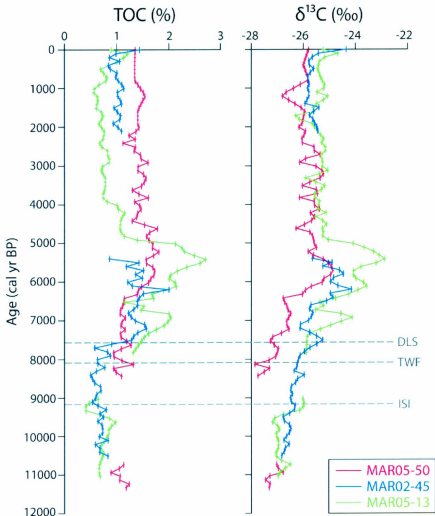


Figure 25: Carbon elemental and isotopic values for cores MAR05-50 (red), MAR02-45 (blue) and MAR05-13 (green) with respect to time. The timing of the initial saline inflow (ISI; from Major et al., 2002), the beginning of a strong, sustained two-way flow (TWF; from Hiscott et al., 2007b) and the disappearance of lacustrine species (DLS; from Ryan et al., 1997) have been added for interpretation purposes.

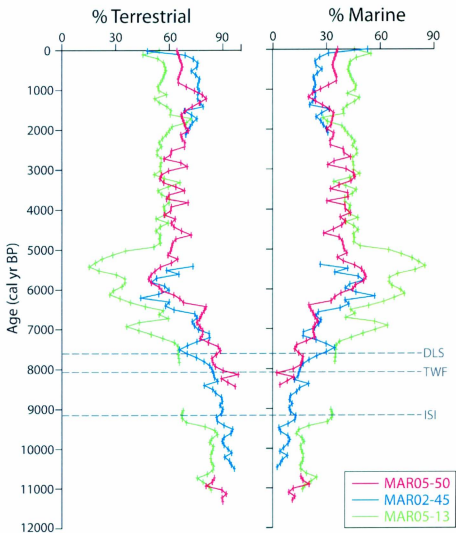


Figure 26: Organic carbon sediment source fractions for cores MAR05-50 (red), MAR02-45 (blue) and MAR05-13 (green) presented with respect to time. Grey lines denote the initial saline inflow (ISI; from Major et al., 2002), the beginning of a strong, sustained two-way flow (TWF; from Hiscott et al., 2007b) and the disappearance of lacustrine species (DLS; from Ryan et al., 1997).

Furthermore, the source of the organic matter similarly shows a noticeable, but progressive shift in both cores MAR02-45 and MAR05-13 from predominantly a terrestrial and/or lacustrine source immediately prior to the first, possibly temporary, influx of saline Mediterranean water at 9,160 cal yr BP (Major et al., 2002) to a clearly marine source by ~6,000 cal yr BP (Figure 26). The time of first influx is not captured in MAR05-50 due to the presence of the  $\alpha_1$  hiatus. These trends are clearly associated with the initial reconnection of the Black Sea with the Mediterranean Sea.

Despite these broad similarities in trends, there are minor, albeit noticeable differences between the TOC and  $\delta^{13}\text{C}$  values of core MAR05-50 compared to cores MAR02-45 and MAR05-13 (Figure 25). For example, the TOC values are slightly higher and the  $\delta^{13}\text{C}$  values are lower at the base of core MAR05-50. These small differences can be interpreted as a slightly higher rate of organic matter influx as well as more terrestrial organic matter input to the site of core MAR05-50 close to the exit of the Bosphorus Strait compared with the background sedimentation characteristic of open shelf core sites to the west (i.e., MAR02-45) and east (i.e., MAR05-13) of the Bosphorus Strait.

Another small difference is the onset of increasing TOC and coincident enrichment in  $\delta^{13}\text{C}$  values. In MAR02-45 and MAR05-13 these changes occur across the interval bracketed by the TWF (~8,085 cal yr BP) and DLS (~7,570 cal yr BP; Figure 25). In these two cores the increasing TOC and enrichment in  $\delta^{13}\text{C}$  values continue up-core to ~6,200 cal yr BP in core MAR02-45 and ~5,400 cal yr BP in core MAR05-13. However, the correlative onset of increasing TOC and enrichment in the  $\delta^{13}\text{C}$  values in core MAR05-50 does not occur until ~6,300 cal yr BP. These small differences are interpreted

to result from an initially lower rate of organic matter influx to the MAR05-50 core site. The timing of the increase in TOC and broadly synchronous enrichment in the  $\delta^{13}\text{C}$  values in core MAR05-50 at  $\sim 6,300$  cal yr BP correspond exactly with the establishment of a fully marine ostracod assemblage in the same core (Figure 22; Williams, 2012).

In core MAR05-13 the interval marked by relatively high TOC percentages as well as heavy  $\delta^{13}\text{C}$  values occur between  $\sim 7,570$  cal yr BP and  $\sim 4,900$  cal yr BP (Figure 25). In core MAR02-45, a similar interval occurs between  $\sim 7,570$  cal yr BP and the onset of the  $\alpha_2$  hiatus at  $\sim 5,465$  cal yr BP. These intervals in these two cores represent a prominent increase in the marine primary productivity across the southwestern Black Sea (Figures 25, 26; Cranshaw, 2007; Hiscott et al., 2007b). In core MAR05-13, dramatic transitions from higher to lower TOC values and from higher to lower  $\delta^{13}\text{C}$  values occur at  $\sim 4,900$  cal yr BP. This transition is not observed in core MAR02-45 because of the  $\alpha_2$  hiatus. The correlative transitions in core MAR05-50 are notably subdued, and are recorded 500 year later at  $\sim 4,400$  cal yr BP (Figures 25, 26). The notably lower TOC percentage throughout the  $\sim 6,300$  cal yr BP to  $\sim 4,400$  cal yr BP interval and the  $\sim 500$  year lag in core MAR05-50 collectively suggest that strong saline inflow from the Bosphorus Strait continued for an additional 500 years, and during that period counteracted regional tendencies. The near synchronous increases in the  $\delta^{13}\text{C}$  values from  $\sim 7,500$  cal yr BP to  $\sim 4,400$  cal yr BP in all three cores suggest that marine primary productivity was notably increased in the southwestern Black Sea during this time. Despite this increase in marine primary productivity (as indicated by the heavier  $\delta^{13}\text{C}$  values), TOC values remain relatively low in cores MAR05-50 and MAR02-45 (Figures

25, 26). This difference between the TOC content of core MAR05-13 and the other two cores can be interpreted as (i) higher marine productivity at site MAR05-13 than that at sites MAR05-50 and MAR02-45 or (ii) a notable increase in the amounts of organic matter preservation at site MAR05-13 compared to the other two sites. The fact that all three cores show high marine primary productivity, as indicated by the  $\delta^{13}\text{C}$  values, suggests that the greater TOC values in core MAR05-13 may best be interpreted as an improvement of the preservation state of organic carbon on the seafloor at this core site.

The geochemical data presented in this thesis (particularly cores MAR05-13 and MAR05-50) show that the marine environment stabilized after  $\sim 4,400$  cal yr BP and a steady biogeochemical system became established in the southwestern Black Sea. Core MAR02-45 is mute about this interval because of the  $\alpha_2$  hiatus. The near constant TOC and  $\delta^{13}\text{C}$  values in all three cores strongly suggest that the physical and chemical oceanographic makeup of the Black Sea shelves became established at  $\sim 4,400$  cal yr BP, with little subsequent deviation from these conditions. This is to say that changes in climate, oceanography and benthic conditions, including organic matter preservation versus degradation rates, were less severe after  $\sim 4,400$  cal yr BP, leading to no drastic changes in the data.

### *5.6.2 Sulphur Results*

Despite the interpretation difficulties associated with sulphate diffusion and sulphide fixation, the data for elemental sulphur and its isotope  $\delta^{34}\text{S}$  from cores MAR05-50, MAR02-45 and MAR-13 show remarkably good general correlation (Figure 27). In all three cores, the TS values follow similar trends, starting with low values close to (or

marginally higher in the case of MAR05-50) the values found in normal oxygenated marine/lacustrine sediments (<0.1% to 0.2%; Holser et al., 1988) and increasing so as to approach levels characteristic of euxinic bottom waters (>1.0% to 1.2%; Masuzawa et al., 1992) after the initiation of sustained two-way flow at ~8,085 cal yr BP (Hiscott et al., 2007b). At ~1,500 cal yr BP, the TS values in all three cores decrease to <0.2%, indicating that sulphur fixation is not complete in the near-surface sediments because of ongoing early diagenesis.

During the interval from ~11,500 cal yr BP to ~9,160 cal yr BP (i.e., onset of ISI; Figure 27) all three cores show very low TS, suggesting an oxygenated environment. The  $\delta^{34}\text{S}$  values hover around 0‰, suggesting that this was probably a closed system, preventing preferential isotopic fractionation. This interpretation is in keeping with the previously published work which suggested that the bottom waters in the Black Sea were isolated (e.g., Hiscott et al., 2007a,b). During this time, vigorous outflow of Black Sea waters into the Marmara Sea (Hiscott et al., 2002, 2007a,b) would have prevented the penetration of Mediterranean waters into the Black Sea basin.

The interval from the ISI (i.e., ~9,160 cal yr BP) to the TWF (~8,085 cal yr BP) is only fully represented in core MAR02-45. In core MAR05-13 the record from ~8,970 cal yr BP to ~7,805 cal yr BP is missing (i.e.,  $\alpha_1$  hiatus), whereas in core MAR05-50 the sedimentary record from ~10,735 cal yr BP to ~8,420 cal yr BP is similarly missing. In core MAR02-45, both the TS and  $\delta^{34}\text{S}$  values show a marked positive shift at ~8,085 cal yr BP (Figure 27). Hiscott et al. (2007b) interpreted this shift to be the result of a “first pulse” of sulphate-rich Mediterranean bottomwater into the Black Sea, where sulphate

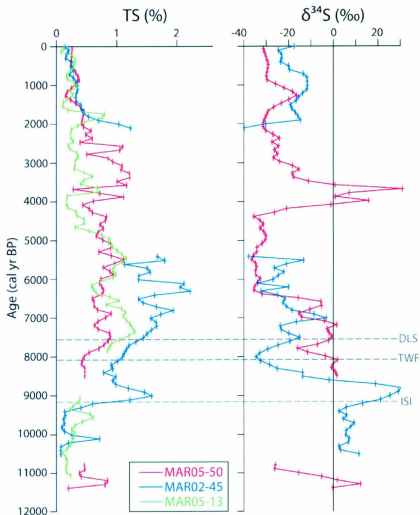


Figure 27: Elemental and isotopic sulphur data for cores MAR05-50 (red), MAR02-45 (blue) and MAR05-13 (green) presented in age domain. Sulphur isotopic data for core MAR05-13 are not included for reasons explained in section 5.5.2.1. The superimposed grey lines denote the initial saline inflow (ISI; from Major et al., 2002), the beginning of sustained two-way flow (TWF; from Hiscott et al., 2007b) and the disappearance of lacustrine species (DLS; from Ryan et al., 1997).

reduction occurred, but bacterial fractionation could not occur due to the existence of a closed biogeochemical system. In core MAR05-50 the sedimentary record starts at ~8,420 cal yr BP and continues up-core without interruption to the present-day depositional surface. In the upper portion of the ISI – TWF interval the geochemical proxies show lower amounts of sulphide production, as indicated by the TS and less bacterial isotopic fractionation as indicated by the  $\delta^{34}\text{S}$  values hovering around 0‰ until the initiation of the sustained two-way flow (TWF, Figure 27). During the  $\alpha_1$  hiatus, the currents at the core site were probably strong enough to prevent deposition (Hiscott et al., 2007b). The sedimentary environment at the core site soon after the  $\alpha_1$  hiatus was probably not conducive for the immediate establishment of a healthy benthic community, accounting for the observed geochemical signatures.

During the period from the initiation of sustained two way flow (i.e., TWF) at ~8,085 cal yr BP to ~5,000 cal yr BP the TS and the  $\delta^{34}\text{S}$  values show increasing rates of preferential isotopic fractionation associated with sulphate reduction in an open system as indicated by a negative shift to  $^{34}\text{S}$ -depleted values and the related sulphide precipitation as indicated by the marked increase in the weight percentage of TS (Figure 27). This interval is also distinct in the TOC and  $\delta^{13}\text{C}$  data, since organic matter becomes increasingly marine from ~8,085 cal yr BP to ~5,000 cal yr BP (Figures 25, 26). The progressive increase in the contribution of marine organic carbon follows a good correlation with the depletion of  $\delta^{34}\text{S}$  values, suggesting that the efficiency of sulphate reduction paralleled an enrichment in  $\delta^{13}\text{C}$  values (compare Figures 25 and 27). It is noteworthy that at ~6,300 cal yr BP the sulphur isotopic values reached their most

depleted values ( $\sim 30$  to  $\sim 35\%$ ), indicating an open geochemical system for sulphate reduction (Figure 27) coincident with the termination of the ostracod faunal turnover zone from Ponto-Caspian to Mediterranean assemblages (Figure 22; Williams, 2012).

In core MAR02-45 the zone of increasingly active sulphate reduction only extends from  $\sim 8,085$  cal yr BP to  $\sim 5,465$  cal yr BP (Figure 27). TS values in core MAR02-45 remain consistently higher than those in cores MAR05-13 and MAR05-50. In fact the TS values are invariably  $>1.0\%$  and as high as  $\sim 2.0\%$ . These high TS values suggest that the MAR02-45 core site must have been situated very close to the chemocline so that the conditions were near euxinic (Raiswell and Berner, 1985). However, the presence of a continuous and diverse ostracod fauna from core MAR02-45 through this interval (Evans, 2004; Hiscott et al., 2007b) precludes the rise of the chemocline to the core site, and strongly suggests that the core site must have been situated beneath oxygenated or dysoxic bottom waters.

The broad shape of the TS curve for core MAR05-50 matches reasonably well with that of core MAR02-45. In core MAR05-13, the interval from  $\sim 8,085$  cal yr BP to  $\sim 5,000$  cal yr BP (Figure 27) shows two zones where the TS values exceed  $1.0\%$ . These intervals are interpreted similar to the correlative interval in core MAR02-45. Except for a very short interval at  $\sim 5,500$  cal yr BP, the TS values in core MAR05-50 does not reach  $>1.0\%$  level, suggesting that the core site was probably oxic/dysoxic during this entire interval. The presence of an abundant and diverse ostracod fauna throughout core MAR05-50 strongly suggests that bottom waters at the core site were oxic (Williams,

2012), possibly explaining the generally lower TS values in core MAR05-50 than in the other two cores.

### *5.6.3 Results from Carbon to Sulphur and Sulphur to Carbon Ratios*

At the base of the cores MAR05-50, MAR02-45 and MAR05-13, the general trend of the TOC/TS ratios shows that sediments were deposited in oxic marine environments with  $\text{TOC/TS} > 2.8$ . This interpretation confirms the earlier assessment of TS and the  $\delta^{34}\text{S}$  data which suggested that this interval was probably oxic to dysoxic. Although this interval from ~11,000 cal yr BP to ~9,160 cal yr BP at the MAR02-45 core site remained oxic, data from core MAR05-13 show that the environment at this site gradually transitioned toward lower oxygen levels at or around 9,600 cal yr BP, prior to the ISI boundary at ~9,160 cal yr BP (Figure 28). Core MAR05-50 does not contribute any information for conditions at this time due to the  $\alpha_1$  hiatus which spans from ~10,735 cal yr BP to ~8,420 cal yr BP (Figure 28). Ignoring time gaps at hiatuses, near constant TS/TOC ratios that are greater than 0.357 begin in all three cores at the ISI boundary and continue until ~2,000 cal yr BP with only occasional, small oscillations toward oxic marine values. After ~2,000 cal yr BP, the data provide the false suggestion of an up-core “freshening” of salinities because of incomplete sulphur fixation in the zone of early diagenesis – because the TS denominator of the TOC/TS ratio is artificially low close to the sediment-water interface, graphs show high or “fresh” TOC/TS values (Figure 28).

The principal concern with the above general interpretation of the carbon to sulphur ratio data is that it suggests that the cores recovered sediments that were deposited in very poorly oxygenated to anoxic conditions. For the data collected from the

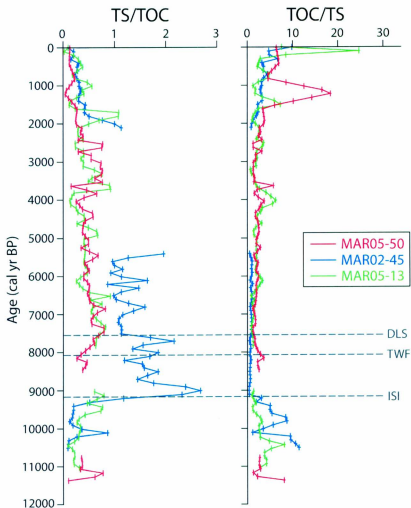


Figure 28: Ratios of TOC/TS and TS/TOC for cores MAR05-50 (red), MAR02-45 (blue) and MAR05-13 (green) presented in age domain. The grey lines denote the initial saline inflow (ISI; from Major et al., 2002), the beginning of sustained two-way flow (TWF; from Hiscott et al., 2007b) and the disappearance of lacustrine species (DLS; from Ryan et al., 1997). The purple shaded zones indicate the standard deviation of the oxic to anoxic transition for normal marine sediments (Bernier, 1986; Rullkötter, 2006).

southwestern Black Sea shelf, it is clear that this statement cannot be true. Firstly, the palaeoceanographic data suggest that the chemocline in this region has never risen to the relatively shallow depths of the three cores (collected in present waters depths of  $\leq 91$  m below sea-level), rather that it had been much lower, progressively rising to the present day level (Deuser et al., 1974; Glenn and Arthur, 1984). Secondly, all three cores show moderate burrow mottling and both MAR02-45 and MAR05-50 possess abundant and diverse ostracod fauna for the entire Holocene interval (Evans, 2004, Williams, 2012, respectively). The presence of these lacustrine and marine fauna precludes the existence of euxinic or anoxic bottom waters on the southwestern Black Sea shelf, and implies that, at the very least, the benthic environment was dysaerobic (i.e., 0.1-1.0 mL/L dissolved oxygen content; Raiswell and Berner, 1985, 1986). It may be that the thresholds proposed in the literature (Table 12) are too restrictive when applied to the samples from the Black Sea shelves.

As mentioned in section 5.2.5, a better explanation for the ratio data of the three cores is that, given the presumed positions of the core sites above the chemocline throughout the Holocene, the benthic conditions might have oscillated between predominantly oxic and dysoxic. This is supported by the fact that most of the ratio data hovers around the normal oxic marine/lacustrine value of Quaternary sediments ( $2.8 \pm 0.8$  as defined by Berner, 1986). Taking the lowest value consistent with the standard deviation, that is  $\text{TOC/TS} = 2.0$ , more data points become consistent with oxic conditions.

## Chapter Six: Discussion

The results of geochemical analyses in 89 sediment samples extracted from a long piston core (MAR05-50P) and its nearby gravity core (MAR05-51G) recovered from the southwestern Black Sea shelf provide a detailed palaeo-oceanographic and palaeo-environmental reconstruction of the region for the last ca. 11,500 years. The comparison of the geochemical data from these cores with two other cores collected west-northwest and east of the exit of the Strait of Bosphorus into the Black Sea allow a regional and holistic evolution of the southwestern Black Sea to be deduced. The following discussion is presented under the following four headings based on chronological age: (i) the last glacial maximum – interglacial transition, (ii) the period of basin isolation, (iii) initial saline inflow and evolution of the two way flow exchange and (iv) the Late Holocene to Present.

### 6.1 Last Glacial Maximum – Interglacial Transition (~20,000 – ~12,630 cal yr BP)

Major et al. (2002) and Ryan et al. (2003) indicated that the Black Sea level stood at ~-140 m during the last glacial maximum, some ~20,000 cal yr BP. During this time they proposed that the Black Sea was a fresh water lake disconnected from the Marmara Sea. The timing of the early post-glacial reconnection of the Black Sea with the Marmara Sea is in dispute. The proponents of the *Oscillating Sea-Level Hypothesis* suggested that between ~17,000 and ~11,000 14C yr BP (~19,735 and ~12,630 cal yr BP) the warming of the climate associated with the glacial-interglacial transition caused waters from the Caspian Sea to enter the Black Sea (referred to, by the authors, as the Late Neoeuxinian

lake) via the Manych Spillway, which connected the Caspian Sea and the Black Sea (Yanko-Hombach et al., 2004; Kerey et al., 2004; Yanko-Hombach, 2007). This event apparently raised the level of the Black Sea to  $\sim$ 20 m, but also produced a small outflow into the Marmara Sea. On the other hand, the proponents of the *Flood Hypothesis* suggested that at  $\sim$ 16,000 to 14,700  $^{14}\text{C}$  yr BP ( $\sim$ 18,760 to  $\sim$ 17,380 cal yr BP) the level of the Black Sea rose to the breach depth of the Strait of Bosphorus, permitting outflow into the Marmara Sea (Ryan et al., 2003). Hiscott et al. (2002, 2007a) mapped a lower delta (i.e., their  $\Delta 2$ , also see Chapter 1) across the northeastern Marmara Sea shelf immediately south of the mouth of the Strait of Bosphorus. They speculated that  $\Delta 2$  might have developed during this period of strong Black Sea outflow associated with this early reconnection between the Black Sea and the Marmara Sea. So the dispute between the *Oscillating Sea-Level Hypothesis* and the *Flood Hypothesis* is in the timing and duration of the initial post-glacial reconnection of the Black Sea with the Marmara Sea: the *Oscillating Sea-Level Hypothesis* suggests that this connection occurred  $\sim$ 975 cal years earlier than suggested by the *Flood Hypothesis*, and that the connection was not severed until the Younger Dryas cool interval some  $\sim$ 11,000  $^{14}\text{C}$  yr BP ( $\sim$ 12,630 cal yr BP). In contrast, the *Flood Hypothesis* suggests that the connection was a short-duration event and that the Black Sea experienced an evaporative drawdown starting at  $\sim$ 14,700  $^{14}\text{C}$  yr BP ( $\sim$ 17,380 cal yr BP), when the level of the Black Sea dropped to  $\sim$ 120 m below present level (Major et al., 2002; Ryan et al. 2003; Hiscott et al., 2007a,b). There is no disagreement between the *Outflow Hypothesis II* and the *Flood Hypothesis* in the timing and duration of this early reconnection because Hiscott et al. (2007a) had no data

pertaining to this time period, and therefore accepted the scenario advanced by Ryan et al. (2003). The core data presented in this thesis do not address these controversies, because the cores do not penetrate into sediments of older than ~11,500 cal yr BP.

## **6.2 Period of basin isolation (~11,300 – ~9,160 cal yr BP)**

The data presented in Chapter 4 and interpreted in Chapter 5 show that from ~11,500 cal yr BP until ~9,160 cal yr BP the southwestern Black Sea shelf was a brackish environment with oxic bottom waters, albeit with depleted levels of dissolved oxygen relative to normal marine conditions. The organic matter preserved in the sediments during this time was of predominantly lacustrine and/or terrestrial origin. The stable isotopic data clearly show that the interval from ~11,500 cal yr BP to ~9,160 cal yr BP represented a closed system which prevented preferential isotopic fractionation during bacterial sulphate reduction, and also prevented abundant sulphide mineral formation. Hiscott et al. (2002, 2007a) suggested that during this interval, specifically between ~10,000 and ~9,000  $^{14}\text{C}$  yr BP (~11,150 to ~9,660 cal yr BP) a prominent delta was developing in the northeastern Marmara Sea (i.e.,  $\Delta 1$ , see Chapter 1). They evaluated the sediment-discharge budgets of all the rivulets around the southern exit of the Strait of Bosphorus, and decided that the discharges of these small streams were not sufficient to account for the sediments contained within this delta. They also noted that the seismic-stratigraphic architecture of the delta shows vertical aggradation during the period of seaward progradation, suggesting that the delta was building into a rising sea-level. Based on these characteristics, they attributed the development of this delta to vigorous outflow from the Black Sea across the Strait of Bosphorus. The core data from MAR05-

50, MAR02-45 and MAR05-13 do not allow consideration of the level of the Black Sea during this interval, and cannot directly support or refute the existence of the vigorous outflow from the Black Sea during this time interval. However, the data do indicate that there is no geochemical and isotopic evidence for inflow of Mediterranean water into the Black Sea during this time. This conclusion is further supported by a recent MSc thesis (Williams, 2012) which shows that this interval is solely represented by a very distinctive Ponto-Caspian brackish ostracod assemblage. The closed oxic bottom-water system in the Black Sea, the Ponto-Caspian ostracod assemblage and vigorous outflow of Black Sea waters into the Marmara Sea are not unrelated observations. The interpretation of a closed geochemical system with oxic bottom waters is in keeping with previously published work which suggested that the bottom waters in the Black Sea were isolated (e.g., Hiscott et al., 2007a,b). It is entirely possible that vigorous outflow of Black Sea waters into the Marmara Sea (Hiscott et al., 2002, 2007a,b) prevented any significant inflow of Mediterranean waters into the Black Sea basin during this time, thus creating an closed geochemical system. Furthermore, because there was no inflow of Mediterranean water into the Black Sea, the shelf waters were brackish, thus the Ponto-Caspian ostracod assemblage flourished.

According to the *Flood Hypothesis*, the Black Sea should have experienced a sustained evaporative drawdown from ~10,000 to ~8,400 <sup>14</sup>C yr BP (~11,150 to 9,160 cal yr BP), when the Black Sea level is proposed to have dropped to ~95 m below its present level (Major, 2002; Ryan et al. 2003). These authors further argued that the level of the Marmara Sea rose before that in the Black Sea, breaking a hypothetical sediment dam

across the Bosphorus Strait (Ryan et al., 1997a,b) at 9,160 cal yr BP, catastrophically inundating the Black Sea, creating the “Great Flood”. The fact that the geochemical data in cores MAR02-45 and MAR05-13 confirm fully subaqueous deposition and continuous sedimentation at these core sites shows that the Black Sea level was never as low as -95 m as suggested by the proponents of the *Flood Hypothesis* (e.g., Major, 2002; Ryan et al. 2003).

### **6.3 Initial saline inflow and two way flow exchange (~9,160 – ~4,400 cal yr BP)**

The geochemical data from core MAR02-45 shows that Mediterranean waters penetrated into the Black Sea starting at ~9,160 cal yr BP. This interval is within the  $\alpha$  hiatus in cores MAR05-50 and MAR05-13. This age (i.e., 9,160 cal yr BP) exactly matches the age proposed by others for catastrophic flooding (Major, 2002; Ryan et al. 2003). However, the proponents of the *Outflow Hypothesis* used the data from core MAR02-45 to counter the arguments of a catastrophic flooding event (Hiscott et al., 2007b). These authors interpreted the notable enrichment in the  $\delta^{34}\text{S}$  values and the co-occurring increase in the TS amounts as a first pulse of Mediterranean water inflow into the Black Sea. They argued that the inflow of Mediterranean water was brief and short lived, but that ... *it was enough to shift the  $^{87}\text{Sr}/^{86}\text{Sr}$  ratio to open marine values, but not enough to maintain an isotopic offset between a heavy reservoir of sea water sulphate and a light reservoir in the sulphide minerals in the sediments ...* Hiscott et al. (2007b) used micropaleontological and geochemical data to suggest that the inflow of the Mediterranean waters into the Black Sea during the “first pulse” was not a catastrophic event, and was not caused by the breach of a sediment dam, but was simply caused by the

weakening of the outflow to the point that some Mediterranean water could penetrate as a tongue of bottom water. This interpretation is supported by palynological studies in the Black Sea (e.g., Mudie et al., 2007) which suggest that the initial first pulse of incoming sulphate was reduced and entirely preserved as abundant  $<5\mu\text{m}$  particles of pyrite. They showed that at  $\sim 9,000$   $^{14}\text{C}$  yr BP ( $\sim 9,660$  cal yr BP) the landmass around the southern Black Sea included a vegetation dominated by *Quercus cerris*, *Tilia*, *Fagus*, *Castanea*, *Ulmus* as well as shade ferns, aquatics and swamp plants. This flora indicates a palaeoclimate with warm winters and year-around precipitation, directly contradicting the proposal by Major et al. (2002) and Ryan et al. (2003) of a dry climate needed to drive an evaporative drawdown of the Black Sea.

Whether the 9,160 cal yr BP event is associated with catastrophic flooding or simply with the weakening of Black Sea outflow remains conjectural: the primary data presented in this thesis for core MAR05-50 do not cover this time interval. These data do, however, provide insight into the oceanographic history after 8,420 cal yr BP, several hundred years before the initiation of sustained two-way flow at 8,085 cal yr BP (as proposed by Hiscott, 2007b).

The elemental carbon and carbon isotopic data show concomitant increases in  $\delta^{13}\text{C}$  values from  $\sim 7,500$  cal yr BP to  $\sim 4,400$  cal yr BP in all three cores, suggesting that marine primary productivity increased in the southwestern Black Sea during this time. In core MAR05-50, the sedimentary record re-started after the  $\alpha_1$  hiatus at  $\sim 8,420$  cal yr BP and continued up-core without interruption to the present-day depositional surface. Between  $\sim 8,420$  cal yr BP and  $\sim 7,570$  cal yr BP the data discussed in Chapters 4 and 5

show lower amounts of sulphide production, and low rates of sulphate reduction. But, this condition rapidly changed by ~7,000 cal yr BP as the environment progressively transitioned into a fully open marine environment with oxic/dysoxic bottom conditions and very active bacterially mediated sulphate reduction in the near-surface sediments.

The period from ~7,000 cal yr BP to ~5,000 cal yr BP shows that the southwestern Black Sea shelf became an open marine environment with organic matter supplied from predominantly marine sources. The data further indicates that the progressive increase in the contribution of the marine organic carbon correlated with depleted  $\delta^{34}\text{S}$  values, suggesting that sulphate reduction accelerated along with the enrichment in the  $\delta^{13}\text{C}$  values. Parallel studies of ostracods shows that at ~6,300 cal yr BP the establishment of an open system with an essentially unlimited supply of sulphate coincided with the termination of the ostracod faunal turnover from Ponto-Caspian to Mediterranean assemblages (Williams, 2012). The interpretations for this time period are in good agreement with the *Outflow Hypothesis* (e.g., Hiscott et al., 2007b), the *Flood Hypothesis* (e.g., Major, 2002; Ryan et al. 2003) as well as the *Oscillating Sea Level Hypothesis* (Kerey et al., 2004; Yanko-Hombach et al., 2004; Yanko-Hombach, 2007). The only possible exception is that the *Oscillating Sea Level Hypothesis* suggests that the watermass communication between the Black Sea and the Marmara Sea may have occurred via a waterway to the east of the modern Bosphorus Strait, called the Sakarya Bosphorus. The data from this thesis cannot add any new insight to this claim.

#### **6.4 Late Holocene to Present (~4,400 – present day)**

The geochemical data presented in this thesis (particularly cores MAR05-13 and MAR05-50) show that the marine environment stabilized after ~4,400 cal yr BP and an open biogeochemical system was well established in the southwestern Black Sea by this time. During this time the sea level reached the present day elevation, allowing full-scale watermass communication across the Strait of Bosphorus. The consistent geochemical and stable isotopic signatures of the sedimentary data in all three cores across the southwestern Black Sea shelf strongly suggest that a full and open-marine biogeochemical environment had reached equilibrium by ~4,400 cal yr BP.

This study clearly provides a glimpse into the evolution of the World's largest anoxic and euxinic basin, and illustrates how seemingly small oceanographic events had profound impacts on the biogeochemical conditions that prevailed in this basin. The preservation of organic matter in ancient semi-isolated basins, such as the North Sea and the Jeanne d'Arc Basin must have had similar evolutionary histories, controlled by palaeo-environmental and palaeo-oceanographic constraints. Thus, it is true that the Black Sea forms an analogue for these ancient deposits, and will continue to provide much needed insight into various fundamental problems in the fields of geology and environmental science.

## Chapter Seven: Conclusion

### 7.1 Summary

The main scientific objective of this thesis was to acquire and interpret the carbon and sulphur geochemical data and to use these as proxies to develop a local palaeo-environmental history, as well as to add to the existing regional history of the southwestern Black Sea shelf. The interpretation of the lithological and geochemical data in cores MAR05-50P and MAR-51G and the correlation with regional composite cores MAR02-45 and MAR05-13 reveals the following salient conclusions.

- A 787 cm-long composite core MAR05-50 was constructed using a 737 cm long-piston core (MAR05-50P) and the upper 50 cm portion of a 157 cm long-gravity core, collected from the southwestern Black Sea shelf on the eastern levee of a prominent saline density-current channel. Radiocarbon dates were collected using a variety of carbonate fossils, which were then calibrated to correct for the apparent reservoir offsets and to conform with tree-ring chronology. An age model using nine radiocarbon dates was constructed to use for interpretation and correlation purposes, resulting in a model that spanned from ~11,500 cal yr BP to present day. The same procedure was used by the author to create age models for the previously published composite cores MAR02-45 (~10,720 cal yr BP to present) and MAR05-13 (~11,236 cal yr BP to present).
- Euhedral gypsum crystals were discovered within the >63-micron fractions of cores MAR05-50P and MAR05-51G, and had been noted to be “growing” on the

exteriors of the wet sediment cores post-collection in the cold storage unit. Given that gypsum is a sulphate mineral, the precipitation of gypsum crystals could have had a detrimental effect on the sulphur isotope values presented in this thesis, especially if the crystallization involved isotopic fractionation or if the HCl treatment dissolved some of the gypsum during sample processing. The abundance of gypsum crystals was counted in each sample interval, and 15 crystals were selected for compositional analysis with a scanning electron microscope which confirmed that they were in fact gypsum. Literature review provided insight on the solubility of gypsum in HCl, which revealed that with the applied treatments, no dissolution of gypsum should have occurred. Stable isotope mass spectrometry results from six difference samples revealed that there was no issue with isotopic fractionation of the sediment samples associated with gypsum precipitation. Thus, it was concluded that the presence of post-collection gypsum has no effect on the integrity of the sulphur geochemistry presented in studies such as this.

- The reservoir age models used in this thesis were based on calibrated radiocarbon dates collected from fossil material. Due to various reservoir effects, the carbon bound in the dated material required calibration in order to interpret the information with respect to solar years, as well as with dates from other regions and environments. The reservoir correction for the Black Sea area is under debate and awaits final resolution based on ongoing studies. A thorough literature review suggests that correction values of 280  $^{14}\text{C}$  yr for dates younger than 7,500  $^{14}\text{C}$  yr BP and 415  $^{14}\text{C}$  yr for dates older than 7,500  $^{14}\text{C}$  yr BP are most appropriate. These

values were used in the Oxcal 4.1 program, which calibrated the samples using the Marine09 calibration curve and the selected reservoir correction value.

- Lithological correlations between cores MAR05-50, MAR02-45 and MAR05-13 show good regional continuity of facies across the southwestern Black Sea shelf. Three regional units (Units A, B and C) are present in all cores, which lie directly above the shelf-crossing transgressive  $\alpha$  unconformity. The local  $\alpha_1$  unconformity (located above the  $\alpha$  unconformity) is found within cores MAR05-50 and MAR05-13, while core MAR02-45 intersects the shallower  $\alpha_2$  unconformity that is absent at the other two core sites. Given that the  $\alpha_1$  and  $\alpha_2$  unconformities are located at different sub-seabed depths, their associated hiatuses in sedimentation also occur at different times. The lithological correlations provide a complete and holistic view for the interval from ~11,500 cal yr BP to present day in the southwestern Black Sea shelf during the Holocene.

- Geochemical results from regional Unit C in MAR50-50 (~11,500 to ~10,635 cal yr BP) show predominately terrestrial/lacustrine organic matter sources (>80%) and a low amount of sulphide mineral production. Interpretation of this unit suggests that the core site was a closed benthic system, as indicated by the lack of preferential isotopic fractionation associated with small TS percentages. Carbon to sulphur ratios lie within the oxic/anoxic boundary region, excluding one TOC/TS peak of 8.1, which possibly indicates benthic waters transitional between brackish and fresh. As a result, this unit is interpreted to have formed in a poorly oxygenated, closed system, supporting the brackish benthic faunal and floral assemblages

suggested by other researchers in this area for this time period (e.g., Mudie et al., 2007; Marret et al., 2009; Mertens et al., 2012; Williams, 2012).

- The results from regional Unit B in MAR05-50 (~8,420 to ~4,700 cal yr BP) show a transitional environment with upwardly increasing marine organic matter input (up to >40% by 6,000 yr BP) and increasing rates of sulphate reduction as indicated by increasing TS (approaching ~1.0%). The benthic environment was likely an open marine system by ~6,300 cal yr BP, indicated by the presence of preferential isotopic fractionation by sulphate reducing microbes ( $\delta^{34}\text{S}$  values from -30‰ to -35‰). The TS/TOC ratios lie above the oxic/anoxic boundary (TS/TOC >0.357), which typically indicates anoxic conditions. However, this geochemical signal is only taken to imply low dissolved oxygen contents, as the presence of moderate bioturbation, as well as benthic fauna (i.e., ostracods) require some amounts of dissolved oxygen to sustain life.

- The carbon elemental and isotopic geochemistry from regional Unit A (~4,700 cal yr BP to the sediment-water interface) indicates a shift to an equilibrium ecosystem similar to that of the modern day. TOC is stable at ~1.25% with ~70% of the organic material originating from terrestrial sources while the other ~30% is derived from marine sources. The carbon to sulphur ratios are low (TOC/TS ~2.1), but within the standard deviation of published values for normal oxic marine sediments. The benthic conditions initially mimicked those observed in Unit B with respect to sulphate reduction; however, there was an anomalous peak of positive  $\delta^{34}\text{S}$  isotopes at ~4,200 cal yr BP lasting some 600 years, associated with an increase in

the TS amounts (~1.0% and above). This short-lived change in the rate and isotopic signatures of sulphate reduction was probably associated with a brief drop in the Black Sea level to ~-15 m at ~4,500 cal yr BP which resulted in a temporary reduction in the availability of seawater sulphate. At ~3,400 cal yr BP, this situation had resolved, and the benthic environment returned to an open-system equilibrium.

- All three cores (MAR05-50, MAR02-45 and MAR05-13) show a notable upward decline in sulphur values in the uppermost ~150 cm. This is attributed to the incomplete precipitation of sulphide minerals in the zone of early diagenesis. Sulphate reduction processes have not gone to completion, therefore all the potential sulphur has not yet been fixed in the sediments. Thus, no palaeo-environmental information could be taken from the sulphur geochemistry of these uppermost sediments.

- Correlation of the geochemical results with the ostracod data also collected in MAR05-50P and MAR05-51G as part of a recent master's thesis (see Williams, 2012) further define the regional Unit B transitional zone. The ostracods clearly show a prominent transition from a solely brackish assemblage to a solely marine assemblage from ~7,500 to ~6,300 cal yr BP. The end of this transition is synchronous with the shift in the sulphur isotopes to open-system sulphate reduction patterns. This confirms the interpretation of a full and renewable (from the viewpoint of sulphate) open-marine benthic environment during the deposition of this unit.

- Correlations between core MAR05-50, and nearby cores MAR02-45 and MAR05-13 provides the opportunity to create a continuous geochemical history of

the southwestern Black Sea shelf. Trends in the carbon, sulphur and ratio data shows good correlation, with only minor variations attributed to local core site variability. For example, there is a local delay of the onset of increasing TOC and enrichment in marine  $\delta^{13}\text{C}$  values in core MAR05-50 in relation to core MAR02-45, which is attributed to an initially lower rate of organic matter influx to the core site MAR05-50. All three cores agree with the basic regional successions of: (i) Unit C indicating brackish conditions, followed by (ii) the transitional Unit B marking the onset of persistent saline inflow from the Mediterranean Sea and (iii) Unit A showing the establishment of an open-marine benthic system at equilibrium with current environmental parameters.

- The results and interpretations presented in this thesis cannot contribute to the reconnection debate until after  $\sim 11,500$  cal yr BP. The data presented in the thesis support (or cannot refute) the major points of both the *Outflow Hypothesis II* and the *Oscillating Sea-Level Hypothesis*. The data confirm the view that the benthic conditions were isolated and brackish from  $\sim 11,300$  cal yr BP until  $\sim 9,160$  cal yr BP, however cannot disprove the *Outflow Hypothesis II* suggestion that there was substantial outflow through the Strait of Bosphorus during this time interval. However, the data do not support some of the components of the *Flood Hypothesis*, which has suggested that the interval from  $\sim 11,300$  cal yr BP until  $\sim 9,160$  cal yr BP was marked by regression with the sea level situated at an elevation of  $\sim 95$  m. Given that cores MAR02-45, MAR05-13 and MAR05-50 are currently located in shallower water depths of 69 m, 75 m and 91 m, respectively, and that the cores show

constant sedimentation during this time interval, a sea level of  $-95$  m is not feasible. Specific data from core MAR05-50 cannot refute the presence of a catastrophic flooding event at 9,160 cal yr BP, as the core contains a hiatus in sedimentation through this period. After this time interval, the data are in good agreement with all three conflicting hypotheses.

## **7.2 Recommendations for Future Work**

The following recommendations are made with the intent of augmenting the current body of geological research in the southwestern Black Sea region, and specifically would complement the results and interpretations of the data presented in this thesis.

1. Ideally, a second longer core at the MAR05-50P core site would be useful to augment the results found in this thesis. This core would need to extend only  $\sim 2$  m deeper in order to penetrate through the  $\alpha$  unconformity. Results from this core would ultimately give a time constraint to the unconformity at the MAR05-50 location, as well as yield information about the evolution of the channel and the benthic conditions surrounding the development of the  $\alpha$  unconformity. Radiocarbon dates from this adjacent core could be used to further identify the age of the  $\alpha_1$  unconformity, and add to the existing age model for this site.

2. It would be beneficial to re-run the sulphur geochemistry for MAR05-13P and MAR05-04G given the issues with the sulphur isotope results from the use of an older mass spectrometer methodology. These new results could be used to assess the margin of error of the older methodology, and thus give perspective on the reliability and

reproducibility of these experiments. As well, the new data could be used to correlate with results from cores MAR05-50 and MAR02-45, in hopes of further constraining the palaeo-environmental conditions, in particular the  $\delta^{34}\text{S}$  isotope enrichment in MAR05-50 during the accumulation of regional Unit A.

3. A second long piston core at site MAR05-13P would be useful for resolving the speculations concerning compression in the lower portion of the existing core, presented in Bradley et al. (in press). The current core is 8.13 m in length, but seismic profiles across the core site suggest that the second core would need to be ~11 m in length in order to transect the level of the  $\alpha$  unconformity. This second core would be useful to constrain the age of this shelf crossing transgressive unconformity in this region of the southwestern Black Sea shelf.

4. It would be interesting to correlate the geochemical results from cores MAR05-50P and MAR05-51G with other multi-proxy data found at this core site, such as palynology and Sr-isotope geochemistry of calcareous fauna found within the sediments. This information would provide further invaluable information about the palaeo-environment (e.g., climate and salinities) at this location, further expanding and reinforcing the palaeo-environmental history of the region.

## Bibliography

- Abedon, S. T., Breitenberger, C.A., Roden, E.E., Williams, J.B. Respiration. In: Jorgensen, S.E. and Fath, B. *Encyclopedia of Ecology*. Oxford: Academic Press; 2008. p. 3010–3020.
- Adeona, K.B. Characterization of cores from the Black and Marmara seas: implications for TOC source and preservation and potential for paleoenvironmental interpretation [dissertation]. St. John's: Memorial University; 2005.
- Aksu, A.E., Hiscott, R.N., Mudie, P.J., Yaşar, D. 1999b. Organic geochemical and palynological evidence for terrigenous origin of the organic matter in Aegean Sea sapropel S1. *Marine Geology* 153, 303–318.
- Aksu, A.E., Hiscott, R.N., Mudie, P.J., Rochon, A., Kaminski, M.A., Abrajano, T., Yaşar, D. 2002a. Persistent Holocene outflow from the Black Sea to the Eastern Mediterranean contradicts Noah's Flood Hypothesis. *GSA Today* 12(5), 4–10.
- Aksu, A.E., Hiscott, R.N., Yaşar, D., İşler, F.I., Marsh, S. 2002b. Seismic stratigraphy of Late Quaternary deposits from the southwestern Black Sea shelf: evidence for non-catastrophic variations in sea-level during the last ~10 000 yr. *Marine Geology* 190, 61–94.
- Aksu, A.E., Hiscott, R.N., Kaminski, M.A., Mudie, P.J., Gillespie, H., Abrajano, T., Yaşar, D. 2002c. Last glacial-Holocene paleoceanography of the Black Sea and Marmara Sea: stable isotopic, foraminiferal and coccolith evidence. *Marine Geology* 190, 119–149.
- Allen, B.M., Power, A.M., O'Riordan, R.M., Myers, A.A., McGrath, D. 2006. Increases in the abundance of the invasive barnacle *Elminius modestus* Darwin in Ireland. *Biology and Environment* 106(2), 155–161.
- Arthur, M.A. and Dean, W.E. 1998. Organic-matter production and preservation and evolution of anoxia in the Holocene Black Sea. *Paleoceanography* 13(4), 395–411.
- Athersuch, J., Horne, D.J., Whittaker, J.E. Marine and Brackish Water Ostracods (Superfamilies Cyprodeacea and Cytheracea). *Synopses of the British Fauna (New Series)*, No. 43. Leiden: E.J. Brill; 1989.
- Bahr, A., Lamy, F., Arz, H.W., Major, C., Kwiecien, O., Wefer, G. 2008. Abrupt changes of temperature and water chemistry in the late Pleistocene and early Holocene Black Sea. *Geochemistry Geophysics Geosystems* 9, 1: 1–16.
- Berner, R.A. 1978. Sulfate reduction and the rate of deposition of marine sediments. *Earth and Planetary Science Letters* 37, 492–498.
- Berner, R.A. 1984. Sedimentary pyrite formation: An update. *Geochimica et Cosmochimica Acta* 48, 605–615.

- Berner, R.A. and Raiswell, R. 1983. Burial of organic carbon and pyrite sulfur in sediments over Phanerozoic time: a new theory. *Geochimica et Cosmochimica Acta* 47, 855–862.
- Berner, R.A. and Canfield, D.E. 1989. A new model for atmospheric oxygen over Phanerozoic time. *American Journal of Science* 289, 333–361.
- Best, R.M. 1999. Noah's Ark and the Ziusudra Epic: Sumerian origins of the Flood Myth. Enlil Press, Ft Myers, Florida.
- Bradley, L.R., Marret, F., Mudie, P.J., Aksu, A.E., and Hiscott, R.N. (in press). Assessing Holocene fossil dinoflagellate cyst records from the south-western shelf of the Black Sea. *Journal of Quaternary Science*.
- Brenna, J.T., Corso, T.N., Tobias, H.J. and Caimi, R.J. 1997. High-precision continuous-flow isotope ratio mass spectrometry. *Mass Spectrometry Reviews* 16, 227–258.
- Bromley, R.G. and Ekdale, A.A. 1984. Chondrites: A Trace Fossil Indicator of Anoxia in Sediments. *Science* 224 (4651), 872–874.
- Brownlow, A.H. *Geochemistry*. Englewood Cliffs: Prentice-Hall Inc.; 1979.
- Calder, J.A. and Parker, P.L. 1968. Stable carbon isotope ratios as indices of petrochemical pollution of aquatic systems. *Environmental Science and Technology* 2(7), 535–539.
- Canfield, D.E. 1989. Sulfate reduction and oxic respiration in marine sediments: implications for organic carbon preservation in euxinic environments. *Deep Sea Research* 36(1), 121–138.
- Canfield, D.E. 1991. Sulfate reduction in deep-sea sediments. *American Journal of Science* 291, 177–188.
- Canfield, D.E. 1994. Factors influencing organic carbon preservation in marine sediments. *Chemical Geology* 114, 315–329.
- Caspers, H., 1957. Black Sea and Sea of Azov. In: J.W. Hedgpeth (Ed.). *Treatise on Marine Ecology and Paleocology*, Geological Society of America, Memoir 67, pp. 801–921.
- Çağatay, M.N., Görür, N., Algan, O., Eastoe, C., Tchepalyga, A., Ongan, D., Kuhn, T., Kuşçu, I. 2000. Late-Glacial–Holocene palaeoceanography of the Sea of Marmara: timing of connections with the Mediterranean and Black Seas. *Marine Geology* 167, 191–206.
- Chepalyga, A. L. 2002a. Black Sea. In Velichko, A. A. (ed.) *Dynamics of Terrestrial Landscape Components and Inner Marine Basins of Northern Eurasia During the Last 130,000 Years*. Moscow, GEOS: 170–182 (in Russian).
- Codispoti, L.A., Friederich, G.E., Murray, J.W., Saka- moto, C.M. 1991. Chemical variability in the Black Sea: implications of continuous vertical profiles that

- penetrated the oxic/anoxic interface. *Deep Sea Research* 38(Suppl. 2), S691–S710.
- Cranshaw, J. Carbon and sulfur elemental and isotopic results from coring of a long piston core on the southwestern Black Sea shelf, Sakarya region: implications for communication between the Black Sea and eastern Mediterranean Sea during the last 10,000 years [dissertation]. St. John's: Memorial University; 2007.
- Degens, E.T. 1969. Biochemistry of stable carbon isotopes. In: Eglinton, E. and Murphy, M.T.J. (Eds). Springer-Verlag, New York, Heidelberg, pp. 304–329.
- Degens, E.T. and Ross, D.A. 1972. Chronology of the Black Sea over the Last 25,000 years. *Chemical Geology* 10, 1–16.
- Deines, P., 1980. The isotopic composition of reduced carbon. In: P. Fritz and J.C. Fontes (Eds.), *Handbook of Environmental Isotope Geochemistry*, pp. 329-406. Elsevier, Amsterdam.
- Deuser, W.G. 1971. Organic carbon budget of the Black Sea. *Deep-Sea Research* 18, 995–1004.
- Deuser, W.G. 1972. Late-Pleistocene and Holocene history of the Black Sea as indicated by stable-isotope studies. *Journal of Geophysical Research* 77(6), 1071–1077.
- Di Iorio, D., Akal, T., Guerrini, P., Yüce, H., Gezgin, E., Özsoy, E. 1999. Oceanographic measurements of the West Black Sea: June 15 to July 5, 1996. Report SR-305, SAC-LANTCEN: NATO, La Spezia.
- Eriksen, U., Friedrich, W.L., Bucharadt, B., Tauber, H. 1990. The Strongyle Caldera: geological, paleontological and stable isotope evidence from radiocarbon dated stromatolites from Santorini. In: Hardy, D.A., Keller, J., Galanopoulos, V.P., Flemming, N.C., Druitt, T.H. (Eds). *Thera and the Aegean World III, Proceedings of the Third International Congress, The Thera Foundation, Santorini, Greece*, 139–150.
- Eriş, K.K., Ryan, W.B.F., Çağatay, M.N., Sancar, U., Lericolais, G., Ménot, G., Bard, E. 2007. The timing and evolution of the post-glacial transgression across the Sea of Marmara shelf south of Istanbul. *Marine Geology* 243, 57–76.
- Evans, J.M. Noah's Flood: Fact or Fiction? An palaeoenvironmental study of Holocene Black Sea Ostracoda [dissertation]. London: University College London; 2004.
- Fairbanks, R.G., 1989. A 17,000-year glacio-eustatic sea level record: influence of glacial melting rates on the Younger Dryas event and deep-ocean circulation. *Nature* 342, 637–642.
- Faure, G. *Principles of Isotope Geology*. New York: John Wiley & Sons; 1977.
- Flood, R.D., Hiscott, R.N., Aksu, A.E. 2009. Morphology and evolution of an anastomosed channel network where saline underflow enters the Black Sea. *Sedimentology* 56, 807–839.

- Fontugne, M.R. 1983. Les isotope stable du carbone organique dans l'océan. Application à la paleoclimatologie. Doctorate thesis, University of Paris, 224 pp.
- Fontugne, M.R. and Calvert, S.E. 1992. Late Pleistocene variability of the carbon isotopic composition of organic matter in the Eastern Mediterranean: monitor of changes in carbon sources and atmospheric CO<sub>2</sub> concentrations. *Paleoceanography* 7(1), 1–20.
- Fontugne, M.R. and Duplessy, J.C. 1978. Carbon isotope ratios of marine plankton related to surface water masses. *Earth and Planetary Science Letters* 41, 365–371.
- Forensic Isotope Ratio Mass Spectrometry. 2012. Available from: URL: <http://www.forensic-isotopes.org>
- Fry, B. and Sherr, E.B. 1984. <sup>13</sup>C measurements as indicators of carbon flow in marine and freshwater ecosystems. *Contributions in Marine Sciences* 27, 13–47.
- Galy, V., Bouchez, J., France-Lanord, C. 2007. Determination of total organic carbon content and δ<sup>13</sup>C in carbonate-rich detrital sediments. *Geostandards and Geoanalytical Research* 31, 199–207.
- Glenn, C.R. and Arthur, M.A. 1985. Sedimentary and geochemical indicators of productivity and oxygen contents in modern and ancient basins: the Holocene Black Sea as the “type” anoxic basin. *Chemical Geology* 48, 325–354.
- Giosan, L., Donnelly, J.P., Constantinescu, S., Filip, F., Ovejanu, I., Vespremeanu-Stroe, A., Vespremeanu, E., Duller, G.A.T. 2006. Young Danube delta documents stable Black Sea level since the middle Holocene: Morphodynamic, paleogeographic, and archaeological implications. *Geology* 34 (9), 757–760.
- Glossary of Geology, 1980. R.L. Bates and J.A. Jackson (Eds). American Geological Institute, Falls Church, Virginia, 751 pp.
- Goddard Earth Sciences Data Information and Service Center (GES-DISC). 2012. Available from: [http://disc.sci.gsfc.nasa.gov/oceancolor/additional/science-focus/ocean-color/dead\\_zones.shtml](http://disc.sci.gsfc.nasa.gov/oceancolor/additional/science-focus/ocean-color/dead_zones.shtml)
- Goldhaber, M.B. and Kaplan, I.R. 1980. Mechanisms of sulfur incorporation and isotope fractionation during early diagenesis in sediments of the Gulf of California. *Marine Chemistry* 9, 95–143.
- Hagen, E., 2001. Northwest African upwelling scenario. *Oceanologica Acta* 24, S113–S128.
- Higham, T. 2012. Available from: URL: <http://www.c14dating.com>
- Hiscott, R.N., Aksu, A.E., Yas-ar, D., Kaminski, M.A., Mudie, P.J., Kostylev, V.E., MacDonald, J.C., Is-ler, F.I., Lord, A.R., 2002. Deltas south of the Bosphorus Strait record persistent Black Sea outflow to the Marmara Sea since 10 ka. *Marine Geology* 190 (1–2), 261–282.

- Hiscott, R.N., Aksu, A.E., Mudie, P.J., Kaminski, M.A., Abrajano, T., Yaşar, D., Rochon, A. 2007a. The Marmara Sea gateway since ~16ky BP: Non-catastrophic causes of paleoceanographic events in the Black Sea at 8.4 and 7.15 ky BP. In: Yanko-Hombach, V., Gilber, A. S., Panin, N. Dolukhanov, P. M. (Eds). *The Black Sea flood question: changes in coastline, climate and human settlement*. Springer, Dordrecht, The Netherlands, 89–117.
- Hiscott, R.N., Aksu, A.E., Mudie, P.J., Marret, F., Abrajano, T., Kaminski, M.A., Evans, J., Çakiroğlu, A.İ., Yaşar, D. 2007b. A gradual drowning of the southwestern Black Sea shelf: Evidence for a progressive rather than abrupt Holocene reconnection with the eastern Mediterranean Sea through the Marmara Sea Gateway. *Quaternary International* 167/168, 19–34.
- Hogan, C.M., Saundry, P. 2012. Sea of Marmara. In: Cutler J.C. Ed. *Encyclopedia of Earth*. Available from: [http://www.eoearth.org/article/Sea\\_of\\_Marmara](http://www.eoearth.org/article/Sea_of_Marmara)
- Holland, H.D. 1973. Systematics of the isotopic composition of sulfur in the oceans during the Phanerozoic and its implications for atmospheric oxygen. *Geochimica et Cosmochimica Acta* 37(12), 2605–2616.
- Holser, W.T., Schidlowski, M., MacKenzie, F.T., and Manard, J.B., 1988. Geochemical Cycles of Carbon and Sulphur. In: Gregor, C.B., Garrels, R.M., MacKenzie, F.T. and Manard, J.B. (Eds.). *Chemical Cycles in the Evolution of the Earth*. John Wiley & Sons: New York, pp. 105–174.
- İzdar, E., Murray, J.W., editors. *Black Sea Oceanography*. Dordrecht: Kluwer Academic Publishers; 1991.
- Jørgensen, B.B. and Kasten, S. 2006. Sulphur Cycling and Methane Oxidation. In: Schulz, H.D. and Zabel, M. (Eds.). *Marine Geochemistry*, 2<sup>nd</sup> edition, Springer: Berlin, pp. 271–310.
- Jørgensen, B.B., Fossing, H., Wirsén, C.O., Jannasch, H.W. 1991. Sulfide oxidation in the anoxic Black Sea chemocline. *Deep-Sea Research* 38 (2) supp. 2, S1083–S1103.
- Jørgensen, B.B., Weber, A., Zopf, J. 2001. Sulfate reduction and anaerobic methane oxidation in Black Sea sediments. *Deep-Sea Research* I 48, 2097–2120.
- Keller, W. 1981. *The Bible as History*, 2<sup>nd</sup> revised edition. William Morrow and Company, New York.
- Kerey, İ.E., Meriç, E., Tunoğlu, C., Kelling, G., Brenner, R.L., Doğan, A.U. 2004. Black Sea-Marmara Sea Quaternary connections: new data from the Bosphorus, Istanbul, Turkey. *Palaeogeography, Palaeoclimatology, Palaeoecology* 204, 277–295.
- Kidd, R.B., Cita, M.B. and Ryan, W.B. 1978. Stratigraphy of Eastern Mediterranean sapropel sequences recovered during DSDP Leg 42A and their

- paleoenvironmental significance. In: Hsü, K. et al. (Eds.) Initial Report of Deep Sea Drilling Project 42: pp. 421–443.
- Kwiecien, O., Arz, H.W., Lamy, F., Wulf, S., Bahr, A., Röhl, U., Haug, G.H. 2008. Estimated reservoir ages of the Black Sea since the last glacial. *Radiocarbon* 50, 1–20.
- Lambert, W.G. and Millard, A.R. 1969. *Atra-Hasis. The Babylonian Story of the Flood*. Clarendon, Oxford.
- Latif, M.A., Özsoy, E., Oguz, T., Ünlüata, Ü. 1991. Observations of the Mediterranean inflow into the Black Sea. *Deep Sea Research* 38(Supp. 2) S711–S723.
- Leventhal, J.S. 1983. An interpretation of carbon and sulfur relationships in Black Sea sediments as indicators of environments of deposition. *Geochimica et Cosmochimica Acta* 47, 133–137.
- Li, Z. and Demopoulos, G.P. 2005. Solubility of CaSO<sub>4</sub> Phases in Aqueous HCl + CaCl<sub>2</sub> Solutions from 283 K to 353 K. *Journal of Chemical and Engineering Data* 50, 1971–1982.
- Major, C., Ryan, W., Lericolais, G., Hajdas, I. 2002. Constraints on Black Sea outflow to the Sea of Marmara during the last glacial–interglacial transition. *Marine Geology* 190, 19–34.
- Major, C.O., Goldstein, S.L., Ryan, W.B.F., Lericolais, G., Piotrowski, A.M., Hajdas, I. 2006. The co-evolution of Black Sea level and composition through the last deglaciation and its paleoclimatic significance. *Quaternary Science Reviews* 25, 2031–2047.
- Marret, F., Mudie, P., Aksu, A., Hiscott, R.N. 2009. A Holocene dinocyst record of a two-step transformation of the Neoeuxinian brackish water lake into the Black Sea. *Quaternary International* 197, 72–86.
- Masuzawa, T., Handa, N., Kitagawa, K., Kusakabe, M. 1992. Sulfate reduction using methane in sediments beneath a bathyal “cold seep” giant clam community off Hatsushima Island, Sagami Bay, Japan. *Earth and Planetary Science Letters* 110, 39–50.
- Mertens, K.N., Bradley, L.R., Takano, Y., Mudie, P.J., Marret, F., Aksu, A.E., Hiscott, R.N., Verleye, T.J., Mousin, E.A., Smyrnova, L.L., Bagheri, S., Mansor, M., Pospelova, V., Matsuoka, K. 2012. Quantitative estimation of Holocene surface salinity variation in the Black Sea using dinoflagellate cyst process length. *Quaternary Science Reviews* 39, 45–59.
- Meyers, P.A. 1994. Preservation of elemental and isotopic source identification of sedimentary organic matter. *Chemical Geology* 114, 289–302.
- Mudie, P.J., Rochon, A., Aksu, A.E. 2002b. Pollen stratigraphy of Late Quaternary cores from Marmara Sea: land–sea correlation and paleoclimatic history. *Marine Geology* 190, 233–260.

- Mudie, P.J., Marret, F., Aksu, A.E., Hiscott, R.N., Gillespie, H. 2007. Palynological evidence for climatic change, anthropogenic activity and outflow of Black Sea water during the late Pleistocene and Holocene: Centennial- to decadal-scale records from the Black and Marmara Seas. *Quaternary International* 167–168, 73–90.
- Murray, J.W., Jannasch, H.W., Honjo, S., Anderson, R.F., Reeburgh, W.S., Top, Z., Friedrich, G.E., Codispoti, L.A., Izdar, E. 1989. Unexpected changes in the oxic/anoxic interface in the Black Sea. *Nature* 338, 411–413.
- Murray, J.W. 1991. The 1988 Black Sea Oceanographic Expedition: introduction and summary. *Deep-Sea Research* 38(Supp. 2), S655–S661.
- Murray, J.W., Top, Z., Özsoy, E. 1991. Hydrographic properties and ventilation of the Black Sea. *Deep-Sea Research* 38(Supp. 2), S663–S689.
- Murray, J.W., Stewart, K., Kassakian, S., Krynytzky, M., DiJulio, D. 2007. Oxic, suboxic, and anoxic conditions in the Black Sea. In: Yanko-Hombach, V., Gilber, A. S., Panin, N. Dolukhanov, P. M. (Eds). *The Black Sea flood question: changes in coastline, climate and human settlement*. Springer, Dordrecht, The Netherlands, 1–21.
- Nesse, W.D. *Introduction to Mineralogy*. New York: Oxford University Press; 2000.
- Neuman, G., 1942. Die absolute Topographie des physikalischen Meeresniveaus und die Oberflächenströmungen des Schwarzen Meeres. *Annalen der Hydrographie und Maritimen Meteorologie* 70, 265–282.
- Oğuz, T., Latun, V.S., Latif, M.A., Vladimirov, V.V., Sur, H.I., Markov, A.A., Özsoy, E., Kovesnikov, L., Eremeev, V., Ünlüata, U. 1993. Circulation in the surface and intermediate layers of the Black Sea. *Deep-Sea Research* I 40, 1597–1612.
- Oğuz, T., Aubrey, D.G., Latun, V.S., Demirov, E., Kovesnikov, L., Sur, H.I., Diaconu, V., Besiktepe, S., Duman, M., Limeburner, R., Eremeev, V. 1994. Mesoscale circulation and thermohaline structure of the Black Sea observed during HydroBlack '91. *Deep-Sea Research* I 41(4), 603–628.
- Östlund HG, Dyrssen D. 1986. Renewal rates of the Black Sea deep water. In: *Proceedings of the Chemical and Physical Oceanography of the Black Sea*. Göteborg, Germany.
- Özsoy, E., Latif, M.A., Tuğrul, S., Ünlüata, U. 1995. Exchanges with Mediterranean, fluxes and boundary mixing processes in the Black Sea. In: Briand, F. (ed.), *Mediterranean Tributary Seas. Bulletin de l'Institut Océanographique, Monaco, Special No. 17, CIESME Science Series 2*, 187–204.
- Özsoy, E., Di Iorio, D., Gregg, M.C., Backhaus, J.O. 2001. Mixing in the Bosphorus Strait and the Black Sea continental shelf: observations and a model of the dense water outflow. *Journal of Marine Systems* 31, 99–135.

- Paytan, A., Kastner, M., Campbell, D., Thiemens, M.H. 1998. Sulfur Isotopic Composition of Cenozoic Seawater Sulfate. *Science* 282, 1459–1461.
- Pichler, H., Friedrich, W. 1976. Radiocarbon dates of Santorini volcanics. *Nature* 262 (5567), 373–374.
- Raiswell, R. and Berner, R.A. 1985. Pyrite formation in euxinic and semi-euxinic sediments. *American Journal of Science* 285, 710–724.
- Raiswell, R. and Berner, R.A. 1986. Pyrite and organic matter in Phanerozoic normal marine shales. *Geochimica et Cosmochimica Acta* 50, 1967–1976.
- Ramsey, C.B. 2012. OxCal 4.1 Manual. Available from: URL: <http://www.c14.arch.ox.ac.uk/oxcal/OxCal.html>
- Reimer, P.J., Baillie, M.G.L., Bard, E., Bayliss, A., Beck, J.W., Blackwell, P.G., Bronk Ramsey, C., Buck, C.E., Burr, G.S., Edwards, R. L., Friedrich, M., Grootes, P.M., Guilderson, T.P., Hajdas, I., Heaton, T.J., Hogg, A.G., Hughen, K.A., Kaiser, K.F., Kromer, B., McCormac, F.G., Manning, S.W., Reimer, R.W., Richards, D.A., Southon, J.R., Talamo, S., Turney, C.S.M., van der Plicht, J., Weyhenmeyer, C.E. 2009. IntCal09 and Marine09 radiocarbon age calibration curves, 0–500,00 years cal BP. *Radiocarbon*, 51(4), 1111–1150.
- Reynolds, R.R. Correlation of two sediment cores recovered from the SW Black Sea shelf using carbon and sulfur elemental and isotopic geochemistry: implications for paleoceanographic communication between the Black Sea and eastern Mediterranean Sea during the last 12,000 years. [dissertation]. St. John's: Memorial University; 2012.
- Ross, D.A., Degens, E.T., MacIlvaine, J. 1970. Black Sea: recent sedimentary history. *Science* 170 (3954), 163–165.
- Rullkötter, J. 2006. Organic Matter: The Driving Force for Early Diagenesis. In: Schulz, H.D. and Zabel, M. (Eds.). *Marine Geochemistry*, 2<sup>nd</sup> edition, Springer: Berlin, pp. 271–310.
- Ryan, W.B.F., Pitman, W.C., Major, C.O., Shimkus, K., Moskalenko, V., Jones, G.A., Dimitrov, P., Gorür, N., Sakiñç, M., Yüce, H. 1997a. An abrupt drowning of the Black Sea shelf. *Marine Geology* 138, 119–126.
- Ryan, W.B.F., Pitman, W.C., Major, C.O., Shimkus, K., Moskalenko, V., Jones, G.A., Dimitrov, P., Gorür, N., Sakiñç, M., Yüce Seyir, H. 1997b. An abrupt drowning of the Black Sea shelf at 7.5 ky BP. *Geo-Eco-Marina* 2, 115–126.
- Ryan, W.B.F. and Pitman, W.C. *Noah's Flood: The New Scientific Discoveries about the Event that Changed History*. New York: Simon & Schuster; 1998.
- Ryan, W.B.F., Major, C.O., Lericolais, G., Goldstein, S.L. 2003. Catastrophic flooding of the Black Sea. *Annual Review Earth and Planetary Sciences* 31, 525–554

- Sackett, W.M. 1986.  $\delta^{13}\text{C}$  signatures of organic carbon in southern high latitude deep sea sediments; paleotemperature implication. *Organic Geochemistry* 9, 63–68.
- Siani, G., Paterne, M., Arnold, M., Bard, E., Métévier, B., Tisnerat, N., Bassinot, F. 2000. Radiocarbon reservoir ages in the Mediterranean Sea and Black Sea. *Radiocarbon* 42(2), 271–280.
- Skinner, L.C. and McCave, I., 2003. Analysis and modelling of gravity- and piston coring based on soil mechanics. *Marine Geology* 199, 181–204.
- Sorokin, Yu.I., 1983. The Black Sea. In: B.H. Ketchum (Ed.), *Estuaries and Enclosed Seas, Ecosystems of the World* 26. Elsevier, Amsterdam, New York, pp. 253–292.
- Soulet, G., Ménot, G., Lericolais, G., Bard, E. 2011a. A revised calendar age for the last reconnection of the Black Sea to the global ocean. *Quaternary Science Reviews* 30 (9-10), 1019–1026.
- Soulet, G., Ménot, G., Garreta, V., Rostek, F., Zaragosi, S., Lericolais, G., Bard, E. 2011b. Black Sea “Lake” reservoir age evolution since the Last Glacial – Hydrologic and climatic implications. *Earth and Planetary Science Letters* 308, 245–258.
- Stuiver, M. and Braziunas, T.F. 1993. Modeling atmospheric  $^{14}\text{C}$  influences and  $^{14}\text{C}$  ages of marine samples to 10000 BC. *Radiocarbon* 35(1), 137–91.
- Swift, D.J.P. 1968. Coastal erosion and transgressive stratigraphy. *Journal of Geology* 76(4), 444–456.
- Taylor, R.E., Aitken, M.J., editors. *Advances in Archaeological and Museum Science, volume 2: Chronometric Dating in Archaeology*. New York: Plenum Press; 1997.
- Thode, H.G. 1991. Sulphur Isotopes in Nature and the Environment: An Overview. In: Krouse, H.R., Grinenko, V.A. (Eds.) *Stable isotopes: Natural and anthropogenic sulphur in the environment*, Scope 43. John Wiley and Sons: New York, 1–26.
- Vinogradov, A.P., Grinenko, V.A., and Ustinov, U.S. 1962. Izotopny sostav soedineii sery v chornomore. (Isotopic composition of sulfur compounds in the Black Sea.) *Geokhimiya* pp. 851–873; *Geochemistry International*, pp. 973–997.
- Walker, M., Johnsen, S., Rasmussen, S.O., Popp, T., Steffensen, J-P., Gibbard, P., Hoek, W., Lowe, J., Andrews, J., Björck, S., Cwynar, L.C., Hughen, K., Kershaw, P., Kromer, B., Litt, T., Lowe, D.J., Nakagawa, T., Newmham, R., Schwander, J. 2009. Formal definition and dating of the GSSP (Global Stratotype Section and Point) for the base of the Holocene using the Greenland NGRIP ice core, and selected auxiliary records. *Journal of Quaternary Science* 24(1), 3–17.
- Waples, D.W. *Geochemistry in Petroleum Exploration*. Boston: International Human Resources Development Corporation; 1985.

- Westrich, J.T. and Berner, R.A. The role of sedimentary organic matter in bacterial sulfate reduction: the G model tested. *Limnology and Oceanography* 29(2), 236–249.
- Yanko-Hombach, V., Meriç, E., Avşar, N., Kerey, E., Görmüş, M. 2004. Micropaleontological evidence of the Black Sea-Marmara Sea connection for the last 800 ka BP. In: 4<sup>th</sup> EMMM 2004, Program and Extended Abstracts of the Fourth International Congress on Environmental Micropalaeontology, Microbiology and Meiobenthology (13-18 September 2004, Isparta, Turkey), Yanko-Hombach, V., Görmüş, M., Ertunç, A., McGann, M., Martin, R., Jacob, J., Ishman, S. (Eds). 228–230.
- Yanko-Hombach, V. 2007. Controversy over Noah's Flood in the Black Sea: geological and foraminiferal evidence from the shelf. In: Yanko-Hombach, V., Gilber, A. S., Panin, N. Dolukhanov, P. M. (Eds). *The Black Sea flood question: changes in coastline, climate and human settlement*. Springer, Dordrecht, The Netherlands, 149–203.
- Yılmaz, Y., Tüysüz, O., Yiğitbaş, E., Can Genç, Ş. and Şengör, A.M.C. 1997. Geology and Tectonic Evolution of the Pontides. In: Robinson, A.G. (Ed.) *Regional and petroleum geology of the Black Sea and surrounding region*. AAPG Memoir 68, 183–226.
- Yılmaz, Y. 2007. Morphotectonic development of the southern Black Sea region and the Bosphorus channel. In: Yanko-Hombach, V., Gilber, A. S., Panin, N. Dolukhanov, P. M. (Eds). *The Black Sea flood question: changes in coastline, climate and human settlement*. Springer, Dordrecht, The Netherlands, 537–570.

## **Appendix A**

### **Carbon and Sulphur Sediment Geochemistry**

**DeltaVPlus-Carlo Erba: Carbon Isotope Analysis**

Run Date: Thursday, September 09, 2010

Client: A. Linegar

Operator: A. Linegar

Isotope:  $\delta^{13}\text{C}$ 

Memorial University

CREAIT Network - TERRA Facility

Stable Isotope Lab

Sample ID	Analysis Comment	Amount (mg)	Peak Amplitude (mV)	Delta of Peak	Mean Delta of All Analyses	StdDev of Deltas of All Analyses	%C for applicable media	Mean %C of All Analyses	StdDev of %C of All Analyses
MUN-Sulfanilamide	primer	0.310	999				55.48	45.38	5.72
MUN-Sulfanilamide	primer	0.310	746	-30.72	-30.60	0.12	42.59	45.38	5.72
MUN-Sulfanilamide	primer	0.310	909	-30.41	-30.60	0.12	51.50	45.38	5.72
MUN-Sulfanilamide	primer	0.329	761	-30.73	-30.60	0.12	40.79	45.38	5.72
MUN-Sulfanilamide	primer	0.311	761	-30.67	-30.60	0.12	43.16	45.38	5.72
MUN-Sulfanilamide	primer	0.312	755	-30.59	-30.60	0.12	42.80	45.38	5.72
MUN-Sulfanilamide	primer	0.320	748	-30.51	-30.60	0.12	41.36	45.38	5.72
Blank capsule		0.000	11						
Blank capsule		0.000	14						
Blank capsule		0.000	12						
MUN-CO-2		0.952	664	-40.49	-40.11	0.47	12.38	12.46	0.20
MUN-CO-2		0.958	660	-40.52	-40.11	0.47	12.24	12.46	0.20
IAEA-CH-6		0.310	810	-11.01	-10.45	0.74	46.22	45.47	0.63
IAEA-CH-6		0.315	816	-11.08	-10.45	0.74	45.82	45.47	0.63
Sulfanilamide		0.253	603	-29.37	-29.52	0.11	42.17	41.57	0.77
Sulfanilamide		0.818	1972	-29.52	-29.52	0.11	42.16	41.57	0.77
M05-50P - 0 cm		14.025	1095	-26.26	-26.26		1.38	1.38	
M05-50P - 10 cm		14.031	1138	-26.25	-26.25		1.43	1.43	
M05-50P - 20 cm		14.049	1102	-25.90	-25.90		1.38	1.38	

=

Sample ID	Analysis Comment	Amount (mg)	Peak Amplitude (mV)	Delta of Peak	Mean Delta of All Analyses	StdDev of Deltas of All Analyses	%C for applicable media	Mean %C of All Analyses	StdDev of %C of All Analyses
M05-50P - 30 cm		14.038	967	-26.32	-26.32		1.21	1.21	
M05-50P - 40 cm		14.045	976	-25.85	-25.85		1.22	1.22	
USGS-24		0.130	702	-16.55	-16.38	0.14	96.51	94.77	3.27
M05-50P - 50 cm		14.001	1031	-26.07	-26.07		1.30	1.30	
M05-50P - 60 cm		14.106	1180	-26.16	-26.16		1.47	1.47	
M05-50P - 70 cm		14.020	861	-26.07	-26.07		1.08	1.08	
M05-50P - 80 cm		14.043	961	-25.65	-25.65		1.21	1.21	
M05-50P - 90 cm		14.045	1135	-25.64	-25.64		1.42	1.42	
MUN-CO-2		0.951	657	-39.81	-40.11	0.47	12.34	12.46	0.20
IAEA-CH-6		0.316	795	-9.61	-10.45	0.74	44.98	45.47	0.63
Sulfanilamide		0.616	1453	-29.44	-29.52	0.11	41.79	41.57	0.77
Sulfanilamide		0.083	192	-29.70	-29.52	0.11	40.10	41.57	0.77
M05-50P - 100 cm		14.077	1053	-25.47	-25.47		1.32	1.32	
M05-50P - 110 cm		14.051	1048	-25.90	-25.90		1.32	1.32	
M05-50P - 120 cm		14.106	1134	-25.34	-25.34		1.43	1.43	
M05-50P - 130 cm		14.183	1320	-26.49	-26.49		1.65	1.65	
M05-50P - 140 cm		14.118	1109	-25.76	-25.76		1.39	1.39	
USGS-24		0.130	703	-16.29	-16.38	0.14	96.80	94.77	3.27
M05-50P - 150 cm		14.074	1253	-25.90	-25.90		1.58	1.58	
M05-50P - 160 cm		14.053	1281	-26.50	-26.50		1.61	1.61	
M05-50P - 170 cm		14.056	1120	-25.60	-25.60		1.41	1.41	
M05-50P - 180 cm		14.107	1066	-25.25	-25.25		1.34	1.34	
M05-50P - 190 cm		14.088	1252	-25.24	-25.24		1.57	1.57	
MUN-CO-2		0.950	673	-39.44	-40.11	0.47	12.69	12.46	0.20

Sample ID	Analysis Comment	Amount (mg)	Peak Amplitude (mV)	Delta of Peak	Mean Delta of All Analyses	StdDev of Deltas of All Analyses	%C for applicable media	Mean %C of All Analyses	StdDev of %C of All Analyses
IAEA-CH-6		0.312	778	-9.69	-10.45	0.74	44.68	45.47	0.63
Sulfanilamide		0.406	940	-29.52	-29.52	0.11	41.48	41.57	0.77
M05-50P - 200 cm		14.033	1181	-26.06	-26.06		1.49	1.49	
M05-50P - 210 cm		14.030	1137	-26.09	-26.09		1.43	1.43	
M05-50P - 220 cm		14.080	1010	-25.57	-25.57		1.28	1.28	
M05-50P - 230 cm		14.030	1125	-24.81	-24.81		1.42	1.42	
M05-50P - 240 cm		14.108	1122	-25.97	-25.97		1.41	1.41	
USGS-24		0.136	688	-16.32	-16.38	0.14	91.00	94.77	3.27
M05-50P - 250 cm		14.029	1285	-26.18	-26.18		1.62	1.62	
M05-50P - 260 cm		14.024	1179	-26.21	-26.21		1.49	1.49	
M05-50P - 270 cm		14.136	1005	-25.39	-25.39		1.26	1.26	
M05-50P - 280 cm		14.044	1118	-25.57	-25.57		1.41	1.41	
M05-50P - 290 cm		14.027	1164	-25.73	-25.73		1.48	1.48	
MUN-CO-2		0.948	668	-40.29	-40.11	0.47	12.63	12.46	0.20
IAEA-CH-6		0.310	786	-10.86	-10.45	0.74	45.62	45.47	0.63
Sulfanilamide		1.019	2412	-29.56	-29.52	0.11	41.72	41.57	0.77

**DeltaVPlus-Carlo Erba: Carbon Isotope Analysis**

Run Date: Friday, September 10, 2010  
 Client: A. Linegar  
 Operator: A. Linegar  
 Isotope:  $\delta^{13}\text{C}$

Memorial University  
 CREAT Network - TERRA Facility  
 Stable Isotope Lab

Sample ID	Analysis Comment	Amount (mg)	Peak Amplitude (mV)	Delta of Peak	Mean Delta of All Analyses	StdDev of Deltas of All Analyses	%C for applicable media	Mean %C of All Analyses	StdDev of %C of All Analyses
MUN-Sulfanilamide	primer	0.317	755	-28.63	-28.60	0.04	42.78	42.27	1.63
MUN-Sulfanilamide	primer	0.312	728	-28.56	-28.60	0.04	43.24	42.27	1.63
MUN-Sulfanilamide	primer	0.323	782	-28.62	-28.60	0.04	43.20	42.27	1.63
MUN-Sulfanilamide	primer	0.319	711	-28.57	-28.60	0.04	39.85	42.27	1.63
Blank capsule		0.000	12						
Blank capsule		0.000	11						
MUN-CO-2		0.950	652	-40.08	-40.11	0.10	12.30	12.45	0.22
MUN-CO-2		0.955	683	-40.18	-40.11	0.10	12.79	12.45	0.22
IAEA-CH-6		0.313	761	-10.43	-10.45	0.09	43.32	42.50	0.85
IAEA-CH-6		0.310	743	-10.51	-10.45	0.09	42.77	42.50	0.85
Sulfanilamide		0.252	587	-29.04	-29.07	0.09	41.73	41.16	1.86
Sulfanilamide		0.810	1889	-29.02	-29.07	0.09	41.29	41.16	1.86
M05-50P - 300 cm		14.009	1151	-25.37	-25.37		1.45	1.45	
M05-50P - 310 cm		14.076	1092	-25.90	-25.90		1.37	1.37	
M05-50P - 320 cm		14.069	1136	-25.45	-25.45		1.43	1.43	
M05-50P - 330 cm		14.025	1018	-25.87	-25.87		1.28	1.28	
M05-50P - 340 cm		14.050	1016	-25.60	-25.60		1.28	1.28	
USGS-24		0.134	678	-15.98	-15.99	0.11	90.89	91.33	2.65
M05-50P - 350 cm		14.025	1448	-26.46	-26.46		1.82	1.82	

<

Sample ID	Analysis Comment	Amount (mg)	Peak Amplitude (mV)	Delta of Peak	Mean Delta of All Analyses	StdDev of Deltas of All Analyses	%C for applicable media	Mean %C of All Analyses	StdDev of %C of All Analyses
M05-50P - 360 cm		14.091	1293	-25.77	-25.77		1.62	1.62	
M05-50P - 370 cm		14.056	1231	-25.66	-25.66		1.54	1.54	
M05-50P - 380 cm		14.102	1352	-25.64	-25.64		1.69	1.69	
M05-50P - 390 cm		14.012	1342	-25.54	-25.54		1.68	1.68	
MUN-CO-2		0.950	668	-39.99	-40.11	0.10	12.54	12.45	0.22
IAEA-CH-6		0.310	747	-10.34	-10.45	0.09	42.85	42.50	0.85
Sulfanilamide		0.610	1463	-29.24	-29.07	0.09	42.48	41.16	1.86
Sulfanilamide		0.082	174	-29.09	-29.07	0.09	37.45	41.16	1.86
M05-50P - 400 cm		14.038	1479	-25.96	-25.96		1.85	1.85	
M05-50P - 410 cm		14.040	1236	-25.35	-25.35		1.55	1.55	
M05-50P - 420 cm		14.022	1245	-25.09	-25.09		1.56	1.56	
M05-50P - 430 cm		14.134	1385	-24.94	-24.94		1.72	1.72	
M05-50P - 440 cm		14.030	1386	-24.90	-24.90		1.73	1.73	
USGS-24		0.129	679	-16.11	-15.99	0.11	94.17	91.33	2.65
M05-50P - 450 cm		14.005	1316	-25.25	-25.25		1.65	1.65	
M05-50P - 460 cm		14.013	1263	-25.34	-25.34		1.59	1.59	
M05-50P - 470 cm		14.043	1101	-25.98	-25.98		1.38	1.38	
M05-50P - 480 cm		14.011	1135	-25.92	-25.92		1.43	1.43	
M05-50P - 490 cm		14.025	879	-26.87	-26.87		1.10	1.10	
MUN-CO-2		0.961	661	-40.24	-40.11	0.10	12.27	12.45	0.22
IAEA-CH-6		0.318	735	-10.56	-10.45	0.09	41.07	42.50	0.85
Sulfanilamide		0.399	944	-29.02	-29.07	0.09	42.02	41.16	1.86
M05-50P - 500 cm		14.108	895	-26.68	-26.68		1.12	1.12	
M05-50P - 510 cm		14.098	842	-26.64	-26.64		1.05	1.05	

Sample ID	Analysis Comment	Amount (mg)	Peak Amplitude (mV)	Delta of Peak	Mean Delta of All Analyses	StdDev of Deltas of All Analyses	%C for applicable media	Mean %C of All Analyses	StdDev of %C of All Analyses
M05-50P - 520 cm		14.119	831	-26.51	-26.51		1.04	1.04	
M05-50P - 530 cm		14.098	939	-26.61	-26.61		1.17	1.17	
M05-50P - 540 cm		14.035	802	-26.71	-26.71		1.01	1.01	
USGS-24		0.131	650	-15.88	-15.99	0.11	88.92	91.33	2.65
M05-50P - 550 cm		14.124	919	-26.54	-26.54		1.15	1.15	
M05-50P - 560 cm		14.114	827	-26.91	-26.91		1.03	1.03	
M05-50P - 570 cm		14.008	864	-27.34	-27.34		1.08	1.08	
M05-50P - 580 cm		14.010	1035	-27.17	-27.17		1.30	1.30	
M05-50P - 590 cm		14.014	832	-26.97	-26.97		1.05	1.05	
MUN-CO-2		0.952	656	-40.06	-40.11	0.10	12.36	12.45	0.22
IAEA-CH-6		0.314	748	-10.41	-10.45	0.09	42.47	42.50	0.85
Sulfanilamide		1.036	2468	-28.99	-29.07	0.09	41.97	41.16	1.86

**DeltaVPlus-Carlo Erba: Carbon Isotope Analysis**

Run Date: Monday, September 13, 2010

Client: A. Linegar

Operator: A. Linegar

Isotope:  $\delta^{13}\text{C}$ 

Memorial University

CREAIT Network - TERRA Facility

Stable Isotope Lab

Sample ID	Analysis Comment	Amount (mg)	Peak Amplitude (mV)	Delta of Peak	Mean Delta of All Analyses	StdDev of Deltas of All Analyses	%C for applicable media	Mean %C of All Analyses	StdDev of %C of All Analyses
MUN-Sulfanilamide	primer	0.319	745	-28.83	-28.70	0.09	42.50	42.69	1.91
MUN-Sulfanilamide	primer	0.313	793	-28.69	-28.70	0.09	45.43	42.69	1.91
MUN-Sulfanilamide	primer	0.312	719	-28.65	-28.70	0.09	41.63	42.69	1.91
MUN-Sulfanilamide	primer	0.312	720	-28.61	-28.70	0.09	41.18	42.69	1.91
Blank capsule		0.000	12						
Blank capsule		0.000	11						
MUN-CO-2		0.947	650	-40.23	-40.11	0.24	12.32	12.67	0.35
MUN-CO-2		0.950	654	-40.31	-40.11	0.24	12.32	12.67	0.35
IAEA-CH-6		0.318	829	-10.58	-10.45	0.20	46.65	44.37	1.32
IAEA-CH-6		0.331	819	-10.66	-10.45	0.20	44.28	44.37	1.32
Sulfanilamide		0.265	618	-29.03	-29.13	0.11	42.06	41.71	0.75
Sulfanilamide		0.810	1919	-29.05	-29.13	0.11	41.62	41.71	0.75
M05-50P - 600 cm		14.094	676	-27.04	-27.04		0.86	0.86	
M05-50P - 610 cm		14.087	784	-27.13	-27.13		0.99	0.99	
M05-50P - 620 cm		14.099	1046	-27.88	-27.88		1.32	1.32	
M05-50P - 630 cm		14.077	650	-27.17	-27.17		0.82	0.82	
M05-50P - 640 cm		14.020	839	-27.75	-27.75		1.07	1.07	
M05-50P - 660 cm		14.053	682	-26.85	-26.92	0.11	0.87	0.87	
USGS-24		0.140	737	-15.97	-15.99	0.02	95.08	94.03	4.12

Sample ID	Analysis Comment	Amount (mg)	Peak Amplitude (mV)	Delta of Peak	Mean Delta of All Analyses	StdDev of Deltas of All Analyses	%C for applicable media	Mean %C of All Analyses	StdDev of %C of All Analyses
M05-50P - 650 cm		14.013	868	-27.02	-27.02		1.11	1.11	
50P-DUP - 660 cm		14.006	694	-27.00	-26.92	0.11	0.89	0.89	
M05-50P - 670 cm		14.010	657	-26.70	-26.70		0.84	0.84	
M05-50P - 680 cm		14.056	870	-27.50	-27.50		1.11	1.11	
M05-50P - 690 cm		14.037	802	-27.46	-27.46		1.03	1.03	
50P-DUP - 430 cm		14.018	1546	-25.68	-25.68		1.96	1.96	
MUN-CO-2		0.968	681	-39.72	-40.11	0.24	12.75	12.67	0.35
IAEA-CH-6		0.326	783	-10.21	-10.45	0.20	43.65	44.37	1.32
Sulfanilamide		0.606	1398	-29.08	-29.13	0.11	41.58	41.71	0.75
Sulfanilamide		0.098	224	-29.34	-29.13	0.11	40.39	41.71	0.75
M05-51G - 10 cm		14.012	1049	-25.84	-25.84		1.34	1.34	
M05-51G - 20 cm		14.005	1042	-26.04	-26.04		1.33	1.33	
M05-51G - 30 cm		14.067	1045	-25.83	-25.83		1.33	1.33	
M05-51G - 40 cm		14.061	1204	-26.88	-26.88		1.54	1.54	
M05-51G - 50 cm		14.013	1088	-25.97	-25.97		1.39	1.39	
50P-DUP - 180 cm		14.091	1056	-25.48	-25.48		1.34	1.34	
USGS-24		0.136	669	-16.00	-15.99	0.02	89.49	94.03	4.12
M05-51G - 60 cm		14.080	1022	-25.68	-25.68		1.31	1.31	
M05-51G - 70 cm		14.090	1015	-26.13	-26.13		1.30	1.30	
M05-51G - 80 cm		14.073	1036	-25.89	-25.89		1.32	1.32	
M05-51G - 90 cm		14.003	1235	-25.51	-25.51		1.58	1.58	
M05-51G - 100 cm		14.007	1027	-25.62	-25.62		1.32	1.32	
M05-51G - 120 cm		14.013	1095	-25.15	-25.38	0.32	1.41	1.41	
MUN-CO-2		0.955	688	-40.06	-40.11	0.24	13.12	12.67	0.35

Sample ID	Analysis Comment	Amount (mg)	Peak Amplitude (mV)	Delta of Peak	Mean Delta of All Analyses	StdDev of Deltas of All Analyses	%C for applicable media	Mean %C of All Analyses	StdDev of %C of All Analyses
IAEA-CH-6		0.333	790	-10.28	-10.45	0.20	43.91	44.37	1.32
Sulfanilamide		0.405	944	-29.16	-29.13	0.11	42.66	41.71	0.75
M05-51G - 110 cm		14.052	801	-25.55	-25.55		1.03	1.03	
51G-DUP - 120 cm		14.114	1151	-25.61	-25.38	0.32	1.46	1.46	
M05-51G - 130 cm		14.063	1090	-25.32	-25.32		1.40	1.40	
M05-51G - 140 cm		14.041	888	-25.40	-25.40		1.14	1.14	
M05-51G - 150 cm		14.035	1094	-25.50	-25.50		1.40	1.40	
50P-DUP - 0 cm		14.083	1096	-25.96	-25.96		1.40	1.40	
USGS-24		0.149	799	-16.01	-15.99	0.02	97.53	94.03	4.12
M05-50P - 700 cm		14.052	939	-27.25	-27.25		1.21	1.21	
M05-50P - 710 cm		14.157	1007	-27.56	-27.56		1.28	1.28	
M05-50P - 720 cm		14.042	705	-26.85	-26.85		0.91	0.91	
M05-50P - 730 cm		14.067	659	-27.00	-27.00		0.85	0.85	
MUN-CO-2		0.963	679	-40.24	-40.11	0.24	12.82	12.67	0.35
IAEA-CH-6		0.317	755	-10.52	-10.45	0.20	43.35	44.37	1.32
Sulfanilamide		1.061	2464	-29.10	-29.13	0.11	41.95	41.71	0.75

**MAT252 Carlo Erba: Sulfur Isotope Analysis**

Run Date: July 21, 2010  
 Client: A. Linegar  
 Operator: A. Linegar, A. Pye  
 Isotope:  $\delta^{34}\text{S}$

Memorial University  
 CREAT Network - TERRA Facility  
 Stable Isotope Lab

Sample ID	Analysis Comment	Amount (mg)	Peak Amplitude (mV)	Delta of Peak	Mean Delta of All Analyses	StdDev of Deltas of All Analyses	%S for applicable media	Mean %S of All Analyses	StdDev of %S of All Analyses
MUN-Sulfanilamide	primer	0.833	3060	1.34	2.02	0.39	17.60	18.41	0.47
MUN-Sulfanilamide	primer	0.817	3087	2.17	2.02	0.39	18.68	18.41	0.47
MUN-Sulfanilamide	primer	0.824	3223	2.03	2.02	0.39	18.92	18.41	0.47
MUN-Sulfanilamide	primer	0.806	2943	2.36	2.02	0.39	18.16	18.41	0.47
MUN-Sulfanilamide	primer	0.804	3037	2.17	2.02	0.39	18.45	18.41	0.47
Sulfanilamide		0.827	3203	2.24	2.24		18.63	18.41	0.47
High org sed B2150		1.525	164	5.28	5.53	0.92	0.90	0.92	0.03
IAEA-S-3		0.850	2167	-32.45	-32.55	0.09	13.77	14.27	0.59
IAEA-S-3		0.849	2431	-32.64	-32.55	0.09	14.93	14.27	0.59
IAEA-S-2		0.861	2239	22.47	22.67	0.23	13.84	13.69	0.20
IAEA-S-2		0.855	2045	22.82	22.67	0.23	13.40	13.69	0.20
MAR05-50P - 0 cm		15.209	868	-32.86	-32.86		0.36	0.36	
MAR05-50P - 10 cm		15.149	1049	-32.28	-32.28		0.42	0.42	
MAR05-50P - 20 cm		15.022	1498	-31.95	-31.95		0.56	0.56	
MAR05-50P - 30 cm		15.670	758	-27.80	-27.80		0.31	0.31	
MAR05-50P - 40 cm		15.109	1311	-28.16	-28.16		0.50	0.50	
High org sed B2150		8.128	1274	4.28	5.53	0.92	0.93	0.92	0.03
High org sed B2150		0.701	66	6.79	5.53	0.92	0.97	0.92	0.03
MAR05-50P - 50 cm		15.222	1377	-26.04	-26.04		0.52	0.52	

Σ

Sample ID	Analysis Comment	Amount (mg)	Peak Amplitude (mV)	Delta of Peak	Mean Delta of All Analyses	StdDev of Deltas of All Analyses	%S for applicable media	Mean %S of All Analyses	StdDev of %S of All Analyses
MAR05-50P - 60 cm		15.256	1681	-22.45	-22.45		0.61	0.61	
MAR05-50P - 70 cm		15.517	833	-28.74	-28.74		0.33	0.33	
MAR05-50P - 80 cm		15.509	2387	-24.47	-24.47		0.80	0.80	
MAR05-50P - 90 cm		15.004	4094	-26.04	-26.04		1.19	1.19	
IAEA-S-3		0.857	2284	-32.56	-32.55	0.09	14.10	14.27	0.59
IAEA-S-2		0.854	2193	22.47	22.67	0.23	13.84	13.69	0.20
IAEA-S-2		0.867	2251	22.91	22.67	0.23	13.66	13.69	0.20
MAR05-50P - 100 cm		15.279	3654	-28.48	-28.48		1.09	1.09	
MAR05-50P - 110 cm		15.373	2548	-25.47	-25.47		0.84	0.84	
MAR05-50P - 120 cm		15.843	1200	-25.96	-25.96		0.44	0.44	
MAR05-50P - 130 cm		15.102	2015	-26.15	-26.15		0.70	0.70	
MAR05-50P - 140 cm		15.080	2489	-28.42	-28.42		0.84	0.84	
High org sed B2150		12.032	2037	5.88	5.53	0.92	0.92	0.92	0.03
High org sed B2150		5.562	832	5.44	5.53	0.92	0.91	0.92	0.03
MAR05-50P - 150 cm		15.603	3407	-25.38	-25.38		1.01	1.01	
MAR05-50P - 160 cm		15.112	2087	-24.59	-24.59		0.73	0.73	
MAR05-50P - 170 cm		15.349	3540	-20.11	-20.11		1.06	1.06	
MAR05-50P - 180 cm		15.484	3079	-14.87	-14.87		0.95	0.95	

**MAT252 Carlo Erba: Sulfur Isotope Analysis**

Run Date: July 22, 2010  
 Client: A. Linegar  
 Operator: A. Linegar, A. Pye  
 Isotope:  $\delta^{34}\text{S}$

Memorial University  
 CREAT Network - TERRA Facility  
 Stable Isotope Lab

Sample ID	Analysis Comment	Amount (mg)	Peak Amplitude (mV)	Delta of Peak	Mean Delta of All Analyses	StdDev of Deltas of All Analyses	%S for applicable media	Mean %S of All Analyses	StdDev of %S of All Analyses
MUN-Sulfanilamide	primer	0.824	3155	1.64	2.23	0.45	17.90	16.27	18.62
MUN-Sulfanilamide	primer	0.818	3050	2.74	2.23	0.45	18.52	16.27	18.62
MUN-Sulfanilamide	primer	0.838	3240	2.26	2.23	0.45	18.50	16.27	18.62
MUN-Sulfanilamide	primer	0.815	3249	2.28	2.23	0.45	18.89	16.27	18.62
Sulfanilamide		0.801	3161	2.45	0.78	2.37	18.72	16.27	18.62
High org sed B2150		1.575	189	4.46	5.52	0.82	0.93	0.50	0.92
IAEA-S-3		0.854	2238	-31.93	-32.55	0.45	13.06		12.94
IAEA-S-3		0.860	2264	-32.65	-32.55	0.45	13.29		12.94
IAEA-S-2		0.849	2626	22.07	22.67	0.43	15.12		12.94
IAEA-S-2		0.860	1845	23.64	22.67	0.43	12.69		12.94
IAEA-S-2		0.853	2185	22.73	22.67	0.43	13.05		12.94
High org sed B2150		8.022	1364	5.67	5.52	0.82	0.91	0.50	0.92
High org sed B2150		0.707	56	6.45	5.52	0.82	1.05	0.50	0.92
MAR05-50P - 190 cm		15.535	4266	-21.31	-21.31		1.25		
MAR05-50P - 200 cm		15.436	2542	-7.67	-7.67		0.81		
MAR05-50P - 210 cm		15.608	5179	7.84	7.84		1.46		
MAR05-50P - 220 cm		15.440	554	30.52	30.52		0.22		
MAR05-50P - 230 cm		15.774	1581	3.21	3.21		0.53		
IAEA-S-3		0.859	2214	-32.20	-32.55	0.45	13.51		12.94

Sample ID	Analysis Comment	Amount (mg)	Peak Amplitude (mV)	Delta of Peak	Mean Delta of All Analyses	StdDev of Deltas of All Analyses	%S for applicable media	Mean %S of All Analyses	StdDev of %S of All Analyses
IAEA-S-3		0.875	2162	-32.33	-32.55	0.45	12.59		12.94
IAEA-S-2		0.853	2092	22.68	22.67	0.43	13.01		12.94
IAEA-S-2		0.863	2127	22.33	22.67	0.43	12.84		12.94
High org sed B2150		2.550	326	5.50	5.52	0.82	0.88	0.50	0.92
Sulfanilamide		1.110	4560	-0.90	0.78	2.37	18.59	16.27	18.62
IAEA-S-3		1.104	3087	-32.94	-32.55	0.45	13.70		12.94
IAEA-S-3		0.605	1647	-32.91	-32.55	0.45	14.22		12.94
IAEA-S-3		0.400	923	-33.24	-32.55	0.45	13.18		12.94
IAEA-S-3		0.259	418	-32.74	-32.55	0.45	11.75		12.94
IAEA-S-3		0.098	160	-32.02	-32.55	0.45	13.51		12.94
IAEA-S-2		0.105	137	22.57	22.67	0.43	11.52		12.94
IAEA-S-2		0.250	473	22.97	22.67	0.43	12.71		12.94
IAEA-S-2		0.407	984	22.43	22.67	0.43	13.32		12.94
IAEA-S-2		0.608	1517	22.43	22.67	0.43	13.35		12.94
IAEA-S-2		1.100	2778	22.84	22.67	0.43	13.30		12.94

**MAT252 Carlo Erba: Sulfur Isotope Analysis**

Run Date: July 26, 2010  
 Client: A. Linegar  
 Operator: A. Linegar, A. Pye  
 Isotope:  $\delta^{34}\text{S}$

Memorial University  
 CREAT Network - TERRA Facility  
 Stable Isotope Lab

Sample ID	Analysis Comment	Amount (mg)	Peak Amplitude (mV)	Delta of Peak	Mean Delta of All Analyses	StdDev of Deltas of All Analyses	%S for applicable media	Mean %S of All Analyses	StdDev of %S of All Analyses
MUN-Sulfanilamide	8 psi dilut	0.812	2397	1.78	1.42	0.61	17.57	18.61	0.73
MUN-Sulfanilamide	primer	0.811	2450	1.92	1.42	0.61	18.23	18.61	0.73
MUN-Sulfanilamide	primer	0.812	2630	1.24	1.42	0.61	19.03	18.61	0.73
MUN-Sulfanilamide	primer	0.828	2780	0.93	1.42	0.61	19.45	18.61	0.73
MUN-Sulfanilamide	primer	0.817	2598	1.24	1.42	0.61	18.78	18.61	0.73
Sulfanilamide		0.807	2562	1.69	-0.76	3.47	18.69	18.64	0.07
High org sed B2150		1.500	111	4.96	4.74	0.46	0.86	0.93	0.07
IAEA-S-3		0.850	1837	-32.26	-32.55	0.39	13.17	13.27	0.39
IAEA-S-3		0.863	1920	-32.85	-32.55	0.39	12.98	13.27	0.39
IAEA-S-2		0.852	1899	22.55	22.67	0.09	12.96	13.37	0.34
IAEA-S-2		0.858	1960	22.73	22.67	0.09	13.27	13.37	0.34
MAR05-50P - 240 cm		15.624	2081	7.95	7.95		0.76	0.76	
MAR05-50P - 250 cm		15.556	3313	-0.34	-0.34		1.12	1.12	
MAR05-50P - 260 cm		15.883	2024	0.66	0.66		0.74	0.74	
MAR05-50P - 270 cm		15.725	1223	20.53	20.53		0.49	0.49	
MAR05-50P - 280 cm		15.568	893	1.66	1.66		0.38	0.38	
High org sed B2150		8.014	1132	5.45	4.74	0.46	0.90	0.93	0.07
High org sed B2150		0.715	54	4.95	4.74	0.46	1.07	0.93	0.07
MAR05-50P - 290 cm		15.576	1050	-12.90	-12.90		0.41	0.41	

XX

Sample ID	Analysis Comment	Amount (mg)	Peak Amplitude (mV)	Delta of Peak	Mean Delta of All Analyses	StdDev of Deltas of All Analyses	%S for applicable media	Mean %S of All Analyses	StdDev of %S of All Analyses
MAR05-50P - 300 cm		15.861	1367	-23.82	-23.82		0.51	0.51	
MAR05-50P - 310 cm		15.015	1221	-24.14	-24.14		0.50	0.50	
MAR05-50P - 320 cm		15.481	1796	-35.82	-35.82		0.67	0.67	
MAR05-50P - 330 cm		15.303	2616	-37.71	-37.71		0.94	0.94	
IAEA-S-3		0.853	1677	-31.99	-32.55	0.39	12.85	13.27	0.39
IAEA-S-3		0.863	1905	-33.07	-32.55	0.39	13.13	13.27	0.39
IAEA-S-2		0.857	1971	22.67	22.67	0.09	13.47	13.37	0.34
IAEA-S-2		0.858	2021	22.73	22.67	0.09	13.76	13.37	0.34
High org sed B2150		12.084	1890	4.58	4.74	0.46	0.93	0.93	0.07
High org sed B2150		5.506	798	4.28	4.74	0.46	0.93	0.93	0.07
High org sed B2150		2.530	308	4.25	4.74	0.46	0.92	0.93	0.07
Sulfanilamide		1.103	3974	-3.22	-0.76	3.47	18.60	18.64	0.07
IAEA-S-3		1.132	2926	-32.54	-32.55	0.39	13.63	13.27	0.39
IAEA-S-3		0.604	1342	-32.60	-32.55	0.39	13.85	13.27	0.39

**MAT252 Carlo Erba: Sulfur Isotope Analysis**

Run Date: July 27, 2010  
 Client: A. Linegar  
 Operator: A. Linegar, A. Pye  
 Isotope:  $\delta^{34}\text{S}$

Memorial University  
 CREAT Network - TERRA Facility  
 Stable Isotope Lab

Sample ID	Analysis Comment	Amount (mg)	Peak Amplitude (mV)	Delta of Peak	Mean Delta of All Analyses	StdDev of Deltas of All Analyses	%S for applicable media	Mean %S of All Analyses	StdDev of %S of All Analyses
MUN-Sulfanilamide	20 psi dilut	0.813	3210	1.24	1.66	0.32	18.20	18.57	0.30
MUN-Sulfanilamide	primer	0.824	3238	2.01	1.66	0.32	18.46	18.57	0.30
MUN-Sulfanilamide	primer	0.830	3311	1.64	1.66	0.32	18.77	18.57	0.30
MUN-Sulfanilamide	primer	0.825	3350	1.76	1.66	0.32	18.84	18.57	0.30
Sulfanilamide		0.808	3275	2.16	0.86	1.84	18.88	18.71	0.25
High org sed B2150		1.507	181	6.56	5.42	0.86	0.92	0.97	0.15
IAEA-S-3		0.866	2207	-32.38	-32.55	0.36	12.73	13.51	0.65
IAEA-S-3		0.857	2365	-32.73	-32.55	0.36	13.23	13.51	0.65
IAEA-S-2		0.857	2307	22.48	22.67	0.09	12.91	13.01	0.36
IAEA-S-2		0.859	2315	22.69	22.67	0.09	12.98	13.01	0.36
MAR05-50P - 340 cm		15.088	1896	-30.71	-30.71		0.61	0.61	
MAR05-50P - 350 cm		15.324	2402	-34.32	-34.32		0.75	0.75	
MAR05-50P - 360 cm		15.351	2022	-32.02	-32.02		0.64	0.64	
MAR05-50P - 370 cm		15.254	1867	-30.79	-30.79		0.60	0.60	
MAR05-50P - 380 cm		15.365	2713	-32.19	-32.19		0.85	0.85	
High org sed B2150		8.188	1427	4.97	5.42	0.86	0.90	0.97	0.15
High org sed B2150		0.702	86	6.27	5.42	0.86	1.27	0.97	0.15
MAR05-50P - 390 cm		15.073	2702	-35.28	-35.28		0.85	0.85	
MAR05-50P - 400 cm		15.574	1858	-35.17	-35.17		0.59	0.59	

Sample ID	Analysis Comment	Amount (mg)	Peak Amplitude (mV)	Delta of Peak	Mean Delta of All Analyses	StdDev of Deltas of All Analyses	%S for applicable media	Mean %S of All Analyses	StdDev of %S of All Analyses
MAR05-50P - 410 cm		15.237	3729	-38.21	-38.21		1.12	1.12	
MAR05-50P - 420 cm		15.304	2934	-35.88	-35.88		0.92	0.92	
MAR05-50P - 430 cm		15.082	2034	-35.14	-35.14		0.67	0.67	
IAEA-S-3		0.859	2298	-32.53	-32.55	0.36	13.07	13.51	0.65
IAEA-S-3		0.854	2333	-32.57	-32.55	0.36	13.28	13.51	0.65
IAEA-S-2		0.854	2316	22.66	22.67	0.09	13.15	13.01	0.36
IAEA-S-2		0.853	2271	22.72	22.67	0.09	13.13	13.01	0.36
MAR05-50P - 440 cm		15.479	3223	-36.55	-36.55		0.98	0.98	
MAR05-50P - 450 cm		15.124	2097	-33.59	-33.59		0.69	0.69	
MAR05-50P - 460 cm		15.096	2040	-35.25	-35.25		0.66	0.66	
MAR05-50P - 470 cm		15.041	2260	-36.78	-36.78		0.73	0.73	
MAR05-50P - 480 cm		15.021	2302	-36.26	-36.26		0.74	0.74	
High org sed B2150		12.014	2170	4.91	5.42	0.86	0.93	0.97	0.15
High org sed B2150		5.519	876	4.33	5.42	0.86	0.89	0.97	0.15
MAR05-50P - 490 cm		15.180	1593	-15.25	-15.25		0.53	0.53	
MAR05-50P - 500 cm		15.521	1844	-3.05	-3.05		0.59	0.59	
MAR05-50P - 510 cm		15.065	1685	-10.05	-10.05		0.56	0.56	
MAR05-50P - 520 cm		15.086	2752	-16.44	-16.44		0.86	0.86	
MAR05-50P - 530 cm		15.620	2370	-14.88	-14.88		0.74	0.74	
IAEA-S-3	not used in cal	0.854	2283	-30.94			13.03	13.51	0.65
IAEA-S-3	11.5hr break	0.860	2419	-32.99	-32.55	0.36	13.40	13.51	0.65
IAEA-S-2		0.866	2225	22.73	22.67	0.09	13.17	13.01	0.36
IAEA-S-2		0.853	2307	22.80	22.67	0.09	13.33	13.01	0.36
High org sed B2150		2.518	329	5.49	5.42	0.86	0.88	0.97	0.15

Sample ID	Analysis Comment	Amount (mg)	Peak Amplitude (mV)	Delta of Peak	Mean Delta of All Analyses	StdDev of Deltas of All Analyses	%S for applicable media	Mean %S of All Analyses	StdDev of %S of All Analyses
Sulfanilamide		1.135	4456	-0.44	0.86	1.84	18.53	18.71	0.25
IAEA-S-3		1.115	3212	-32.46	-32.55	0.36	13.80	13.51	0.65
IAEA-S-3		0.618	1578	-31.83	-32.55	0.36	13.35	13.51	0.65
IAEA-S-3		0.405	991	-32.64	-32.55	0.36	13.31	13.51	0.65
IAEA-S-3		0.253	649	-33.09	-32.55	0.36	14.85	13.51	0.65
IAEA-S-3		0.102	201	-32.27	-32.55	0.36	14.56	13.51	0.65
IAEA-S-2		0.106	167	22.71	22.67	0.09	12.47	13.01	0.36
IAEA-S-2		0.259	548	22.75	22.67	0.09	12.42	13.01	0.36
IAEA-S-2		0.401	926	22.57	22.67	0.09	12.76	13.01	0.36
IAEA-S-2		0.601	1541	22.62	22.67	0.09	13.23	13.01	0.36
IAEA-S-2		1.116	3195	22.63	22.67	0.09	13.60	13.01	0.36

**MAT252 Carlo Erba: Sulfur Isotope Analysis**

Run Date: July 29, 2010  
 Client: A. Linegar  
 Operator: A. Linegar, A. Pye  
 Isotope:  $\delta^{34}\text{S}$

Memorial University  
 CREAT Network - TERRA Facility  
 Stable Isotope Lab

Sample ID	Analysis Comment	Amount (mg)	Peak Amplitude (mV)	Delta of Peak	Mean Delta of All Analyses	StdDev of Deltas of All Analyses	%S for applicable media	Mean %S of All Analyses	StdDev of %S of All Analyses
MUN-Sulfanilamide	8 psi dilut	0.807	3155	1.24	1.90	0.44	18.62	19.33	0.53
MUN-Sulfanilamide	primer	0.820	3259	2.21	1.90	0.44	19.72	19.33	0.53
MUN-Sulfanilamide	primer	0.818	3307	2.07	1.90	0.44	19.73	19.33	0.53
MUN-Sulfanilamide	primer	0.819	3223	2.06	1.90	0.44	19.24	19.33	0.53
Sulfanilamide		0.813	3076	2.41	1.04	1.93	18.68	18.65	0.04
High org sed B2150		1.518	196	6.18	4.78	0.73	0.90	0.92	0.03
IAEA-S-3		0.856	2129	-31.87	-32.55	0.70	13.20	5.40	6.40
IAEA-S-3		0.857	2391	-32.31	-32.55	0.70	14.08	13.45	0.72
IAEA-S-2		0.859	2124	22.63	22.67	0.35	13.23	13.13	0.68
IAEA-S-2		0.869	2298	22.29	22.67	0.35	13.37	13.13	0.68
MAR05-50P - 540 cm		15.215	1621	2.63	2.63		0.56	0.56	
MAR05-50P - 550 cm		15.370	1838	-4.00	-4.00		0.62	0.62	
MAR05-50P - 560 cm		15.058	2550	-2.86	-2.86		0.86	0.86	
MAR05-50P - 570 cm		15.051	2468	-1.10	-1.10		0.84	0.84	
MAR05-50P - 580 cm		15.154	2272	-6.12	-6.12		0.76	0.76	
High org sed B2150		8.098	1376	4.63	4.78	0.73	0.94	0.92	0.03
High org sed B2150		0.705	75	4.63	4.78	0.73	0.97	0.92	0.03
MAR05-50P - 590 cm		15.056	1849	-17.58	-17.58		0.65	0.65	
MAR05-50P - 600 cm		15.425	1177	-10.72	-10.72		0.43	0.43	

XX

Sample ID	Analysis Comment	Amount (mg)	Peak Amplitude (mV)	Delta of Peak	Mean Delta of All Analyses	StdDev of Deltas of All Analyses	%S for applicable media	Mean %S of All Analyses	StdDev of %S of All Analyses
MAR05-50P - 610 cm		15.056	1056	1.36	1.36		0.39	0.39	
MAR05-50P - 620 cm		15.218	984	-1.07	-1.07		0.36	0.36	
MAR05-50P - 630 cm		15.224	1167	-2.17	-2.17		0.43	0.43	
IAEA-S-3		0.858	2200	-32.27	-32.55	0.70	13.44	13.45	0.72
IAEA-S-3		0.851	2239	-32.11	-32.55	0.70	13.58	13.45	0.72
IAEA-S-2		0.870	2229	22.35	22.67	0.35	13.62	13.13	0.68
IAEA-S-2		0.859	2010	22.64	22.67	0.35	13.04	13.13	0.68
MAR05-50P - 640 cm		15.284	1167	1.06	1.06		0.42	0.42	
MAR05-50P - 650 cm		15.107	1127	-27.83	-27.83		0.41	0.41	
MAR05-50P - 670 cm		15.025	823	-13.31	-13.31		0.31	0.31	
MAR05-50P - 680 cm		15.210	1029	-4.03	-4.03		0.38	0.38	
High org sed B2150		12.055	2010	4.43	4.78	0.73	0.91	0.92	0.03
High org sed B2150		5.504	870	4.77	4.78	0.73	0.94	0.92	0.03
MAR05-50P - 690 cm		15.092	2260	0.67	0.67		0.80	0.80	
MAR05-51G - 10 cm		15.033	546	-32.28	-32.28		0.21	0.21	
MAR05-51G - 20 cm		15.073	477	-30.05	-30.05		0.19	0.19	
MAR05-51G - 30 cm		15.203	909	-31.28	-31.28		0.34	0.34	
MAR05-51G - 40 cm		15.095	174	-16.60	-16.60		0.08	0.08	
IAEA-S-3	not used in cal	0.867	1831				13.23	13.45	0.72
IAEA-S-3		0.865	2239	-33.02	-32.55	0.70	13.46	13.45	0.72
IAEA-S-2		0.851	2207	22.48	22.67	0.35	13.58	13.13	0.68
IAEA-S-2		0.868	2200	22.52	22.67	0.35	13.36	13.13	0.68
High org sed B2150		2.518	349	4.04	4.78	0.73	0.88	0.92	0.03
Sulfanilamide		1.116	4435	-0.32	1.04	1.93	18.62	18.65	0.04

Sample ID	Analysis Comment	Amount (mg)	Peak Amplitude (mV)	Delta of Peak	Mean Delta of All Analyses	StdDev of Deltas of All Analyses	%S for applicable media	Mean %S of All Analyses	StdDev of %S of All Analyses
IAEA-S-3		1.104	2897	-33.19	-32.55	0.70	13.47	13.45	0.72
IAEA-S-3		0.610	1195	-32.74	-32.55	0.70	11.93	13.45	0.72
IAEA-S-3		0.409	993	-33.59	-32.55	0.70	13.79	13.45	0.72
IAEA-S-3		0.251	521	-33.11	-32.55	0.70	12.90	13.45	0.72
IAEA-S-3		0.113	238	-31.29	-32.55	0.70	14.83	13.45	0.72
IAEA-S-2		0.100	141	22.25	22.67	0.35	11.26	13.13	0.68
IAEA-S-2		0.251	502	23.02	22.67	0.35	12.66	13.13	0.68
IAEA-S-2		0.411	938	22.78	22.67	0.35	13.41	13.13	0.68
IAEA-S-2		0.604	1439	23.29	22.67	0.35	13.52	13.13	0.68
IAEA-S-2		1.118	2778	23.12	22.67	0.35	13.36	13.13	0.68

**MAT252 Carlo Erba: Sulfur Isotope Analysis**

Run Date: July 30, 2010  
 Client: A. Linegar  
 Operator: A. Linegar, A. Pye  
 Isotope:  $\delta^{34}\text{S}$

Memorial University  
 CREAT Network - TERRA Facility  
 Stable Isotope Lab

Sample ID	Analysis Comment	Amount (mg)	Peak Amplitude (mV)	Delta of Peak	Mean Delta of All Analyses	StdDev of Deltas of All Analyses	%S for applicable media	Mean %S of All Analyses	StdDev of %S of All Analyses
MUN-Sulfanilamide	primer	0.804	3053	-0.20	-0.55	0.69	17.70	18.69	0.82
MUN-Sulfanilamide	primer	0.810	3305	-1.58	-0.55	0.69	19.66	18.69	0.82
MUN-Sulfanilamide	primer	0.812	3191	-0.32	-0.55	0.69	18.95	18.69	0.82
MUN-Sulfanilamide	primer	0.813	3112	-0.11	-0.55	0.69	18.46	18.69	0.82
Sulfanilamide		0.803	3093	0.23	0.23		18.56	18.56	
High org sed B2150		1.518	184	4.65	4.99	0.26	0.92	0.93	0.03
IAEA-S-3		0.867	2236	-32.12	-32.55	0.39	13.65	13.56	0.47
IAEA-S-3		0.865	2337	-32.66	-32.55	0.39	13.63	13.56	0.47
IAEA-S-2		0.864	2268	22.56	22.67	0.08	13.37	13.59	0.29
IAEA-S-2		0.856	2186	22.73	22.67	0.08	13.30	13.59	0.29
MAR05-51G - 50 cm		15.483	1130	-29.96	-29.96		0.41	0.41	
MAR05-51G - 60 cm		15.209	565	-27.88	-27.88		0.23	0.23	
MAR05-51G - 70 cm		15.393	1006	-28.82	-28.82		0.38	0.38	
MAR05-51G - 80 cm		15.025	644	-23.31	-23.31		0.26	0.26	
MAR05-51G - 90 cm		15.336	1401	-30.01	-30.01		0.51	0.51	
MAR05-51G - 100 cm		15.150	1170	-33.91	-33.91		0.43	0.43	
High org sed B2150		8.012	1223	5.06	4.99	0.26	0.91	0.93	0.03
High org sed B2150		0.709	68	5.27	4.99	0.26	0.97	0.93	0.03
MAR05-51G - 110 cm		15.041	482	-34.53	-34.53		0.20	0.20	

Sample ID	Analysis Comment	Amount (mg)	Peak Amplitude (mV)	Delta of Peak	Mean Delta of All Analyses	StdDev of Deltas of All Analyses	%S for applicable media	Mean %S of All Analyses	StdDev of %S of All Analyses
MAR05-51G - 120 cm		15.145	1719	-39.02	-39.02		0.61	0.61	
MAR05-51G - 130 cm		15.062	1771	-37.61	-37.61		0.64	0.64	
MAR05-51G - 140 cm		15.014	731	-33.36	-33.36		0.29	0.29	
MAR05-51G - 150 cm		15.226	1796	-34.11	-34.11		0.63	0.63	
IAEA-S-3	glitch in chrom	0.860	1967				12.91	13.56	0.47
IAEA-S-3		0.853	2264	-32.87	-32.55	0.39	14.04	13.56	0.47
IAEA-S-2		0.853	2273	22.64	22.67	0.08	13.78	13.59	0.29
IAEA-S-2		0.858	2313	22.75	22.67	0.08	13.89	13.59	0.29
MAR05-50P - 700 cm		15.028	2388	13.30	13.30		0.84	0.84	
MAR05-50P - 710 cm		15.271	397	-4.39	-4.39		0.17	0.17	
MAR05-50P - 720 cm		15.344	211	4.74	4.74		0.10	0.10	
MAR05-50P - 730 cm		15.240	533	17.68	17.68		0.22	0.22	
High org sed B2150		12.104	2062	4.96	4.99	0.26	0.93	0.93	0.03
High org sed B2150	HV tripped	5.524	834						

**MAT252 Carlo Erba: Sulfur Isotope Analysis**

Run Date: September 22, 2010  
 Client: A. Linegar  
 Operator: A. Linegar, A. Pye  
 Isotope:  $\delta^{34}\text{S}$

Memorial University  
 CREAT Network - TERRA Facility  
 Stable Isotope Lab

Sample ID	Analysis Comment	Amount (mg)	Peak Amplitude (mV)	Delta of Peak	Mean Delta of All Analyses	StdDev of Deltas of All Analyses	%S for applicable media	Mean %S of All Analyses	StdDev of %S of All Analyses
W95-32 PY	9 psi dilut	0.120	1458	7.44	7.33	0.23	46.40	47.70	1.21
W95-32 PY	primer	0.116	1432	7.06	7.33	0.23	47.91	47.70	1.21
W95-32 PY	primer	0.129	1661	7.48	7.33	0.23	48.79	47.70	1.21
IAEA-S-3		0.506	1877	-32.63	-32.55	0.20	13.50	13.45	0.26
IAEA-S-3		0.520	1865	-32.46	-32.55	0.20	13.30	13.45	0.26
IAEA-S-2		0.520	1824	22.74	22.67	0.08	12.88	13.24	0.23
IAEA-S-2		0.501	1769	22.60	22.67	0.08	13.18	13.24	0.23
IAEA-S-1		0.568	2089	0.12	-0.12	0.34	13.15	13.37	0.31
IAEA-S-1		0.579	2227	-0.35	-0.12	0.34	13.59	13.37	0.31
IAEA-S-3		0.511	1921	-32.59	-32.55	0.20	13.58	13.45	0.26
IAEA-S-3		0.526	1968	-32.52	-32.55	0.20	13.51	13.45	0.26
IAEA-S-2		0.515	1847	22.74	22.67	0.08	13.28	13.24	0.23
IAEA-S-2		0.530	1977	22.52	22.67	0.08	13.51	13.24	0.23
IAEA-S-2		0.412	1409	22.73	22.67	0.08	13.14	13.24	0.23
IAEA-S-2		0.317	934	22.69	22.67	0.08	13.03	13.24	0.23
IAEA-S-3		0.335	1040	-32.90	-32.55	0.20	13.00	13.45	0.26
IAEA-S-3		0.420	1453	-32.18	-32.55	0.20	13.22	13.45	0.26
DUP: M05-50P - 20 cm		15.098	2221	-30.33	-30.33		0.53	0.53	
DUP: M05-50P - 200 cm		15.288	3706	-7.94	-7.94		0.79	0.79	

XXX

Sample ID	Analysis Comment	Amount (mg)	Peak Amplitude (mV)	Delta of Peak	Mean Delta of All Analyses	StdDev of Deltas of All Analyses	%S for applicable media	Mean %S of All Analyses	StdDev of %S of All Analyses
DUP: M05-50P - 320 cm		15.048	2823	-33.61	-33.61		0.65	0.65	
DUP: M05-50P - 390 cm		15.053	3917	-34.83	-34.83		0.85	0.85	
DUP: M05-50P - 620 cm		15.051	1484	-2.06	-2.06		0.39	0.39	
High org sed B2150		0.710	88	6.19	5.72	0.39	1.15	0.94	0.11
High org sed B2150		1.557	204	6.17	5.72	0.39	0.85	0.94	0.11
High org sed B2150		2.505	417	5.31	5.72	0.39	0.87	0.94	0.11
High org sed B2150		5.521	1223	5.36	5.72	0.39	0.91	0.94	0.11
High org sed B2150		8.061	2042	5.77	5.72	0.39	0.96	0.94	0.11
High org sed B2150		12.187	3144	5.54	5.72	0.39	0.90	0.94	0.11
Sulfanilamide		0.801	4869	1.08	1.08		18.69	18.69	
Sulfanilamide	peak too large	1.116	6199						
IAEA-S-3		0.858	3604	-32.65	-32.55	0.20	13.72	13.45	0.26
IAEA-S-3		0.854	3613	-32.47	-32.55	0.20	13.76	13.45	0.26
IAEA-S-2		0.858	3470	22.71	22.67	0.08	13.52	13.24	0.23
IAEA-S-2		0.857	3501	22.63	22.67	0.08	13.39	13.24	0.23

**MAT252 Carlo Erba: Sulfur Isotope Analysis**

Run Date: December 6, 2010  
 Client: A. Linegar  
 Operator: A. Linegar, A. Pye  
 Isotope:  $\delta^{34}\text{S}$

Memorial University  
 CREAT Network - TERRA Facility  
 Stable Isotope Lab

Sample ID	Analysis Comment	Amount (mg)	Peak Amplitude (mV)	Delta of Peak	Mean Delta of All Analyses	StdDev of Deltas of All Analyses	%S for applicable media	Mean %S of All Analyses	StdDev of %S of All Analyses
W95-32 PY	primer	0.091	2126	6.31	6.94	0.45	38.45	44.99	4.55
W95-32 PY	primer	0.084	1323	7.06	6.94	0.45	46.18	44.99	4.55
W95-32 PY	primer	0.095	1962	7.37	6.94	0.45	49.02	44.99	4.55
W95-32 PY	primer	0.092	1880	7.00	6.94	0.45	46.31	44.99	4.55
IAEA-S-3		0.352	2058	-32.51	-32.55	0.20	12.96	13.15	0.39
IAEA-S-3		0.360	2086	-32.60	-32.55	0.20	13.00	13.15	0.39
IAEA-S-2		0.341	1843	22.65	22.67	0.09	12.99	13.00	0.23
IAEA-S-2		0.339	1774	22.69	22.67	0.09	13.29	13.00	0.23
IAEA-S-1		0.357	1278	0.04	0.18	0.18	12.72	12.63	0.40
IAEA-S-1		0.347	880	0.43	0.18	0.18	12.07	12.63	0.40
MAR05-50P - 660 cm		9.464	1020	-29.74	-29.74		0.43	0.43	
IAEA-S-3		0.339	1110	-32.29	-32.55	0.20	13.73	13.15	0.39
IAEA-S-3		0.376	1199	-32.82	-32.55	0.20	12.90	13.15	0.39
IAEA-S-2		0.366	1145	22.79	22.67	0.09	13.14	13.00	0.23
IAEA-S-2		0.352	987	22.55	22.67	0.09	12.64	13.00	0.23
IAEA-S-1		0.346	784	0.08	0.18	0.18	12.69	12.63	0.40
IAEA-S-1		0.362	948	0.16	0.18	0.18	13.02	12.63	0.40
IAEA-S-3		0.356	642	-32.39	-32.55	0.20	12.78	13.15	0.39
IAEA-S-3		0.335	702	-32.69	-32.55	0.20	13.54	13.15	0.39

Sample ID	Analysis Comment	Amount (mg)	Peak Amplitude (mV)	Delta of Peak	Mean Delta of All Analyses	StdDev of Deltas of All Analyses	%S for applicable media	Mean %S of All Analyses	StdDev of %S of All Analyses
IAEA-S-2		0.351	687	22.60	22.67	0.09	12.87	13.00	0.23
IAEA-S-2		0.352	686	22.74	22.67	0.09	13.06	13.00	0.23
High org sed B2150		6.604	985	5.18	5.42	0.20	0.92	0.92	0.02
High org sed B2150		5.226	581	5.65	5.42	0.20	0.91	0.92	0.02
High org sed B2150		4.140	340	5.37	5.42	0.20	0.92	0.92	0.02
High org sed B2150		3.150	220	5.47	5.42	0.20	0.94	0.92	0.02
High org sed B2150	peak too small	1.679	41	3.39			0.90	0.92	0.02

## **Appendix B**

### **Gypsum Crystal Counts and Geochemistry**

Core		Depth (cm)	Dry Weight Batch 1 (mg)	# of Gypsum Crystals	Crystals/mg	Classification	Abundance Class	Dry Weight Batch 2 (mg)	# of Gypsum Crystals	Crystals/mg	Classification	Abundance Class
MAR05-51G	10	0.0864	0	0	None	0	0	0.1375	0	0	None	0
	20	0.0963	0	0	None	0	0	0.5161	0	0	None	0
	30	0.0427	0	0	None	0	0	0.1023	0	0	None	0
	40	0.0429	0	0	None	0	0	0.0935	0	0	None	0
	50	0.0730	0	0	None	0	0	0.1090	0	0	None	0
	60	0.2047	0	0	None	0	0	0.2350	0	0	None	0
	70	0.2599	0	0	None	0	0	0.1627	0	0	None	0
	80	0.0511	0	0	None	0	0	0.1292	0	0	None	0
	90	0.9124	0	0	None	0	0	0.3756	0	0	None	0
	100	0.0881	0	0	None	0	0	0.1439	0	0	None	0
	110	0.1784	0	0	None	0	0	0.2923	0	0	None	0
	120	0.2070	0	0	None	0	0	0.1049	0	0	None	0
	130	0.1200	8	67	Common	4	0	0.6090	0	0	None	0
	140	0.0476	0	0	None	0	0	0.1552	0	0	None	0
	150	1.1082	0	0	None	0	0	0.1455	0	0	None	0
MAR05-50P	0	0.2156	0	0	None	0	0	0.6042	0	0	None	0
	10	0.6132	0	0	None	0	0	0.8229	0	0	None	0
	20	0.0631	0	0	None	0	0	0.2199	0	0	None	0
	30	0.0837	0	0	None	0	0	0.1785	0	0	None	0
	40	0.1166	0	0	None	0	0	0.3214	0	0	None	0
	50	0.1718	0	0	None	0	0	0.4060	0	0	None	0
	60	0.4689	0	0	None	0	0	0.2753	0	0	None	0
	70	0.2370	0	0	None	0	0	0.2079	0	0	None	0
	80	0.0628	0	0	None	0	0	0.2212	0	0	None	0
	90	0.0396	0	0	None	0	0	0.0451	0	0	None	0
	100	0.0811	0	0	None	0	0	0.1275	0	0	None	0
	110	0.0696	0	0	None	0	0	0.0919	0	0	None	0
	120	0.0863	0	0	None	0	0	0.1517	0	0	None	0
	130	0.0218	0	0	None	0	0	0.2003	35	175	Frequent	3
	140	0.0390	0	0	None	0	0	0.1048	60	573	Abundant	5
	150	0.0339	0	0	None	0	0	0.1253	13	104	Frequent	3
	160	0.0436	0	0	None	0	0	0.0852	57	669	Abundant	5
	170	0.0587	0	0	None	0	0	0.2492	0	0	None	0
	180	0.1273	0	0	None	0	0	1.1627	0	0	None	0
	190	0.0491	0	0	None	0	0	0.0923	9	98	Frequent	3
	200	0.0225	0	0	None	0	0	0.1596	0	0	None	0
	210	0.0968	0	0	None	0	0	0.3246	0	0	None	0
	220	0.0252	0	0	None	0	0	0.1414	0	0	None	0
	230	0.0688	0	0	None	0	0	0.1522	0	0	None	0
240	0.0374	0	0	None	0	0	0.2030	0	0	None	0	
250	0.0513	0	0	None	0	0	0.1532	4	26	Occasional	2	
260	0.0947	0	0	None	0	0	0.1370	0	0	None	0	
270	0.1329	0	0	None	0	0	0.4298	7	16	Occasional	2	
280	0.3300	0	0	None	0	0	0.7608	3	4	Rare	1	
290	0.2231	0	0	None	0	0	0.5631	0	0	None	0	

Core	Depth (cm)	Dry Weight Batch 1 (mg)	# of Gypsum Crystals	Crystals/mg	Classification	Abundance Class	Dry Weight Batch 2 (mg)	# of Gypsum Crystals	Crystals/mg	Classification	Abundance Class
MAR05-S0P	300	0.3388	0	0	None	0	0.5236	0	0	None	0
	310	0.1765	0	0	None	0	0.4169	54	130	Frequent	3
	320	0.3481	0	0	None	0	0.3777	21	56	Frequent	3
	330	1.0400	0	0	None	0	0.6280	85	135	Frequent	3
	340	0.4729	0	0	None	0	2.7466	10	4	Rare	1
	350	0.1642	85	518	Abundant	5	0.2153	0	0	None	0
	360	0.0804	0	0	None	0	0.1343	0	0	None	0
	370	0.0598	46	769	Abundant	5	0.1027	0	0	None	0
	380	0.2375	3	13	Occasional	2	0.5055	0	0	None	0
	390	0.0314	0	0	None	0	0.1648	0	0	None	0
	400	0.0377	0	0	None	0	0.1192	0	0	None	0
	410	0.0277	0	0	None	0	0.0702	4	57	Frequent	3
	420	0.0587	35	596	Abundant	5	0.3645	640	1756	Abundant	5
	430	0.1060	145	1368	Abundant	5	0.5642	1744	3091	Abundant	5
	440	0.6541	21	32	Frequent	3	0.8623	260	302	Common	4
	450	0.2600	107	412	Common	4	0.3160	832	2633	Abundant	5
	460	0.3950	128	324	Common	4	0.9461	512	541	Abundant	5
	470	0.2910	440	1512	Abundant	5	0.9227	2240	2428	Abundant	5
	480	0.5240	480	916	Abundant	5	0.9014	912	1012	Abundant	5
	490	0.2366	82	347	Common	4	0.5383	672	1248	Abundant	5
	500	0.3018	95	315	Common	4	0.3555	904	2543	Abundant	5
	510	0.5505	248	450	Common	4	0.9897	249	252	Common	4
	520	0.4305	880	2044	Abundant	5	0.9044	736	814	Abundant	5
	530	0.5322	392	737	Abundant	5	0.7848	111	141	Frequent	3
	540	0.7508	113	151	Frequent	3	1.1659	528	453	Common	4
	550	0.2127	50	235	Common	4	0.3446	75	218	Common	4
	560	0.2065	55	266	Common	4	0.4200	216	514	Abundant	5
	570	0.3020	0	0	None	0	0.3158	46	146	Frequent	3
	580	0.1492	0	0	None	0	0.4132	195	472	Common	4
	590	0.3384	0	0	None	0	0.9955	10	10	Occasional	2
600	0.3056	0	0	None	0	0.4669	28	60	Frequent	3	
610	0.2893	0	0	None	0	0.7788	10	13	Occasional	2	
620	0.4842	0	0	None	0	0.6484	6	9	Rare	1	
630	0.2521	3	12	Occasional	2	0.5982	12	20	Occasional	2	
640	0.4975	0	0	None	0	0.9931	3	3	Rare	1	
650	0.1697	0	0	None	0	0.5945	1	2	Rare	1	
660	0.4115	0	0	None	0	0.2139	4	19	Occasional	2	
670	1.1150	0	0	None	0	2.1360	0	0	None	0	
680	0.2317	0	0	None	0	0.5953	5	8	Rare	1	
690	0.5735	0	0	None	0	2.3970	3	1	Rare	1	
700	0.6157	0	0	None	0	0.4234	3	7	Rare	1	
710	0.3420	0	0	None	0	0.5199	13	25	Occasional	2	
720	0.3081	0	0	None	0	0.9385	0	0	None	0	
730	1.7161	0	0	None	0	1.5913	0	0	None	0	

**MAT252-Carlo Erba: Sulfur Isotope Analysis**

Run Date: Wednesday, December 21, 2011  
 Client: A. Linegar  
 Operator: A. Pye  
 Isotope:  $\delta^{34}\text{S}_{\text{VCDT}}$

**Memorial University  
 CREAT Network - TERRA Facility  
 Stable Isotope Lab**

Sample ID	Analysis Comment	Amount (mg)	Peak Amplitude (mV)	Delta of Peak	Mean	StdDev of	Last Name
					Delta of All Analyses	Deltas of All Analyses	
W95-32 PY	primer	0.083	3202	6.84	6.93	0.13	Reference
W95-32 PY	primer	0.095	4986	7.08	6.93	0.13	Reference
W95-32 PY	primer	0.092	3429	6.76	6.93	0.13	Reference
W95-32 PY	primer	0.093	4084	6.98	6.93	0.13	Reference
W95-32 PY	primer	0.098	4407	6.98	6.93	0.13	Reference
IAEA-S-3		0.357	3664	-32.46	-32.55	0.20	Reference
IAEA-S-3		0.348	2846	-32.58	-32.55	0.20	Reference
IAEA-S-2		0.345	3882	22.85	22.67	0.17	Reference
IAEA-S-2		0.381	4151	22.64	22.67	0.17	Reference
B1-430 cm		0.257	3962	-29.72	-29.72		Linegar
B1-460 cm		0.240	2523	-27.27	-27.27		Linegar
B1-470 cm		0.243	3092	-29.32	-29.32		Linegar
B1-490 cm		0.243	2406	-9.93	-9.93		Linegar
B1-520 cm		0.250	2426	-4.48	-4.48		Linegar
IAEA-S-1		0.340	3517	-0.04	0.10	0.21	Reference
IAEA-S-1		0.369	3971	0.18	0.10	0.21	Reference
B1-540 cm		0.239	3352	1.85	1.85		Linegar
B2-430 cm		0.245	3113	-28.98	-28.98		Linegar
B2-460 cm		0.246	3595	-26.87	-26.87		Linegar
B2-470 cm		0.243	3181	-27.06	-27.06		Linegar
B2-490 cm		0.254	3480	-12.47	-12.47		Linegar
IAEA-S-3		0.358	3670	-32.30	-32.55	0.20	Reference
IAEA-S-3		0.343	3635	-32.75	-32.55	0.20	Reference
IAEA-S-2		0.339	3274	22.89	22.67	0.17	Reference
IAEA-S-2		0.348	3648	22.60	22.67	0.17	Reference
B2-520 cm		0.240	2311	-7.00	-7.00		Linegar
B2-540 cm		0.240	2283	1.07	1.07		Linegar
DUP-B2-430		0.241	2741	-28.67	-28.67		Linegar
DUP-B2-540		0.254	2991	1.19	1.19		Linegar
DUP-B1-470		0.243	3596	-29.40	-29.40		Linegar
IAEA-S-1		0.352	3901	0.35	0.10	0.21	Reference
IAEA-S-1		0.365	2781	-0.11	0.10	0.21	Reference
IAEA-S-3		0.345	3822	-32.36	-32.55	0.20	Reference
IAEA-S-3		0.357	3964	-32.65	-32.55	0.20	Reference
IAEA-S-2		0.339	3688	22.93	22.67	0.17	Reference
IAEA-S-2		0.343	3507	22.59	22.67	0.17	Reference
IAEA-S-2		0.526	4445	22.52	22.67	0.17	Reference
IAEA-S-2		0.237	2276	22.40	22.67	0.17	Reference
IAEA-S-2		0.127	1203	22.56	22.67	0.17	Reference
IAEA-S-2		0.058	336	22.71	22.67	0.17	Reference
IAEA-S-3		0.068	411	-32.32	-32.55	0.20	Reference
IAEA-S-3		0.123	903	-32.93	-32.55	0.20	Reference
IAEA-S-3		0.522	2163	-32.58	-32.55	0.20	Reference
IAEA-S-3		0.450	5114	-32.56	-32.55	0.20	Reference

## Appendix C: Gypsum Crystals



Plate 1: Low magnification secondary electron scanning electron microscope image of a gypsum crystal. Gypsum crystal was taken at 490 cm depth in core MAR05-50P.

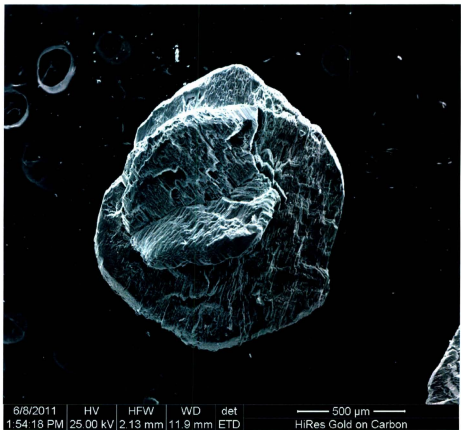


Plate 2: Low magnification secondary electron scanning electron microscope image of a gypsum crystal showing a twinned crystal. Crystal was taken from 490 cm depth in core MAR05-50P.

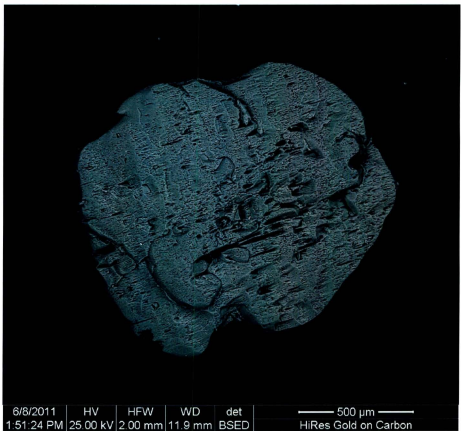


Plate 3: Low magnification backscatter electron image of a gypsum crystal (also shown in Plate 1).



Plate 4: High magnification image of an iron (Fe) inclusion in a gypsum crystal from depth 490 cm.

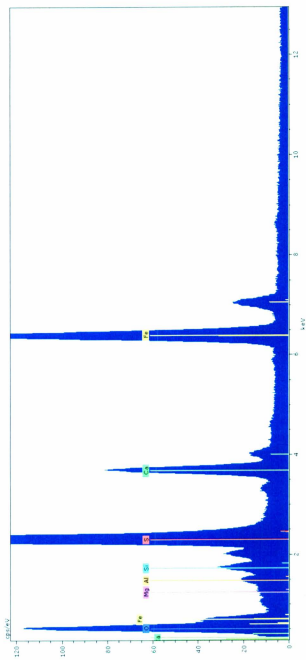


Figure 29: Scanning electron microscope compositional spectrum of inclusions found in a gypsum crystal. The spectrum shows an inclusion of iron (Plate 4) within the  $\text{CaSO}_4 \cdot 2\text{H}_2\text{O}$  matrix.



Plate 5: High magnification backscatter electron image of an inclusion containing iron (Fe), magnesium (Mg) and aluminium (Al) in a gypsum crystal.





